STUDIES OF TIROS AND NIMBUS RADIOMETRIC OBSERVATIONS

EARL S. MERRITT
PAUL E. SHERR
W.K. WIDGER, JR.
CLINTON J. BOWLEY

FINAL REPORT
CONTRACT NO. NAS 5-10151

MARCH 1967

NATIONAL AERONAUTICS AND SPACE ADMINISTRATION
GODDARD SPACE FLIGHT CENTER
GREENBELT, MARYLAND

ALLIED RESEARCH ASSOCIATES, INC.
VIRGINIA ROAD, CONCORD, MASSACHUSETTS

STUDIES OF TIROS AND NIMBUS RADIOMETRIC OBSERVATIONS

EARL S. MERRITT
PAUL E. SHERR
W.K. WIDGER, JR.
CLINTON J. BOWLEY

FINAL REPORT
CONTRACT NO. NAS 5-10151

MARCH 1967

NATIONAL AERONAUTICS AND SPACE ADMINISTRATION
GODDARD SPACE FLIGHT CENTER
GREENBELT, MARYLAND

ALLIED RESEARCH ASSOCIATES, INC.
VIRGINIA ROAD, CONCORD, MASSACHUSETTS

FOREWORD

This report presents results of selected analyses of TIROS and Nimbus radiometric observations. This was conducted by personnel of the Geophysics Division of Allied Research Associates, Inc., Concord Massachusetts. Support for these studies was provided by the National Aeronautics and Space Administration, under Contract No. NAS5-10151 for the Laboratory for Atmospheric and Biological Sciences, Goddard Space Flight Center, Greenbelt, Maryland.

Credits for individual sections of this report are applicable as follows:

Mr. Merritt	Section 2, Appendices A and B and the Motion Picture.
Dr. Widger and Mr. Sherr	Sections 3.1 and 3.2
Mr. Bowley	Portions of Section 2 (particularly with respect to the Motion Picture preparation).

The authors wish to acknowledge the significant contributions of Mr. James Willand of Allied for invaluable assistance in the preparation of the technical illustrative material of Section 3.1 and 3.2 and in the data processing aspects of Section 2.

ABSTRACT

Selected studies of TIROS and Nimbus radiometric observations are presented:

A. TIROS VII 8-12μ "window" investigations of the diurnal variation in cloudiness over Indonesia and Malaysia during June-September 1963. This study revealed a pronounced semi-diurnal cloud cycle with maxima at 0500L and 1700L and minima at 1400L and 2200L over land areas. Ocean areas revealed a similar cycle but the amplitude of the variation was much smaller than that over the land. Average cloud heights inferred from the "window" observation suggests that cloud heights may average about one kilometer higher during the day (0600-1800L).

B. Preparation of a 16mm sound-on-film, color motion picture of the diurnal cycle of TIROS VII 8-12μ "window" observations. This film uses the composited hourly analyses of a cloud "day" to prepare a time lapse presentation of the diurnal cycle. Supplementary material provides explanation of the overall procedures involved in preparation of the analyses.

C. Analysis of hurricane Alma of June 1966 using Nimbus II Medium Resolution Infrared (MRIR) observations in addition to ESSA and Nimbus II photographic observations. This analysis showed a marked difference in size between the H_2O 6.4-6.9μ canopy and the 10-11μ "window" or reflected channels. The size difference could be attributed to the existence of amounts of water vapor and unseen ice crystals outside of the visible canopy due to advection in the outflow layer and to the effects of subsidence around the canopy edge which may have evaporated the visible cloudiness.

Analysis of the time change in visible canopy area during the period from inception through hurricane stage, to the beginning of dissipation, indicate rapid change in area during the formative period decreasing to zero change on the day of upgrade to hurricane intensity. Analysis of a simple incompressible model hurricane in which all vertical motions are confined to "hot" cumulus towers suggest that the percentage of coverage of the area by convective "hot" towers may remain nearly constant from disturbance inception to hurricane.

D. The analysis of HRIR digitized data for three cases previously investigated using the data in pictorial form were selected. The cases include:

1. A Gulf of Alaska Storm with Cloud Vortex. Analyses were prepared on machine mapped HRIR, TIROS IR and hand plotted HRIR and comparisons made to the HRIR pictorial and Nimbus AVCS data. As expected, the vortex pattern can be easily recognized in all data forms. Hand plotted data allow the study of mesoscale systems within larger synoptic scale patterns.

2. Rain Band Case Study. Data for a frontal band over New England has been analyzed at a 1:2 million machine mapped scale and at a 1:1 million hand-plotted scale. The choice of presentation scale contributes to the interpretability of the data. The pictorial form is convenient for comparison to AVCS, the 1:2 million machine map allows easy recognition of sub-synoptic scale features and the full resolution data allows mesoscale interpretation but makes larger scale recognition more difficult. The occurrence of measureable precipitation is reasonably correlated with cloud top temperature.

3. Anomalous Bright Band (Daylight HRIR). Digitized data reveal the anomalous pictorial form was not an artifact. Apparent blackbody temperatures indicate radiation reaching the sensor was composed of some reflected, ground emitted energy, since temperatures were warmer than land surface temperatures.

TABLE OF CONTENTS

TABLE OF CONTENTS (cont'd)

LIST OF FIGURES

LIST OF FIGURES (cont)

LIST OF TABLES

1. INTRODUCTION

1.1 Background and Summary

This report presents the results of studies of selected TIROS and Nimbus radiometric observations. The primary goal of the project was the preparation of a motion picture depicting the diurnal variation of TIROS VII 8-12μ "window" radiation and, therefore, of average cloudiness, over the island areas of Indonesia, Malaysia and New Guinea.† In addition to this movie, the following selected analyses of Nimbus I and II data were completed and are presented in this report:

a. An analysis of certain aspects of Hurricane Alma - 1966, using Nimbus II MRIR and HRIR observations. (This study was presented in Progress Report No. 3. It is included in this report as Appendix B.)

b. Quantitative comparisons of a vortex case observed by Nimbus I HRIR and TIROS VII Channel 2 (8-12μ "window").

c. Quantitative analysis of Nimbus I HRIR data for 9 September 1964 (meso-scale New England rainband case).

d. Quantitative analysis of an apparently anomalous bright band near the British Isles, in the daylight Nimbus I HRIR data for 11 September 1964.

The discussions of the tropical island area diurnal variations, as shown by the TIROS VII 8-12μ window data (Section 2), will center on a presentation of the even-hour, smoothed analysis cels‡ used in the movie, and their comparison with the original unsmoothed TIROS VII analysis (included as Appendix A).

The Hurricane Alma, Nimbus II analysis will be included only as Appendix B.

The Nimbus I HRIR analyses are presented as Section 3.

---

† This motion picture is a 16 mm color sound presentation. While it is inherently a separate item, it should be considered an integral part of this Final Report.

‡ An analysis cel contains all the material required for one step of an animation sequence.

2. DIURNAL STUDIES

2.1 Area

The area chosen for study, i.e., the areas of Indonesia, Malaysia and New Guinea between 10N and 10S and 95E and 150E, is shown in Figure 1. The area straddles the equator between the subtropical surface pressure ridges of the Pacific and Indian Oceans. It has a diverse distribution of islands, straits, gulfs, peninsulas, and archipelagos. Many of the land areas have very rugged terrain, with frequent mountain barriers (shaded on Fig. 1) oriented along the major axes of the land areas.

2.2 Climatological Considerations

The Indonesian region is well known for its extensive cloudiness. During much of the year transient disturbances, moving along the ITCZ/ETZ, influence the production of these clouds. During the period from late June through to late September, however, most of the cloudiness appears to be related to the land and sea wind regimes, and to heating of the land surface. A study of the area, using TIROS IV, was prepared by Saha (1966). His study, for April and May concluded:

> "...However, in the light of evidence furnished by the TIROS radiation data, we may conclude that, given a synoptic situation in the equatorial trough zone, (ETZ) we may expect to see cloud towers growing preferentially over large land masses and islands within this zone, particularly in such areas where there are mountain ranges normal to the prevailing wind and relatively little or moderate vertical cloud growth over the wide ocean areas, except, perhaps when the latter areas are disturbed by an activation of the equatorial trough or by such synoptic disturbances as depressions or tropical storms."

This result is very similar to an earlier statement by Palmer et al., (1955):

> "About mid-day, even though there may be little cloud over the sea, large cumulus will have built up to a height varying between 8,000 and 15,000 feet above the mountain crest, depending on the latitude of the island and its position with respect to the semi-permanent oceanic highs. Already rain will be falling on the windward side of the mountain chain, and, as the afternoon progresses,

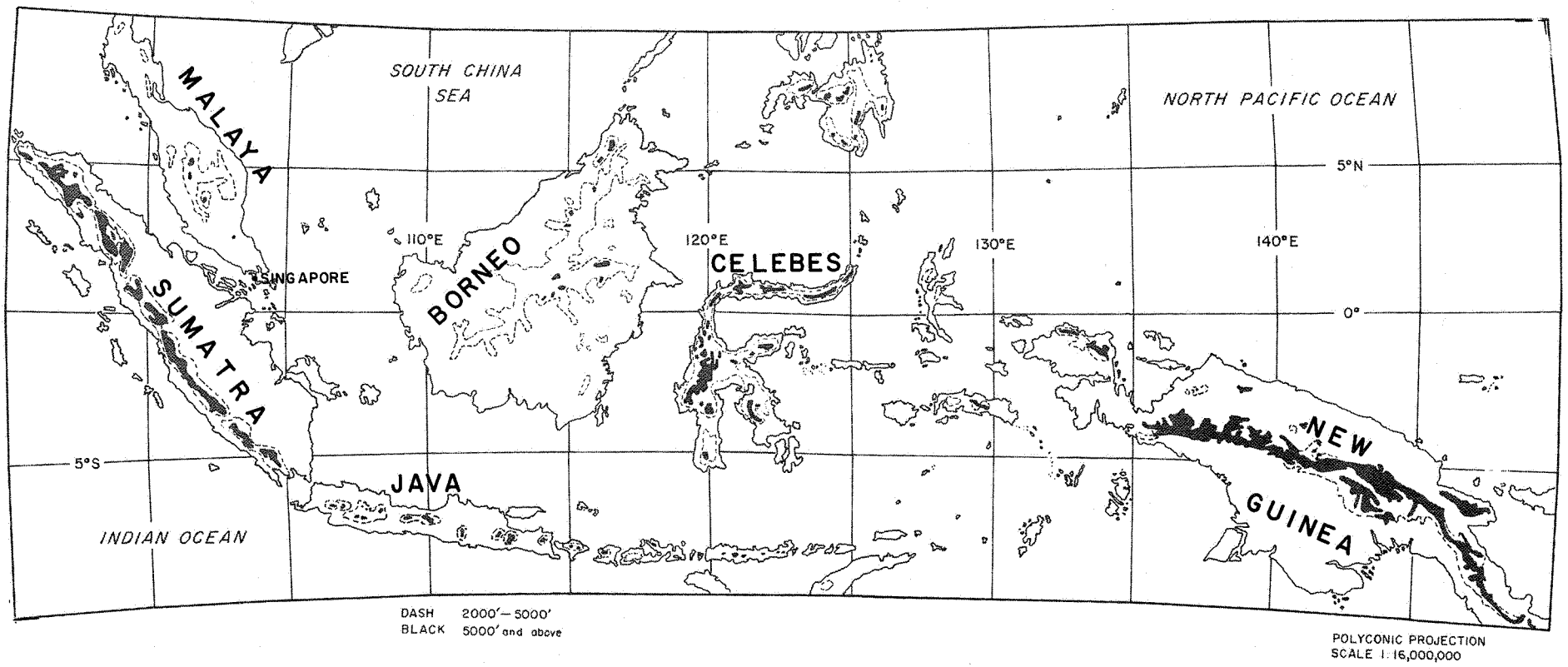

Fig. 1 MAP SHOWING INDONESIA, MALAYSIAN AREA OF INTEREST

the cumulus will spread horizontally along the chain and over the leeward slopes. At the same time the tops will grow into the higher atmosphere. Depending upon the latitude, time of the year, and other factors which need not be elaborated here, the tops, reaching their maximum development towards the middle of the afternoon, may grow to as little as 16,000 feet or to as much as 45,000 feet. If cumulonimbus is produced by this process, it may be accompanied by thunder and lightning, and, towards the latter part of the afternoon, will give rise to a great variety of clouds, such as altostratus, altocumulus, stratocumulus and various types of cirrus. From time to time, incipient cumulonimbus cells may become detached from the peaks and drift over the leeward side of the island; if this occurs, sporadic and isolated thunderstorms will briefly strike stations situated on the leeward plain and may even affect the neighboring sea downwind. By 7:00 or 8:00 P.M., the lower portions of the orographic cumulus, or cumulonimbus, will have vanished. Patches of cloud at the altocumulus and cirrus level, however, may persist. At the same time, or a little later, cumulus will be observed forming in a line parallel with the coast, usually on the leeward side. By about midnight, this oceanic cumulus will be quite evident to an observer on the leeward shore, and its dimensions and structure can be easily explored by aircraft on a moonlit night. If the diurnal cycle of convection is extreme, the oceanic cumulus will continue to grow during the night, reaching maximum dimensions just before dawn. Therefore, an aircraft taking off before dawn from a leeward airfield may find itself involved with a nocturnal thunderstorm off-shore at a distance between five and twenty-five miles, depending upon the terrain, season, etc. The mountain peaks may be quite clear of cloud at this time. Isolated cumulus or cumulonimbus accompanied by showers, may drift toward the land from the pre-existing line, so that a leeward station may have a secondary maximum of showers between 6:00 and 9:00 A.M. local time. By 10:00 A.M., the off-shore cloud will usually completely disappear and the first orographic cumulus will begin to build up on the peaks; then the cycle is repeated with varying intensity, depending on the synoptic situation. During the whole of this cycle, the cloud over the open sea may show very little variation."

Studies by La Seur and Garstang (1964) over a much smaller island, Barbados (West Indies), show a semi-diurnal variation in cloud amount, but greatly influenced by the synoptic situation.

As discussed below, the TIROS VII analyses show a semi-diurnal cycle, similar to that described by La Seur and Garstang (1964).

2.3 Data Processing

The data used in the analyses were selected from the TIROS VII Radiation Data Catalog and Users' Manual, Vol. 1, for 19 June - 30 September 1963. Case selection was guided by review of the available TIROS VI and VII photographs, and inferences from synoptic analyses of the area. The cases selected for use in the motion picture were chosen as periods free of transient cloud influences. However, some cases of minor transient influences may have been inadvertently included.

The majority of the analyses were prepared from single open mode data, with closed and alternating mode data used, when necessary, to assure complete coverage. Orbits for which data were computer mapped and manually analyzed are summarized in Table 1. The underlined orbits are those used to prepare the analyses used for the movie.

2.4 Analysis Procedures

The orbits listed in Table 1 were processed on an IBM 7094, and printouts prepared on an IBM 1460. Program control was accomplished through the NASA Mercator Mapping Program (MSC-2) (Staff Members, GSFC, 1962) using a scale of 1:2,500,000. Nadir angles were limited to less than 60^{o}. No correction was made for limb darkening. Consideration was given, however, to correlations due to overall sensor degradation, and to floor-wall asymmetries. Data Listings were used, to a limited extent, to assure proper data spot locations and reasonable swath lengths, (for discussion see Sherr 1966).

Each analysis was prepared on vellum, using a 1:2,500,000 Mercator map with smoothed topography as an underlay. Initial planning for the program had envisioned photographic reduction of the large vellum analyses to the size used for preparation of the individual "cels" of the motion picture; however, this proved

Table 1

List of TIROS VII 8-12μ Analyses

LST	Sumatra Malaysia Java	Borneo Celebes	New Guinea
24		181	1289
23		802	151
22	240, 802, 831	239, 254	224, 282
21	313, 846	312, 1436	238, 311
20	342, 875, 919	341, 904, 1480	
19	948, 963, 1481		
18	459, 977,	444, 458	
17		502, 517	501, 516
16	532, 1094	531, 560, 561	
15	029, 605, 1123, 1138	575, 1152	530, 559, 574
14	634, 1211	662, 1196, 1225	603, 632
13	1284	706	
12	175, 751, 1269	735, 736, 765, 1266, 1298	705
11	780	779, 794	749, 793
10	277, 309, 853	808	837
09	306, 882	838	851, 895,
08	911	881, 896, 1473	939, 968
07	940	910, 925, 954, 969	909
06	452, 984	437, 983	953
05			
04	569, 1101	554, 1101, 1159	005, 1099
03	1130	006, 035, 1188	034, 1143
02	627, 1203, 1918, 1291	1246	
01		729	1216, 1245, 1304
00	744, 1276	152	

awkward and basically uncalled for, considering the final smoothing requirement for the movie. We instead used careful hand transfers of the analyses. This permitted more emphasis on the maintenance of meteorological integrity during the successive approximations required to insure cinematic smoothness.

2.5 Diurnal Temperature Variation

2.5.1 Procedure

In order to obtain a quantitative presentation of the diurnal TIROS VII 8-12μ "window" temperature cycle, necessary for proper smoothing of the analyses to be used in the planned movie, averages were obtained from the analyses which are presented in Appendix A, composited at two hour intervals. These averages were obtained for each island, and for selected ocean areas. Figure 2 shows these areas.

The procedures followed in each case were: (1) divide the area into small subsections of approximately equal size, (2) obtain an estimate of the average TIROS VII "window" temperatures in each subsection, and (3) average the estimates from each subsection to obtain a mean. Additional mean values were obtained from processed analyses not included in the composite analysis.

2.5.2 Examples

Figures 3 and 4 present the curves† of diurnal 8-12μ "window" temperature variations for each of the areas in Figure 2, and for an overall mean of the entire analysis area. Notice the general tendency for a semi-diurnal variation, with temperature minima (cloudiness maxima) at 0200-0800 LMT (Local Mean Time) and 1600-2000 LMT, and temperature maxima (cloud minima) at 1200-1400 LMT and 2200-2400 LMT. The area mean (Fig. 4M) depicts this cycle most clearly but it is more or less reflected, in spite of noise, in each curve. It is obvious that random selection of analyses has introduced non-representative, noisy data into the sample. In spite of these non-representative data, significant similarities exist among the various island and ocean areas.

---

† Uncorrected for floor/wall differences, and sun phase related response variations. Analysis of the sun phase variation has indicated that these variations do not influence the overall appearance of the curves.

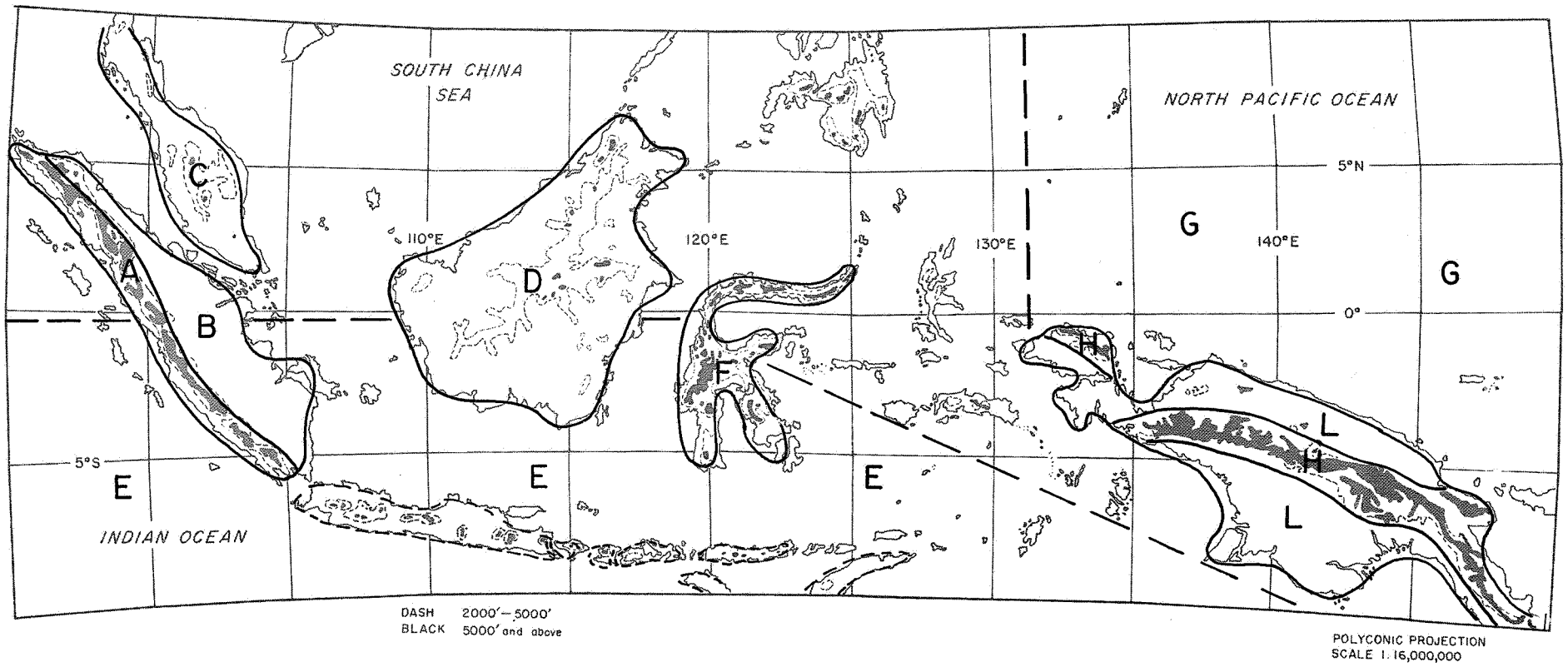

Fig. 2 AREAS USED FOR PREPARATION OF DIURNAL TEMP. VARIATIONS – (REF. FIGS. 3 & 4)

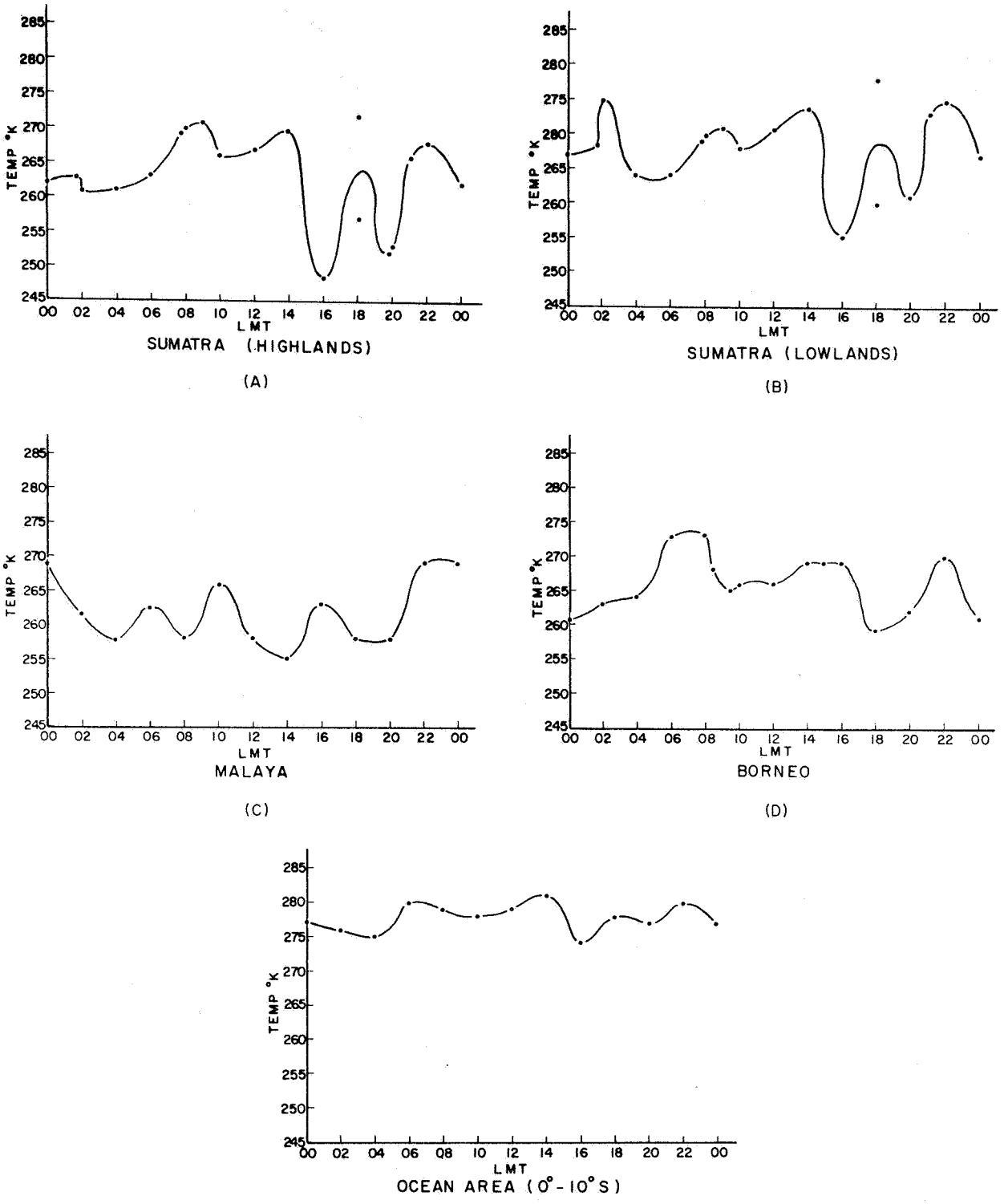

Figure 3 Diurnal Variation of TIROS VII 8-12μ Averaged Temperatures

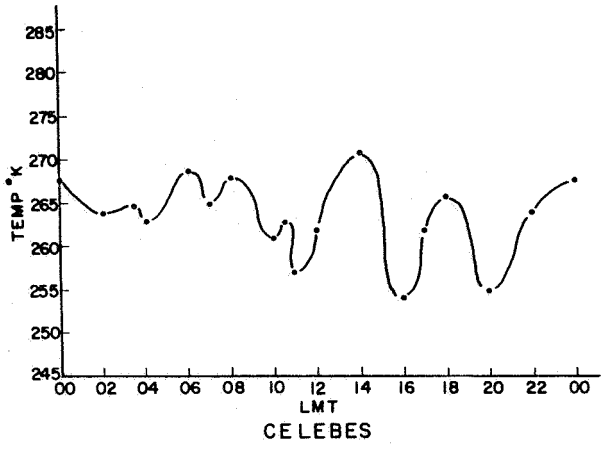

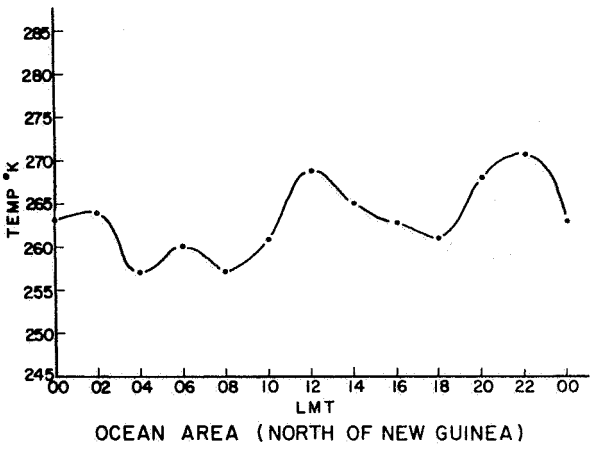

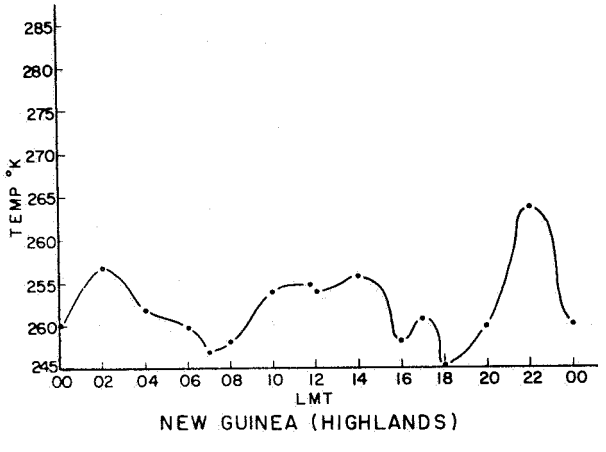

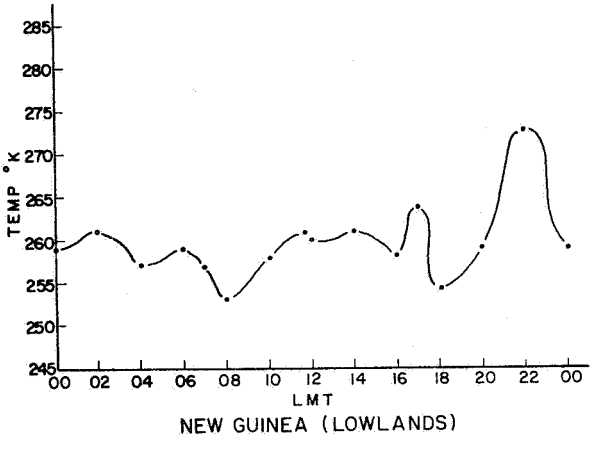

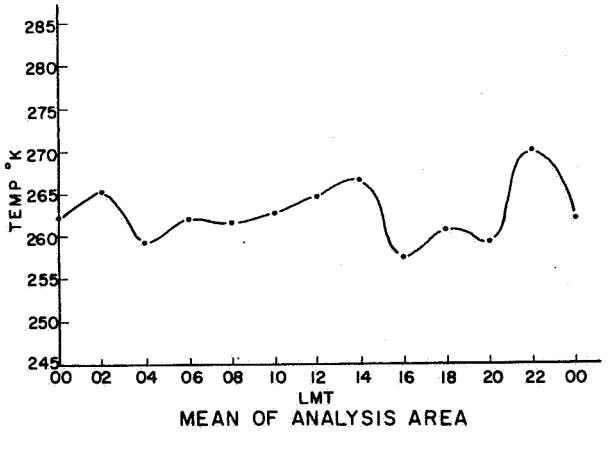

Figure 4 Diurnal Variation of TIROS VII 8-12μ Averaged Temperatures

2.5.3 Land Area Versus Oceans

Comparison of the variations in "window" temperatures over an ocean area (Fig. 3E; area E in Fig. 2)† and an adjacent land area such as Sumatra (Fig. 3A; area A in Fig. 2) dramatically reveals the land control of free and mechanically forced convection within the analysis area. Averaged "window" temperature differences of nearly 30°K exist during the 1600 LMT temperature minimum, in spite of the oscillations in the curves.

2.5.4 Discussion of Area North of New Guinea

The area north of New Guinea was described as follows in the First Quarterly Progress Report (Merritt and Bowley 1966): "An area of persistent cold temperatures (high clouds) over the open ocean northeast of New Guinea is observed on all analyses, regardless of the time of day." It was first assumed that this cloudiness is associated with the ITCZ/ETZ, is therefore produced through some form of dynamical forcing, and is not different, in kind, from cloudiness in tropical or extratropical storms. We should not expect any regular diurnal cycle in these types of cloudiness. It is obvious, however, (Fig. 4G) that a regular cycle does exist, and is similar to that observed over each of the other areas. The reasons for this are not obvious. Some possibilities will be discussed in the next section.

---

† In the First Quarterly Report, a difference in response between floor and wall sensors (observed by NASA, GSFC: TIROS VII Radiation Data Catalog and User's Manual, Vol. III; and by Mr. Krishna Rao of the National Environment Satellite Center of ESSA) was discussed briefly. Their studies had indicated that, from day of launch, wall measurements were 3-5°K higher than similar floor measurements. Floor measurements over the Indonesian area occur between 0600 LMT and 1800 LMT, and wall measurements between 1800 LMT and 0600 LMT. Thus the ocean area diurnal curve can be used as a coarse check on this value. After correction for (1) symmetrical degradation and (2) the apparent sun phase related response variations, the mean wall sensor measurements appear to be no more than 1°K higher than the floor measurements. Possible sources of error in this estimate are (1) the influence of diurnal cloud variations, i.e., the 2200 LMT temperature maxima feature in all diurnal curves; and (2) the limitation of the data record length; i.e., only 30-35 selected orbits were used to prepare the curve.

2.5.5 Discussion of Possible Causes of the Observed Cycle

The causes of diurnal variations in cloudiness and precipitation, over small islands and the open sea, were discussed by LaSeur and Garstang (1964) as follows:

> "A complex relationship apparently exists between the synoptic scale system and land effects . . . A tentative suggestion seems to be that the obstacle effect plays a major role in the production of cloud and precipitation. This and other interactions may explain why studies based upon observations taken on land have not shown a semi-diurnal or even diurnal cycle, while, from time to time, studies made over the oceans or atolls have demonstrated the existence of such cycles...
>
> ". . . there seems to be at least three mechanisms involved in producing the observed distributions of precipitation and cloudiness over the open ocean. A diurnal cycle can be produced by at least two mechansims:
>
> "i. solar radiation: the effect may be to inhibit cloud growth over the ocean during the day (through absorption of solar energy by water vapor). . . and to enhance cloud growth at night through cooling . . .
>
> "ii. sensible heat transport: while this is related to radiation, it depends largely upon the out-of-phase relationship between air and sea surface temperature. It is also related to any diurnal variation in the wind speed as will be described in the next paragraph.
>
> "The semi-diurnal cycle appears to depend upon at least one recognizable mechanism:
>
> "iii. the atmospheric tide: this mechanism, which is directly related to the semi-diurnal pressure oscillation, is called upon to produce a response in the wind field which produces the required divergence to create a semi-diurnal cycle in precipitation."

Most of the TIROS VII 8-12μ "window" curves presented in Figures 3 and 4 can be explained in terms of the LaSeur and Garstang mechanisms. The area northeast of New Guinea, however, would appear to fall outside these explanations unless the atmospheric tide mechanism can be assumed to produce large enough variations in the velocity field to influence dynamically forced cloudiness areas. This speculation deserves further study.

2.6 Composited Unsmoothed Two-Hourly Analyses

Analyses of the TIROS VII 8-12μ "window" radiation temperatures, selected from the listings presented in Table 1, have been composited at two hourly intervals (see Figures in Appendix A). These analyses were used in preparation of the diurnal curves presented in Figures 3 and 4. The same two-hourly composited analyses were used as a basis for preparing the smoothed analyses, used in the planned motion picture and discussed in Section 2.7.

2.6.1 Land Control Over Cloudiness

Comparisons between the ocean area averaged temperatures and those over adjacent Sumatra (Section 2.5.3) dramatically pointed up the predominance of land related cloudiness in that area. The analyses in Figures 1 to 11 of Appendix A show that this relationship is not confined to the Sumatra area. Nearly all major islands are colder (in the 8-12μ radiation data) than the ocean areas surrounding them. Exceptions to this occur (1) over the areas north of 5°N, where transient disturbances are frequent; (2) northeast of New Guinea, where the previously discussed ITCZ/ETZ selected cloudiness occurs; and (3) over Java where the scale of cloudiness is frequently less than the TIROS VII radiometer scan spot size.

2.6.2 Comparisons of Observed Diurnal Variations With a TIROS III Study

Rasool (1964) performed a study of averaged day to night cloud cover variations, using quasi-global averages of TIROS III 8-12μ "window' observations for the period July to September 1961. This study concluded that the percentage of cloud cover over the southern hemisphere increased by a factor of two or three from day to night. This result was subject to much discussion, which culminated in an article

by Winston (1965) suggesting that Rasool's conclusions were in error. Winston further suggested that an answer to the dilemma might be found in analyses of areas where data from individual orbits, at twelve-hour intervals, could be viewed. Since the Indonesian analyses prepared under this contract may approximate those suggested by Winston, we have examined our results for information relevent to the controversy.

Rasool's analysis was based in part on the following assumptions:

> "Reasonably thick clouds . . . are practically opaque to infrared radiation of wavelength >4μ (Shiffrin 1961). As there is very little water vapor above the clouds, and if we may assume that the albedo of the clouds in the far infrared is negligible, the radiometer in the presence of thick clouds will record energy corresponding to the cloud top temperatures.
>
> "If, therefore, for any given instant, both the TIROS measured temperatures and the actual surface temperatures are available, a knowledge of the temperature lapse rate in the atmosphere will enable one to obtain a quick estimate of cloud top height. On the other hand, on a climatological basis, if the satellite-measured temperatures for a given region are averaged over a season, then the departure of this temperature from the mean ground temperature will be mainly dependent on three variables— cloud amount, cloud height, and water vapor distribution in the atmosphere. . . . the effect of water vapor is comparatively small, and from our knowledge of climatological distribution of water vapor over the globe, its effect on the temperature measured by the satellite can be accounted for."

He then constructed a family of curves (his Figures 3 and 4) which related ΔT (the difference between the (climatological) mean surface temperature for the appropriate time of day and the satellite-observed blackbody temperature) to cloud height and percentage of sky cover. Since his averaged TIROS III Channel 2 temperatures varied little between the day and night averages (06-18 Day and 18-06 night), his ΔT shows a marked day/night average difference. The difference in ΔT, assuming constant cloud heights regardless of time of day, produced the conclusion of higher cloud percentage amounts over the southern hemisphere at night. He, however, further qualified his results by stating:

"these results are based on the debatable assumption that, on an average, for a given latitudinal belt, cloud top heights do not change from day to night."

He stated that a 2-4 km higher cloud at night would be required to provide the same cloud cover percentage for day and night.

Our Indonesian diurnal analyses, prepared during a similar (i.e., June-September 1963) synoptic period, when transient disturbances are at a minimum, may provide measurements to permit evaluation of Rasool's assumption of a constant day to night cloud height. Average TIROS VII temperatures (including a $1^{\circ}K$ floor/wall difference) for the entire 10N-10S, 95E-150E belt, as taken from Figure 4M, show 263.7K for 18-06 LMT (night) and 262.3K, 06-18 LMT (day). For a mean surface temperature of 300K, and a $4^{\circ}K$ diurnal surface temperature range, adapted from Haurwitz and Austin (1944), we find ΔT's of 32.3K and 37.3K for night and day, respectively. Assuming 100 percent cloud cover, this indicates approximately 1 km higher cloud tops during the day, or conversely a 20 percent decrease in the night-time cloud cover for a constant cloud height. This is not a large variation, but is opposite in sense from the data presented by Rasool.† However, the small difference within an equally small total sample limits the weight that can be given to these results.

2.7 Motion Picture of Diurnal Cycle

The selected unsmoothed TIROS VII 8-12μ "window" analyses discussed in Section 2, and included in this report as Appendix A, provided the basic analyses for production of a 14 minute animated color film. This film depicts the diurnal changes in "window" radiation, and the cloudiness inferred therefrom, by treating the individual, snythesized hourly analyses as time lapse views from a synchronous satellite for a single 24-hour "day." An optical sound-on-film narration is utilized to provide explanatory comments as to the procedures used for analysis, and to emphasize certain points of interest.

---

† TIROS VII ΔT data presented by Rasool (1965), in his answer to Winston's note, is in agreement with our analysis.

2.7.1 Smoothed Analyses Preparation, and Comparisons with the Unsmoothed Analyses

In order to achieve reasonable cinematic smoothness, it was necessary to subjectively smooth the original TIROS VII analyses. This was, in general, a very subjective process. However, we attempted to retain the overall cycle by reference to the averaged T_{bb} values produced over each island and ocean area (see Figs. 3 and r). The final results of the smoothing process are shown as Figures 5 to 16. These are black and white reproductions of the color originals used in the movie. Only the even hour cels are presented, since the odd hour analyses were obtained by linear interpolation between adjacent even hours. The color time lapse projection permits a "four dimensional" view of the inferred diurnal cloud patterns. The color code as presented in black and white in Figures 5 to 16 is:

COLOR	ALTITUDE (KILOFEET)	TEMPERATURE (DEGREES KELVIN)
Red	< 5	> 290
Orange	5 - 14	290 - 275
Yellow	14 - 21	275 - 260
Green	21 - 28	260 - 245
Blue	28 - 36	245 - 230
Purple	36 - 43	230 - 215
Black	> 43	< 215

Comparison with the unsmoothed analyses in Appendix A will reveal the following:

1. The correspondence between the unsmoothed and smoothed presentations is best between about 5N to 10S.

2. A typhoon, which appears north of New Guinea on the smoothed analyses, has a counterpart in the unsmoothed presentation at only 1000L and perhaps at 2000L. There were frequent data gaps in that region, and it was necessary for artistic purposes. Analyses on a given day would typically not show a typhoon, although frequent high cloudiness (cold T_{bb}'s) were frequent in that region.

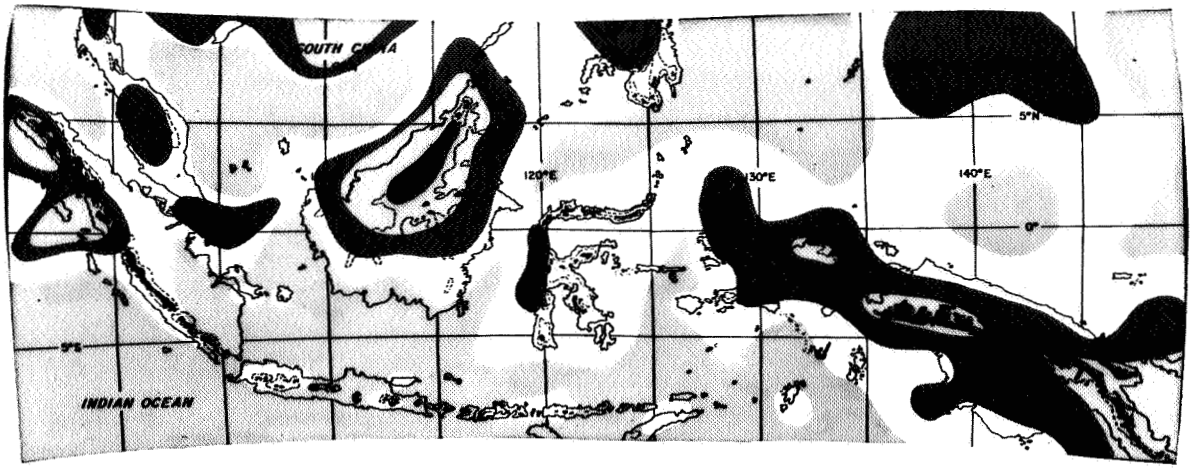

Figure 5 0000 LST Analysis

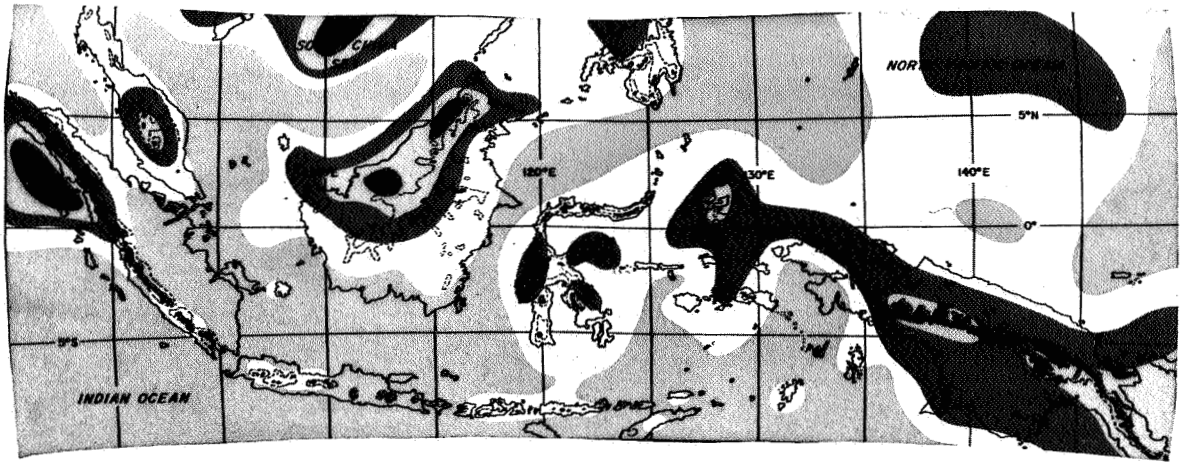

Figure 6 0200 LST Analysis

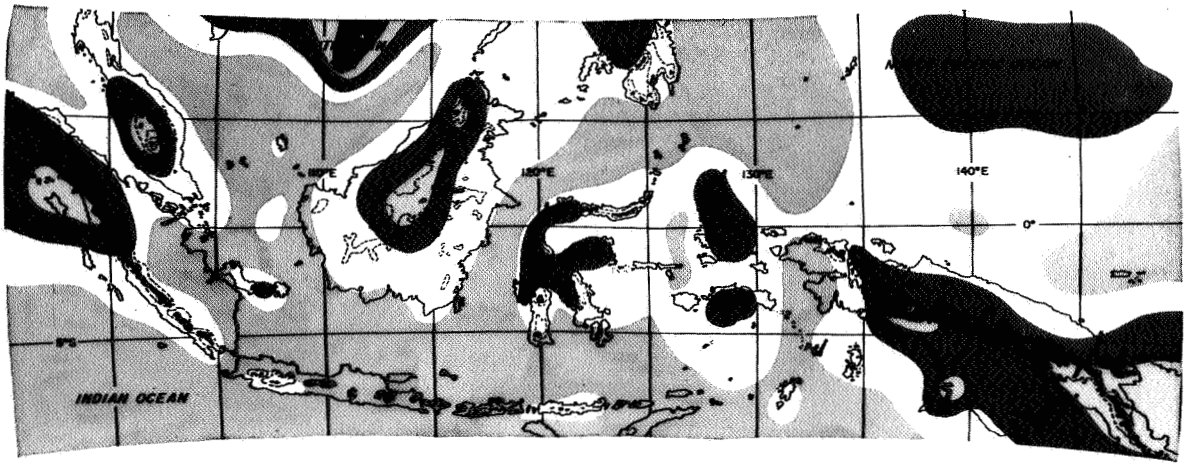

Figure 7 0400 LST Analysis

Figures 5 thru 16 Smoothed TIROS VII 8-12μ "Window" Analyses

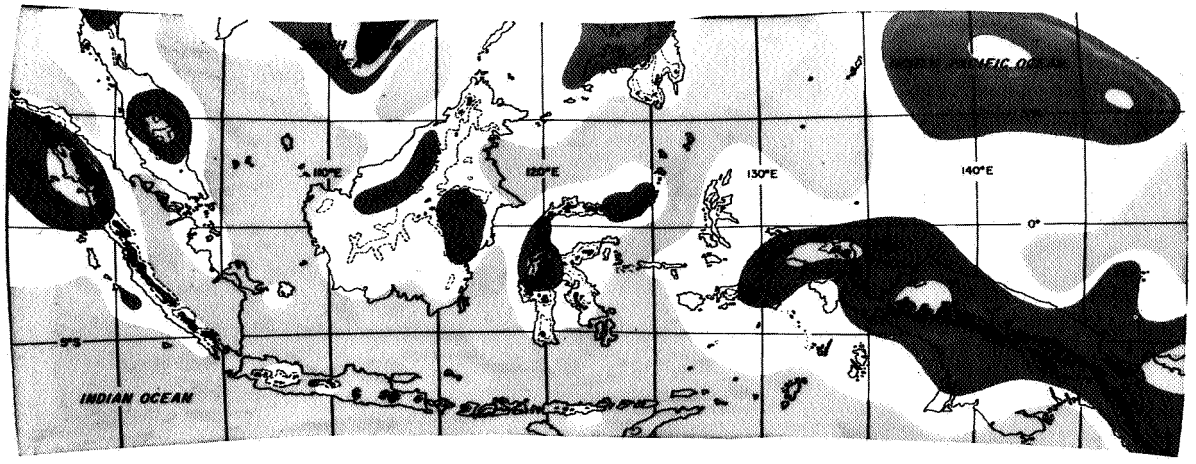

Figure 8 0600 LST Analysis

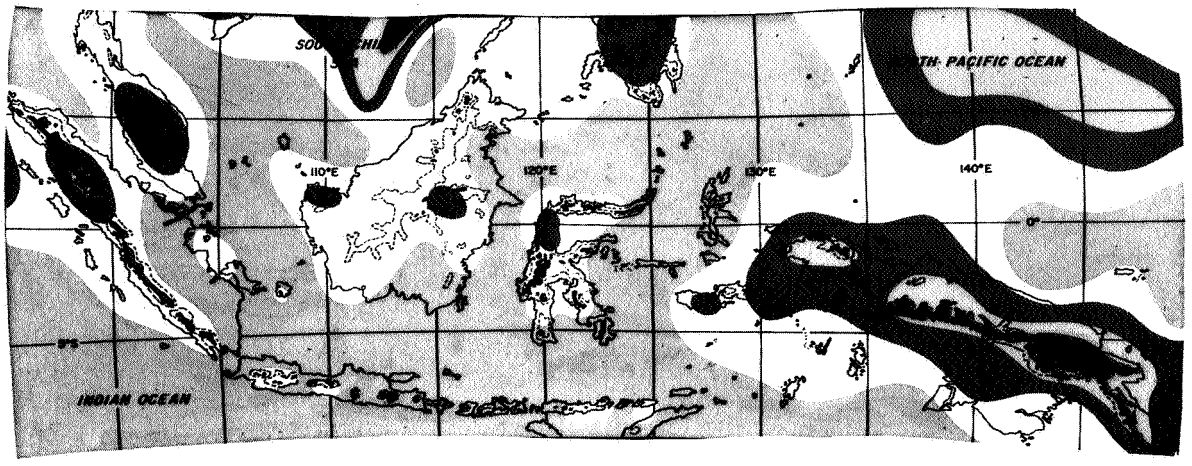

Figure 9 0800 LST Analysis

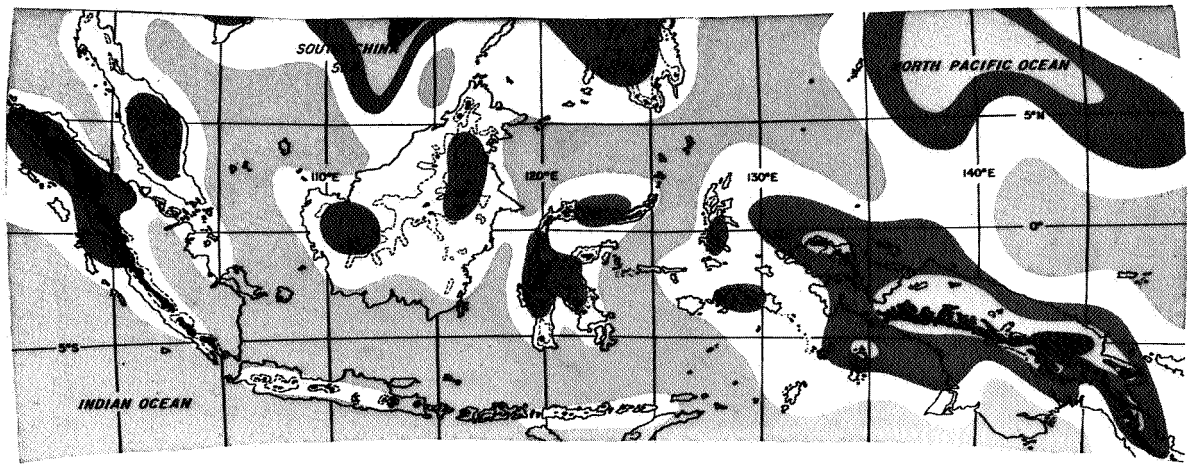

Figure 10 1000 LST Analysis

Figures 5 thru 16 (Cont'd)

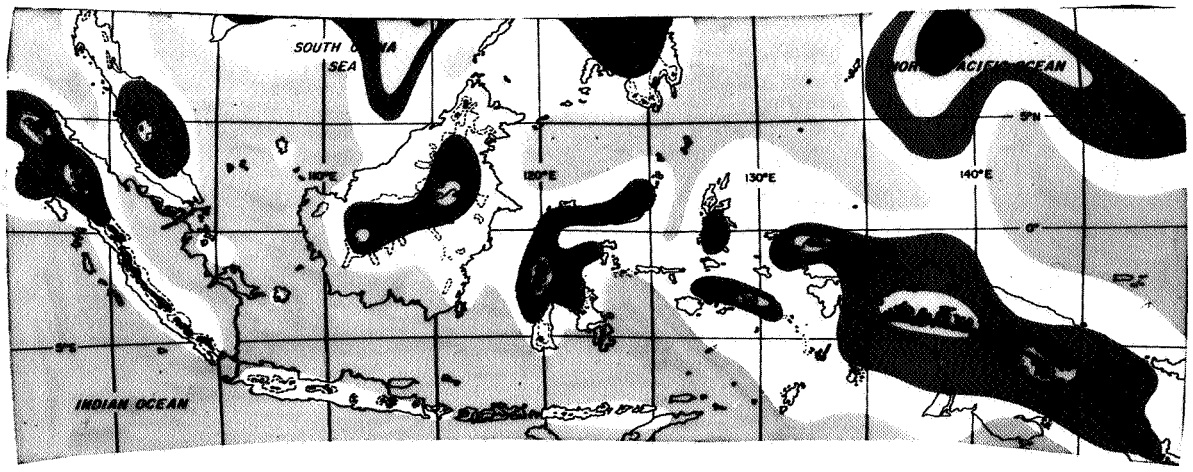

Figure 11 1200 LST Analysis

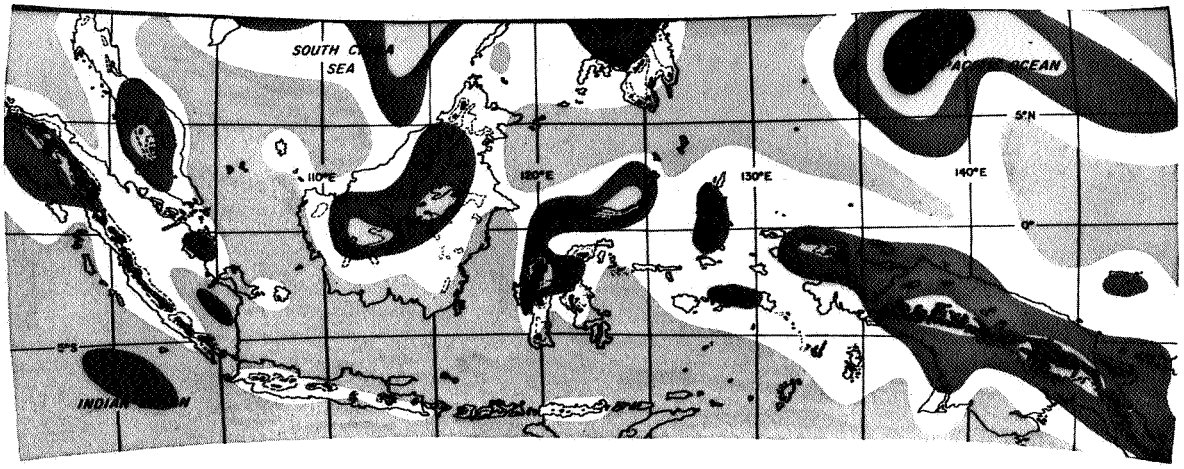

Figure 12 1400 LST Analysis

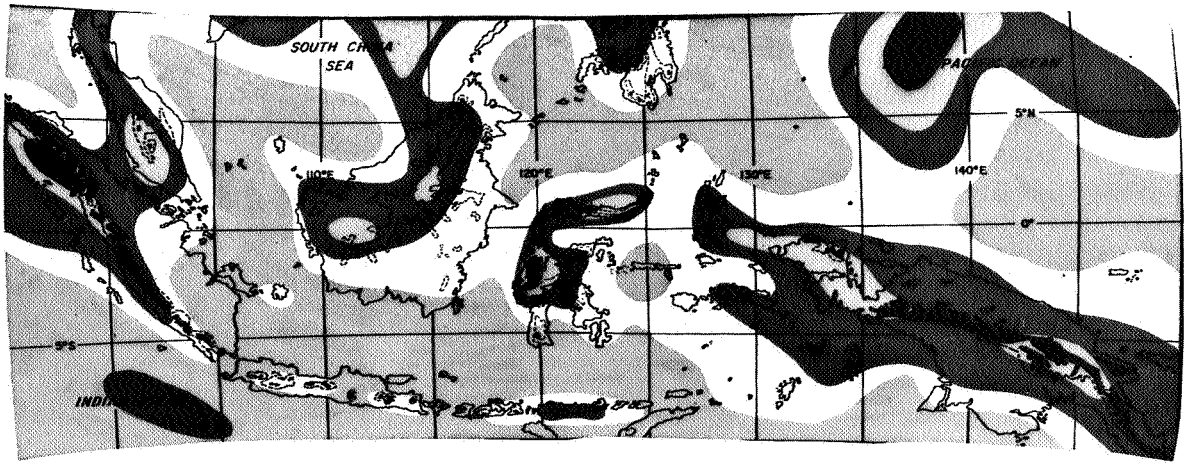

Figure 13 1600 LST Analysis

Figures 5 thru 16 (Cont'd)

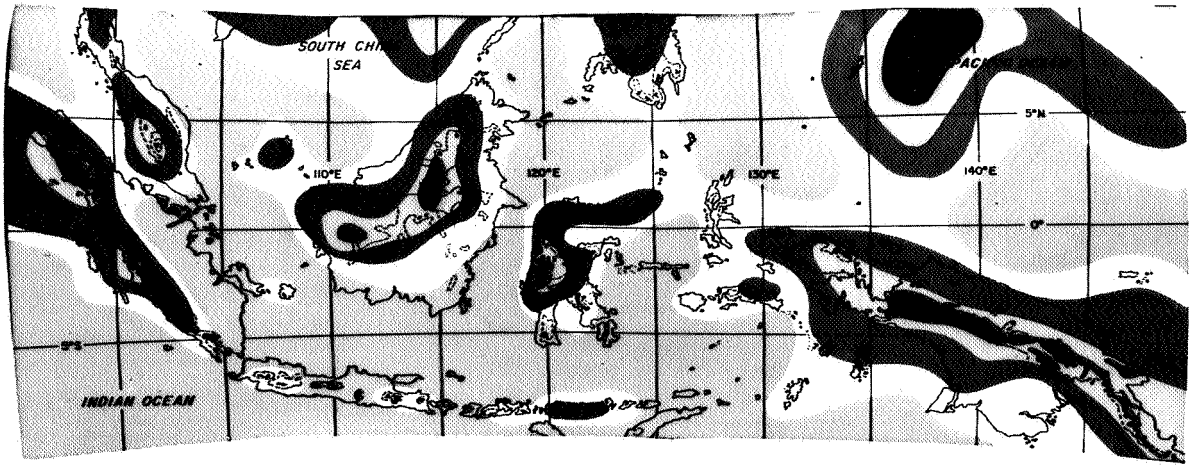

Figure 14 1800 LST Analysis

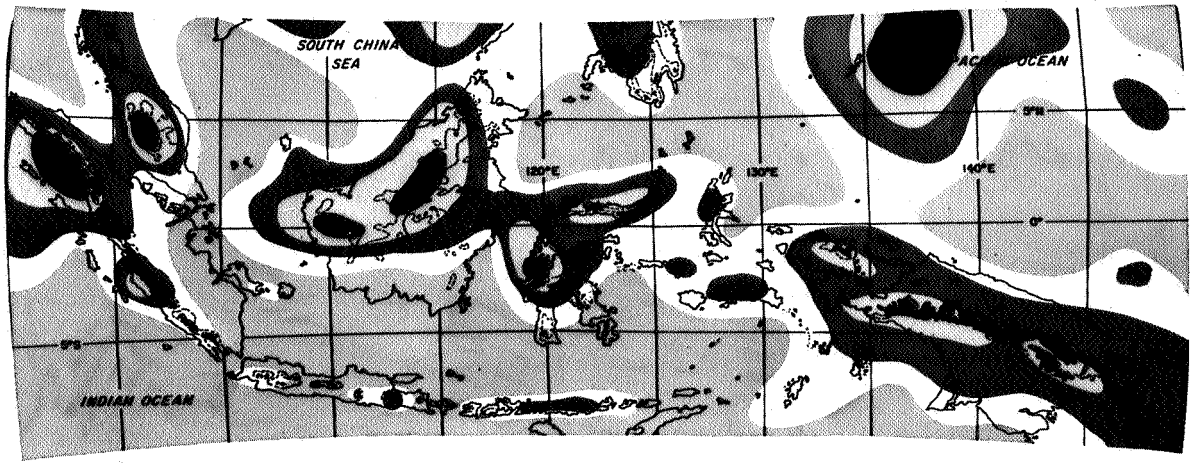

Figure 15 2000 LST Analysis

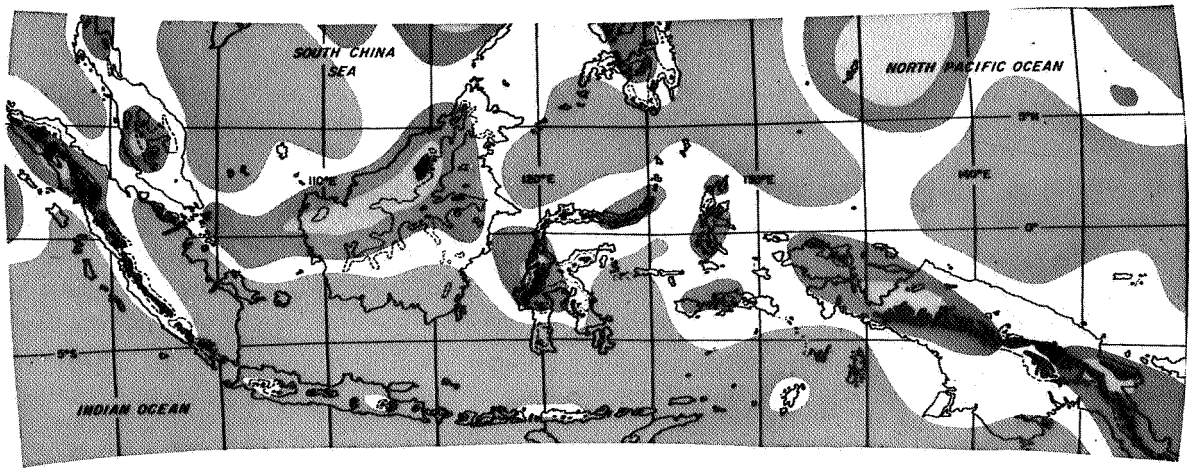

Figure 16 2200 LST Analysis

Figures 5 thru 16 (Cont'd)

3. The area from 5N to 10S displays a marked cyclical pattern. The region north of 5N was frequently influenced by transient disturbances during the June-September 1963 period of analysis. It was, in part, because of these transient systems that the typhoon discussed in (2), and an eastward propagating cold band over the South China Sea, were introduced.

2.7.2 Features to be Observed in the Time Lapse Presentation

The prominent features to be observed are:

1. An overall decrease in high cloud (areas of green, blue or black in the color film) over the islands from 0001L to about 0300L.

2. A brief increase in high cloud cover over the Straits of Malacca (eastern Sumatra) and the Celebes, between 0400L and 0600L.

3. A marked decrease in high clouds, over all areas except New Guinea, from 0700L to 0900L.

4. An increase in high clouds over all islands (except New Guinea), beginning at 1100L and reaching an apparent maximum at about 1900L.

5. The westward drift of high cloudiness from the Celebes, Borneo and Sumatra which begins at about 1900L, after the late afternoon cloudiness maximum has apparently peaked.

6. The minimum of variation in cloud height or cover over the high mountain ridges of New Guinea.

7. The islands of Java, Timor, etc., are small relative to the scan spot size of TIROS; furthermore, there is a minimum of cloudiness over these islands during June-September. Therefore, the appearance of yellow in these areas means a small area of fairly high cloudiness. These areas appear to coincide with the highest mountain areas.

In summary, the smoothed presentation follows the diurnal curves, prepared from the unsmoothed analyses, quite well. The land influence on cloud production is even more impressive in the time lapse presentation than on the individual analyses. It may be well to point out that the averaging interval employed does not permit detailed analyses of much of the day-to-night horizontal translations of cloudiness and precipitation at the scale examined by Ramage (1962).

3. NIMBUS HRIR ANALYSES

3.1 Gulf of Alaska Vortex Case Study

A large cloud vortex has been chosen to demonstrate: (1) the utility of the digitized HRIR data from Nimbus, (2) comparisons between Nimbus HRIR and TIROS scanning radiometer resolutions, and (3) the advantages of the joint use of pictorial (both TV and HRIR) and the digitized IR data.

The period from approximately 2200 GMT, 19 September through 2100 GMT, 20 September 1964 has been chosen for this case. This time period roughly centers on the Nimbus HRIR observation of the vortex system taken near 1200 GMT 20 September 1964. This synoptic situation and the pictorial HRIR data have been discussed by Widger, et al (1966), in pages 73-91 of their Appendix C. Their Figure 43 (HRIR data in pictorial form) and Figure 44 (the same data in rectified form) are reproduced here as Figure 19. The corresponding synoptic data reveal a large mature vortex, centered about a nearly vertical closed contour and wind circulation pattern.

The following discussion will emphasize the similarities and the relative detail to be found in the several formats of data analyzed i.e., (1) AVCS, (2) HRIR pictorial, (3) digitized HRIR, and (4) digitized TIROS IR data. The data sample (Fig. 17) is composed of the following observations:

a. Nimbus I AVCS, at 2221 GMT, 19 September
b. Nimbus I HRIR digitized data, 1200 GMT, 20 September
c. Nimbus I HRIR pictorial data, 1200 GMT, 20 September
d. TIROS digitized IR for approximately 2040 GMT, 20 September
e. Nimbus I AVCS 2120 GMT, 20 September.

Schematic presentations of these data may be found in Figure 17 (detailed analyses for each of these observation times will be presented in subsequent figures).

In order to make the IR data from TIROS VII compatible with the HRIR data, we have made a sensor degradation correction. This correction is a function of the uncorrected blackbody temperature (see Staff Members, NASA A&M Division, 1965 for details of this correction).

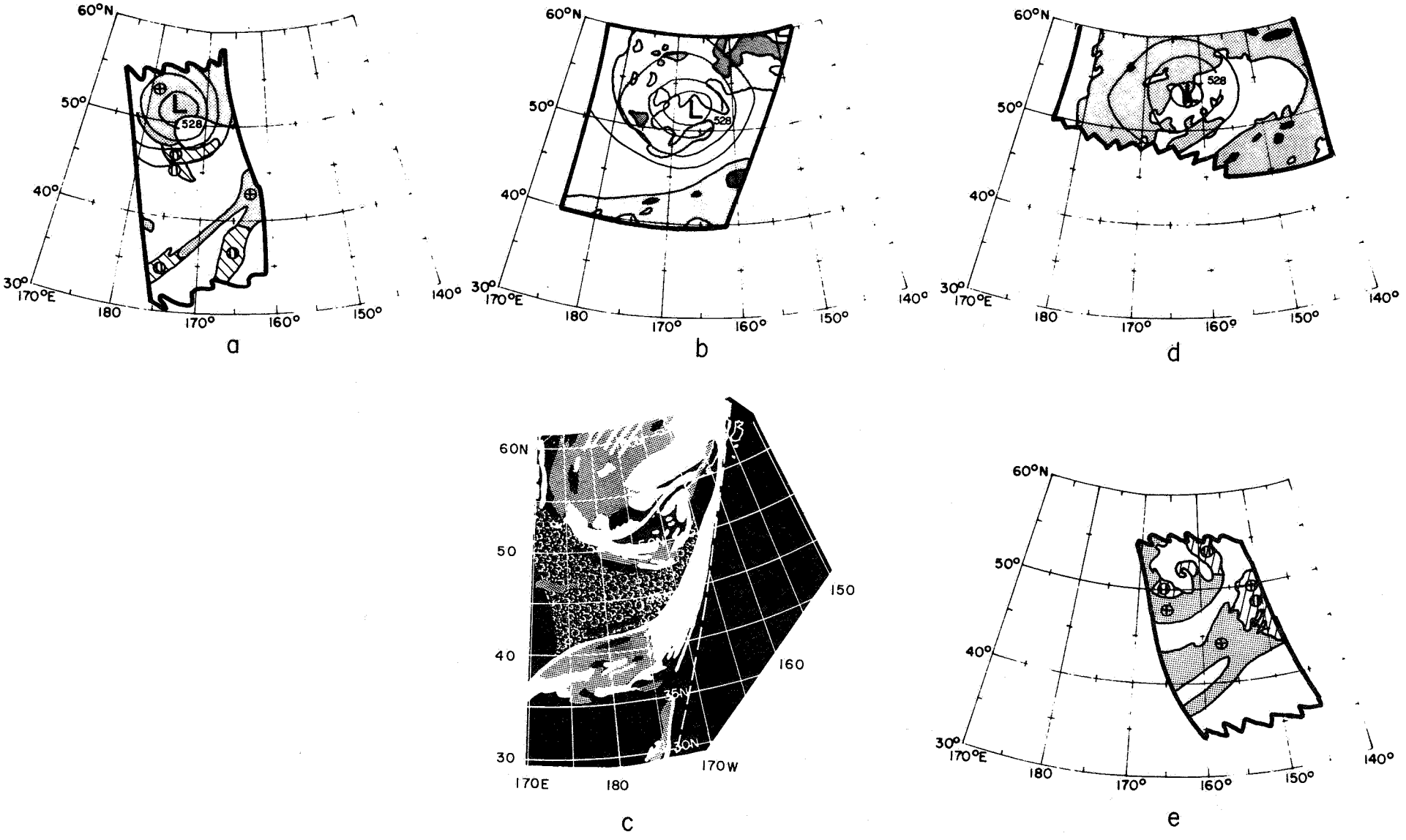

Figure 17 Schematic Presentations of Satellite Data, a) Nimbus AVCS, b) Nimbus HRIR Digitized, c) Nimbus HRIR Pictorial, d) Tiros IR Digitized, and e) Nimbus AVCS.

3.1.1 Nimbus AVCS Observation

The AVCS cameras of Nimbus I, at 2221 GMT, 19 September, observed bright clouds which appear to form a vortex pattern (although this is somewhat difficult to ascertain from these pictures alone). Extensive low level cumuliform cloudiness was being advected from under the western areas of the bright cloud, near 50N forming a hook shaped pattern which terminates near 48N, 168W. A nephanalyses showing the probable orientation of this cloud mass is shown in Figure 17. The actual picture is shown in Figure 18. The frontal cloud band seems to be very narrow, at least in the area south of 44N. Extensive small cumuliform clouds were present in the cold air behind this cold frontal band. The center of the hooked cloud mass would appear to be near 48.5N, 170W. Little or no indication of cloud top height can be inferred from the AVCS pictures, although the areas north of approximately 51°N seem to be very bright and relatively smooth in texture, suggesting cirriform cloudiness.

3.1.2 Nimbus HRIR Observation Approximately 1200 GMT, 20 September

The HRIR sensor viewed this cloud vortex approximately 13 hours later and the pictorial presentation of these data, together with a rectification (taken from Widger, et al, 1966) are shown in Figure 19. Figure 20 presents an analysis of the digitized form of the same observation, machine plotted on a 1:2 million map scale. In this figure the detailed cloud top temperature field provides some information about the three-dimensional structure of the cloud system. The shaded area in Figure 20 includes all temperatures colder than 260°K (minus 13°C) and thus depicts the pattern of the middle and high cloud. The isolines drawn on this figure are for each 10°K. The original analysis was drawn for 5° isoline increments, but, for the purpose of illustration, isotherms more frequent than every 10° provided an unduly dense analysis.

Some comparisons between these three forms of the HRIR data (Figs. 19a, 19b and 20) can be made. The area of coldest temperature (that enclosed by the 240°K isoline) corresponds with the brightest area in the pictorial presentation. More detail in the cloud pattern, at least for temperatures colder than 240°K, is afforded in the digital data presentation. However, for the recognition of narrow banding, the pictorial presentation is better (probably because of its better resolution). For

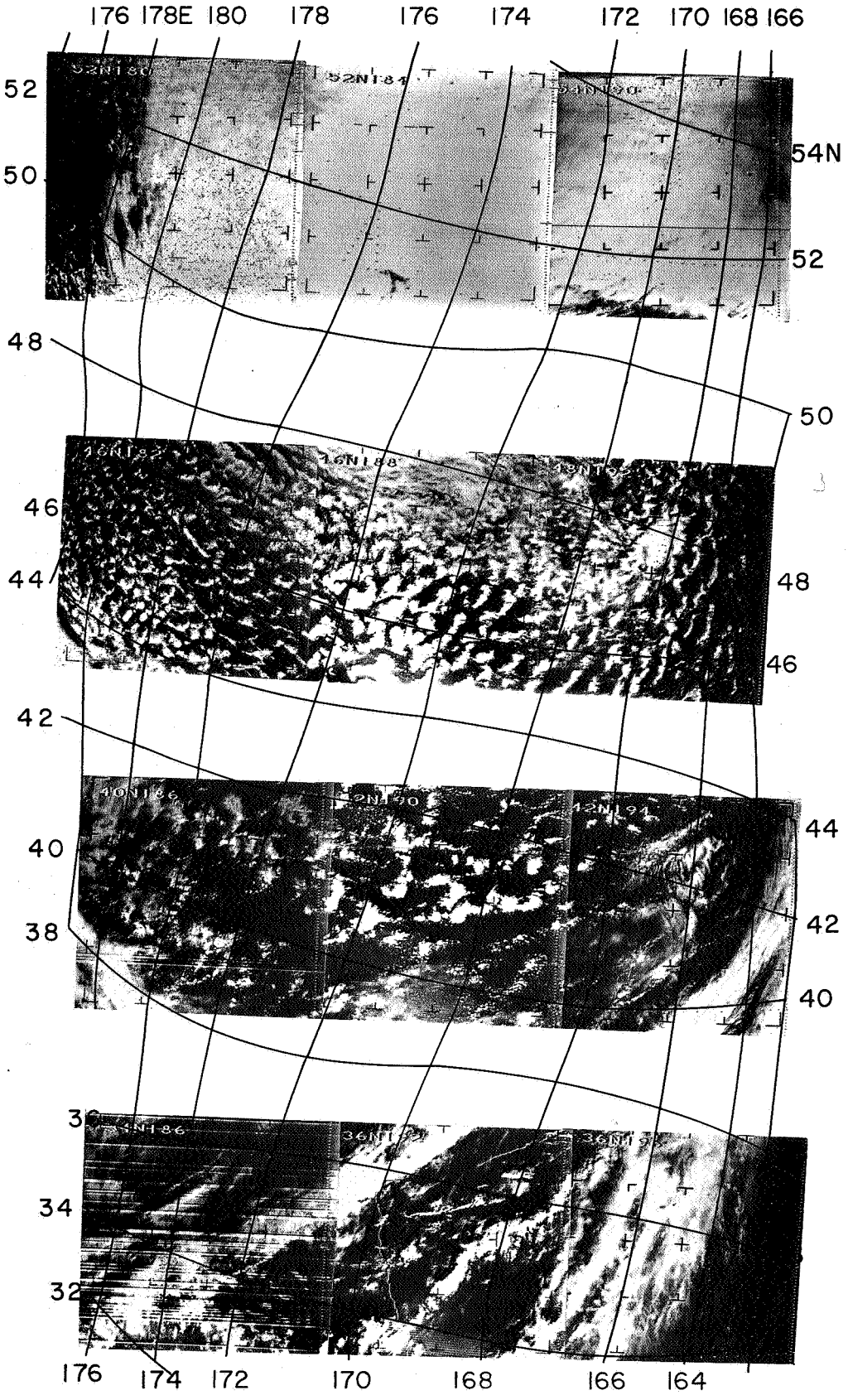

Figure 18 Nimbus I AVCS Mosaic, Orbit 330/331

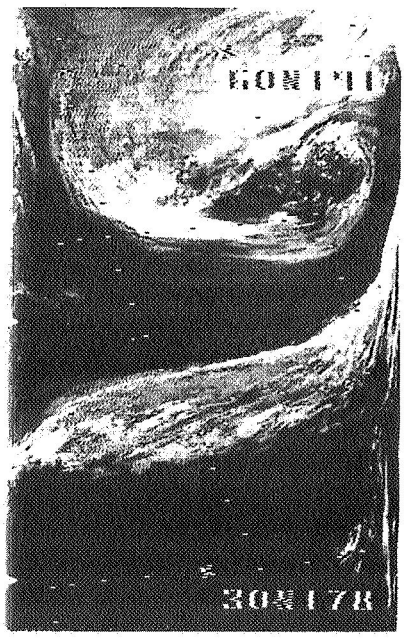

a. HRIR Strip, 20 September 1964

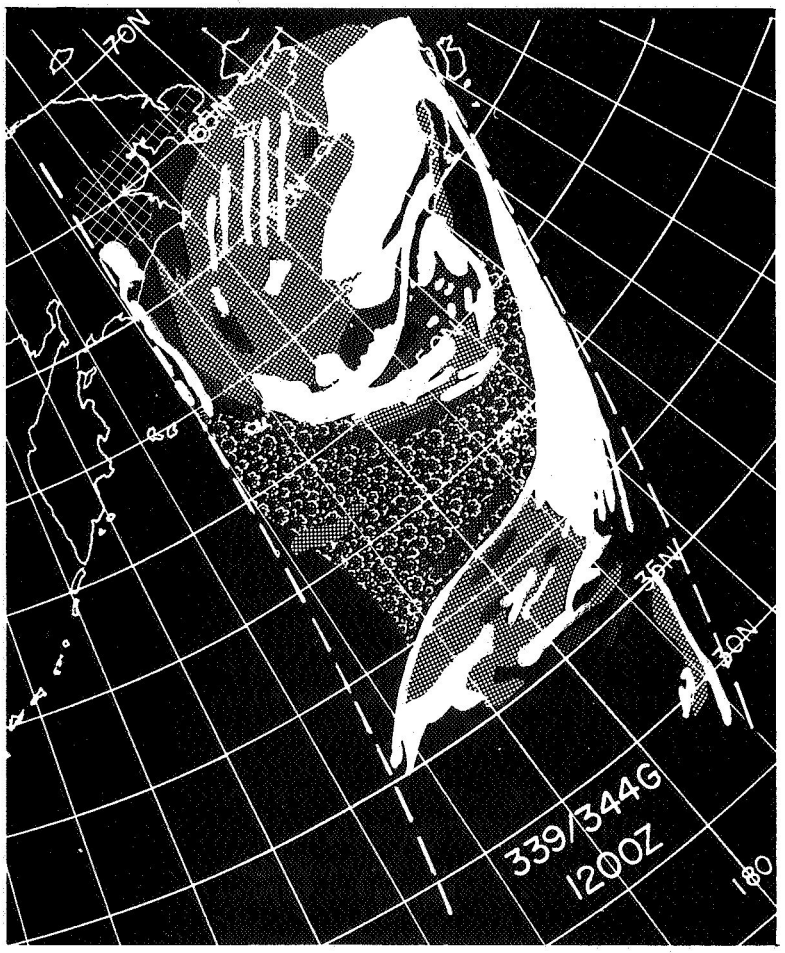

b. Rectification of HRIR Data

Figure 19 HRIR Data for Orbit 339

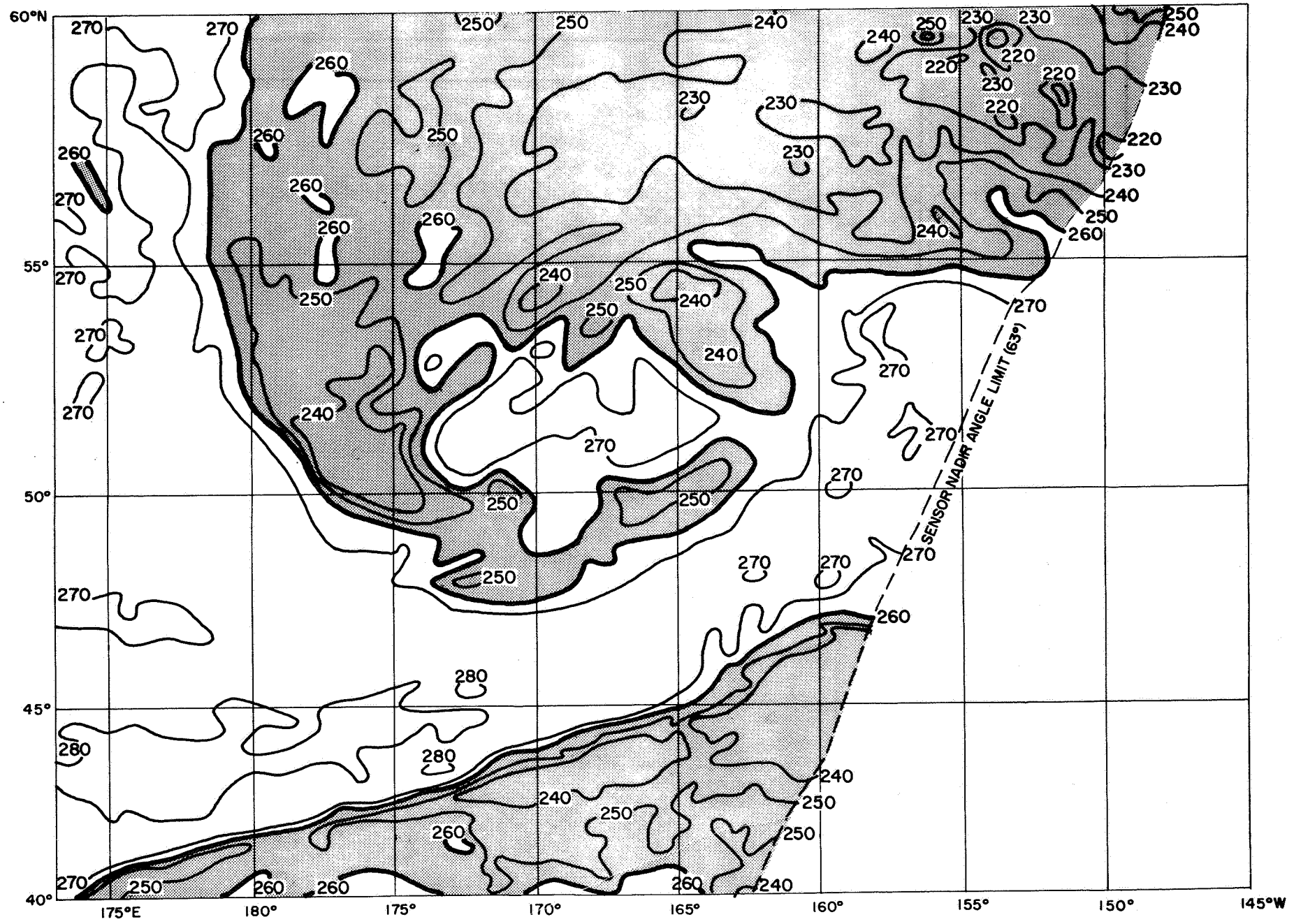

Figure 20 HRIR Analysis from Digitzed Data, 1200 GMT, 20 September.

example, note the apparent banding in the pictorial presentation near 170W to 180 and between 58 and 63N. No such banding is apparent in the digital presentation in this area (south of 60°N). However, areas of temperature warmer than 260°K do appear between approximately 55 to 58N, 174 to 179W, suggesting that high clouds do not completely cover this area, i.e., that holes exist. The frontal band, which in the pictorial presentation appears to be continuous along the eastern boundary of the orbital pass, is not visible in the digital data north of 47°. This results from the fact that a sensor nadir angle limit of 63° was imposte on the data in the machine map. South of 45° however, the frontal band is clearly marked from 165W to 175E. The northern edge of the frontal band correlates well in both presentations. However, east of 170W the edge of the frontal band seems to be displaced further south in the digitized data, suggesting that the rectification in Figure 19 is probably not as accurate as might be desired near the edge of the data pass. In the area between 170W and 175E, where the correspondence of the northern edge of the band is good, the middle to high cloud areas (shaded grey in the digitized data) correspond reasonably well to the areas as depicted in the pictorial data. However the fine scale banding west of 175W is not evident in the digitized data; rather, only a suggestion of the broken nature of the cloud band is given by the areas of temperatures warmer than 270°. The narrow band along the northern edge of the frontal band in the pictorial data, from 175W to 175E, is only remotely discernible as such in the digitized data, where a colder band can be seen along 43N to 45N.

The southern edge of the middle to high cloudiness, generally along 55N from 160 to 170W, is depicted in the digitized data by the 260° isotherm, and correlates reasonably well with the area enclosed by the cross hatching of the rectified pictorial data. Similarly, along the frontal band, the area enclosed by the 260° isoline corresponds roughly with the area enclosed by either the white or the cross-hatched stipling.

3.1.3 Nimbus AVCS and TIROS IR Observations

Approximately 10 hours later (about 2120 GMT, 20 September) the Nimbus AVCS cameras again photographed the storm area. These photographs are presented in mosaic form in Figure 21. Approximately 40 minutes earlier, TIROS VII crossed the storm area and obtained data from the IR sensors. The Channel 2 data (8-13μ water vapor window channel) are presented in Figure 22. The isolines in this analysis of the TIROS VII data are given in degrees K (corrected for sensor

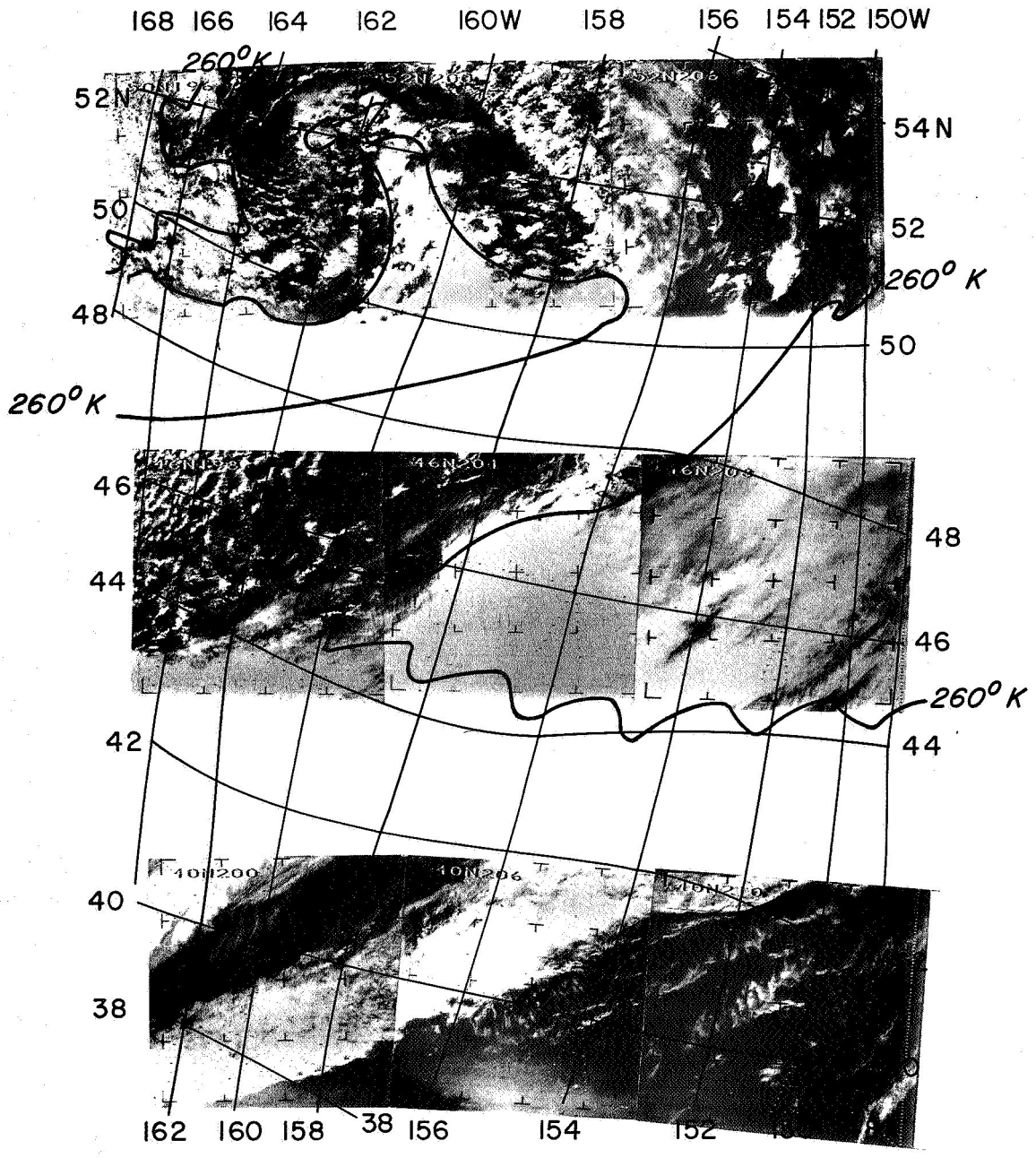

Figure 21 Nimbus I AVCS Mosaic, Orbit 344/345

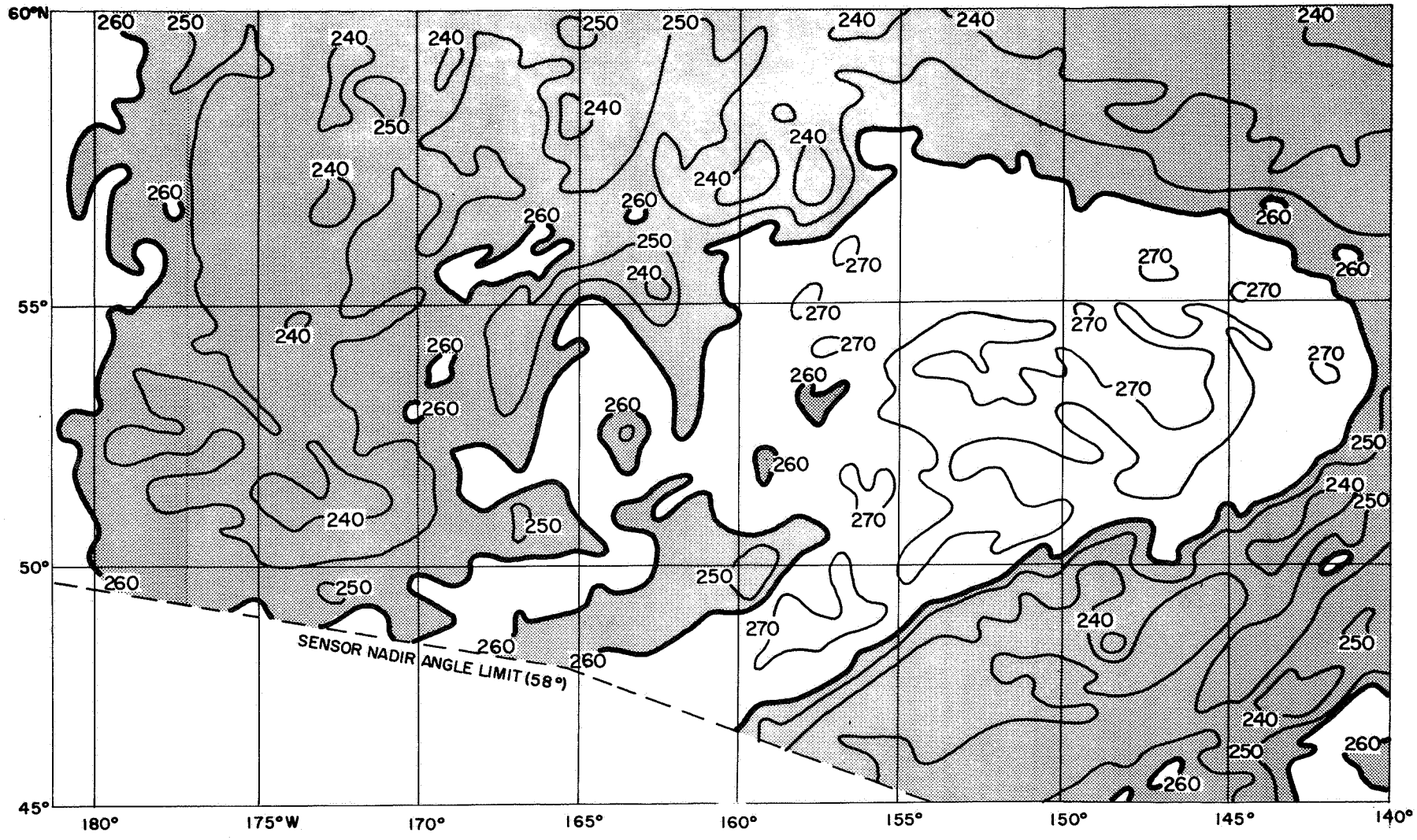

Figure 22 Analysis of Tiros VII IR Data, 2040 GMT, 20 September.

degradation, see Staff Members, NASA A & M Division , 1965). Thus, the 260°K isoline in this figure should represent the same isothermal radiating surface as in the Nimbus HRIR digitized data (Fig. 20).

Both types of satellite data for about 2120 GMT, 20 September confirm the location of the center of the cyclone to be approximately 53N, 163W. Where the area of coverage of the two figures is common to both, the pattern definition is similar. The IR data do not reveal the detail of the lower cloud structure, while the AVCS data does not reveal the detail in the middle and high cloud structure.

The analyses as prepared from the Nimbus HRIR and the TIROS VII IR are entirely compatible. It is to be noted, however, that although the center of the circulation moved approximately 300 miles eastward in the previous 12 hours, the westward or rear edge of the middle and high cloud, as defined by the 260°K isoline, did not move eastward at the same rate. Indeed, at 50N, the 260° isoline enclosed an area at least as far west as that described in the HRIR digitized data (Fig. 20). The middle and high clouds seem to be advecting southward along the west side of the vortex and this band, particularly near 50°N, has broadened considerably.

In Figure 21 the 260° isoline, taken from the TIROS VII IR data of Figure 22. has been superimposed on the Nimbus AVCS picture taken approximately 40 minutes after the IR data. In the area of dual coverage, the correspondence between the 260° isoline and the bright cloud pattern is exceptional. Note however that, in the vicinity of 45 to 49N, 148 to 154W, the AVCS picture shows broken cloudiness under a cirrus deck. The resolution of TIROS VII is unable to detect this cloud structure, and records temperatures colder than 260° (and for the most part colder than 250°) for this entire area. This is similar to the results found by Sherr and Rogers (1965), in their report using TIROS IV IR data, and again by Rogers and Sherr (1966) using TIROS VII data.

3.2 Rain Band Case Study

A frontal band over New England studied by Widger, et al (1966) using the HRIR pictorial data, has been subjected to more detailed analyses using the digitized HRIR data. In the pictorial data presentation, this frontal cloud band appeared to have many smaller scale bands imbedded in it, which were roughly parallel to the major band (see the map of the rectified cloud pattern in Fig. 26). Widger concluded

that these bands were a manifestation of the mesoscale structure reported by Elliott and Hovind (1965). They reported larger mesoscale bands, separated by distances of the order of 200 to 300 km, and lesser bands more closely spaced (of the order of 60 km apart). Rough correlations between these banded structures and the occurrence of precipitation at many stations in New England were made by Widger, et al (1966). They reported that, for at least eleven of the twenty-five recording precipitation stations, there was a reasonable correlation between (1) the HRIR pattern of higher and lower clouds and (2) either the time sequence of precipitation or the lack of measurable precipitation. For many of the other stations, they concluded that the correlation was not unreasonable in the light of the small rates of precipitation generally associated with this system and the convective variations that doubtless occurred during the time period considered. The present study is an extension of the earlier case, and attempts to determine the utility of the digitized HRIR data at the mesoscale. Time and resources remaining under the present contract were only sufficient to plot and perform minimum analyses of the digitized HRIR data for this case. Further studies are suggested in Section 4.

3.2.1 Comparisons of the Digitized and Pictorial Forms of the HRIR Data

Figure 23 presents the pictorial form of the data, taken from Widger et al, (1966). The area of the frontal band chosen for study lies near the right edge of the picture somewhat north of 40°. In particular, the area of concern includes 42 to 46N and 66 to 74W. The digitized data were obtained in two forms: machine plotted at a scale of 1:2 million, and hand plotted data (from the machine listing) on a 1:1 million map scale. For the finer scale format, every data point was plotted and analyzed for each 10°K. These analyses of cloud top temperatures are presented in Figures 24 and 25. On the original maps used for the analyses, a 2°K interval was convenient for the machine mapped data while a 5°K interval was chosen for the hand plotted data. The hand plotted data afforded so much detail that analysis at a 2°K interval on a 1:1 million map is difficult. Further advantages of these analysis intervals will be discussed in a later paragraph.

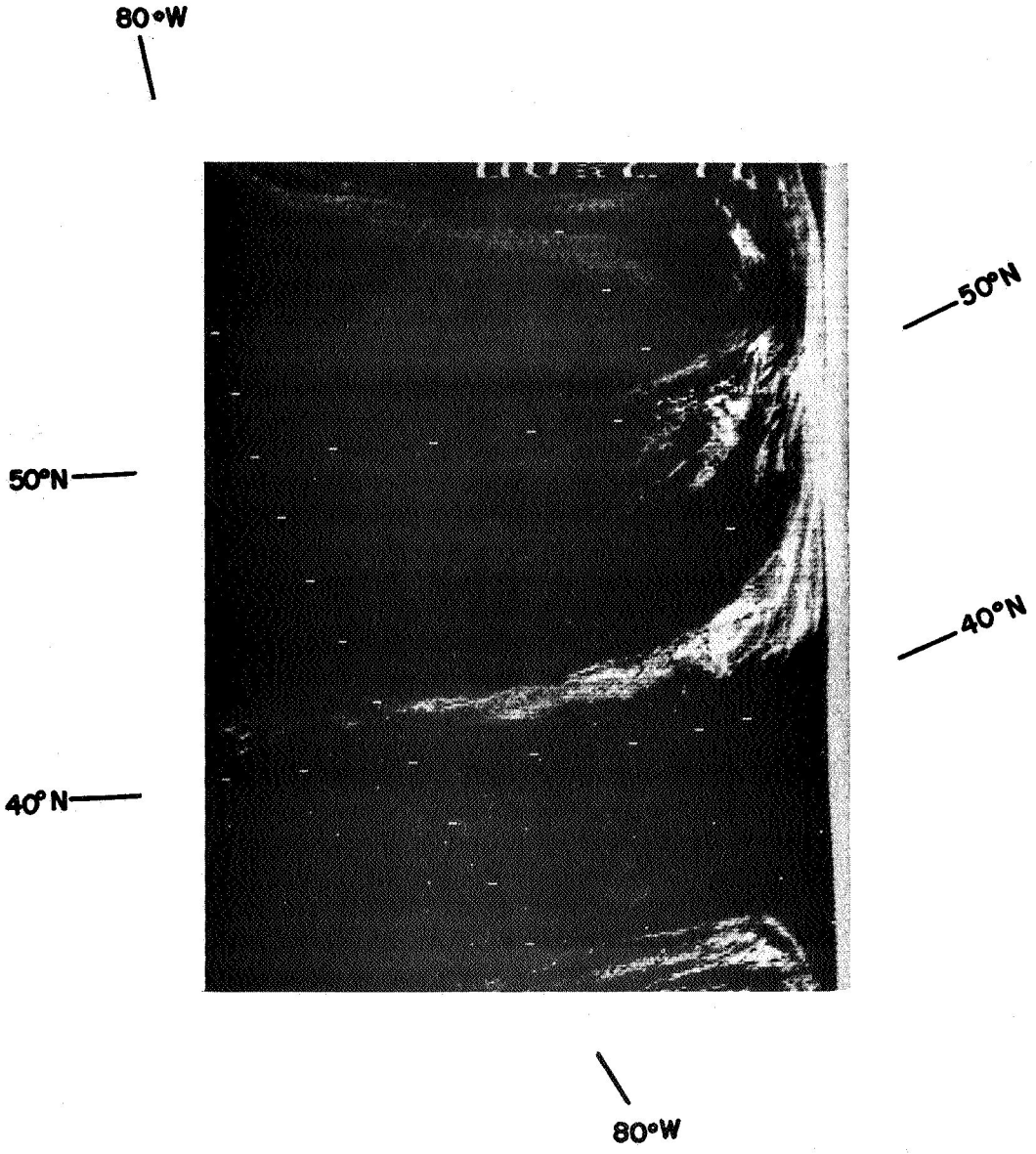

Figure 23 HRIR Observation of a Frontal Cloud Pattern Over New England. A Portion of Orbit 174, about 0025 EST, 9 September 1964.

Figure 24 is an analysis of the machine prepared, 1:2 million map, and includes a slightly larger area than the hand plotted analysis, which is shown in Figure 25. The area of Figure 25 has been outlined on Figure 24 with the heavy dashed line. Figure 26 shows the rectification prepared by Widger et al, with boundaries of the areas of Figures 24 and 25 superposed.

Examination of these three figures reveals that distinct banding can be recognized in the rectified pictorial form (Fig. 26, lines DD, EE, and FF). In the 1:2 million machine mapped data, only a vague suggestion of bands can be seen. Instead, the cloud pattern appears cellular in nature. Note the closed temperature isolines, which represent cloud height contours, in Figure 24. On the original map used for the analysis of Figure 24, isotherms were drawn for each 2^{o} of temperature, and the cellular appearance was far more dramatic. Unfortunately, the 2^{o} isotherm interval was impossible to properly reproduce and only 10^{o} intervals plus some dashed 5^{o} lines, were used. In Figure 25, the cellular structure is still evident. However, the added detail obtained by plotting each data point and analyzing for 5^{o} temperature intervals makes it more difficult to recognize even the cellular structure (in Fig. 25, 10^{o} intervals are shown for illustration). Close examination does however, reveal that a cellular structure still remains.

Certain common features can be recognized in all three figures. For example, in Figure 26, a very narrow band of clouds (stippling) appears to cross 69W near 43.5N. Temperatures colder than 250^{o}K can be seen in both Figures 24 and 25 in this general vicinity, isolated from the main cloud band to the north and northwest. At the full resolution of the data (Fig. 25), the area enclosed by the 250^{o}K isoline appears as a general east-west band between 68 and 69^{o}W. However, no such banded structure, but only isolated areas of colder than 250^{o}K, can be seen in Figure 24 in this area. Another common feature in the three figures is the southward bulge of cold temperature which lies along and near 71W between approximately 43 and 44^{o}N. The major difference between the appearance of the three figures is in the apparent clear or lower cloud areas (or bands) near or between the banded clouds. For example, in Figure 26, a clear or lower cloud area includes the area from Augusta to Lincoln, and near Errol, New Hampshire. No such clear areas are apparent on either Figure 24 or 25. Isolated areas of temperatures warmer than 250^{o} can, however, be seen within the overall frontal band in Figure 25. No explanation for this discrepancy is offered here and a need for further study of this matter is suggested.

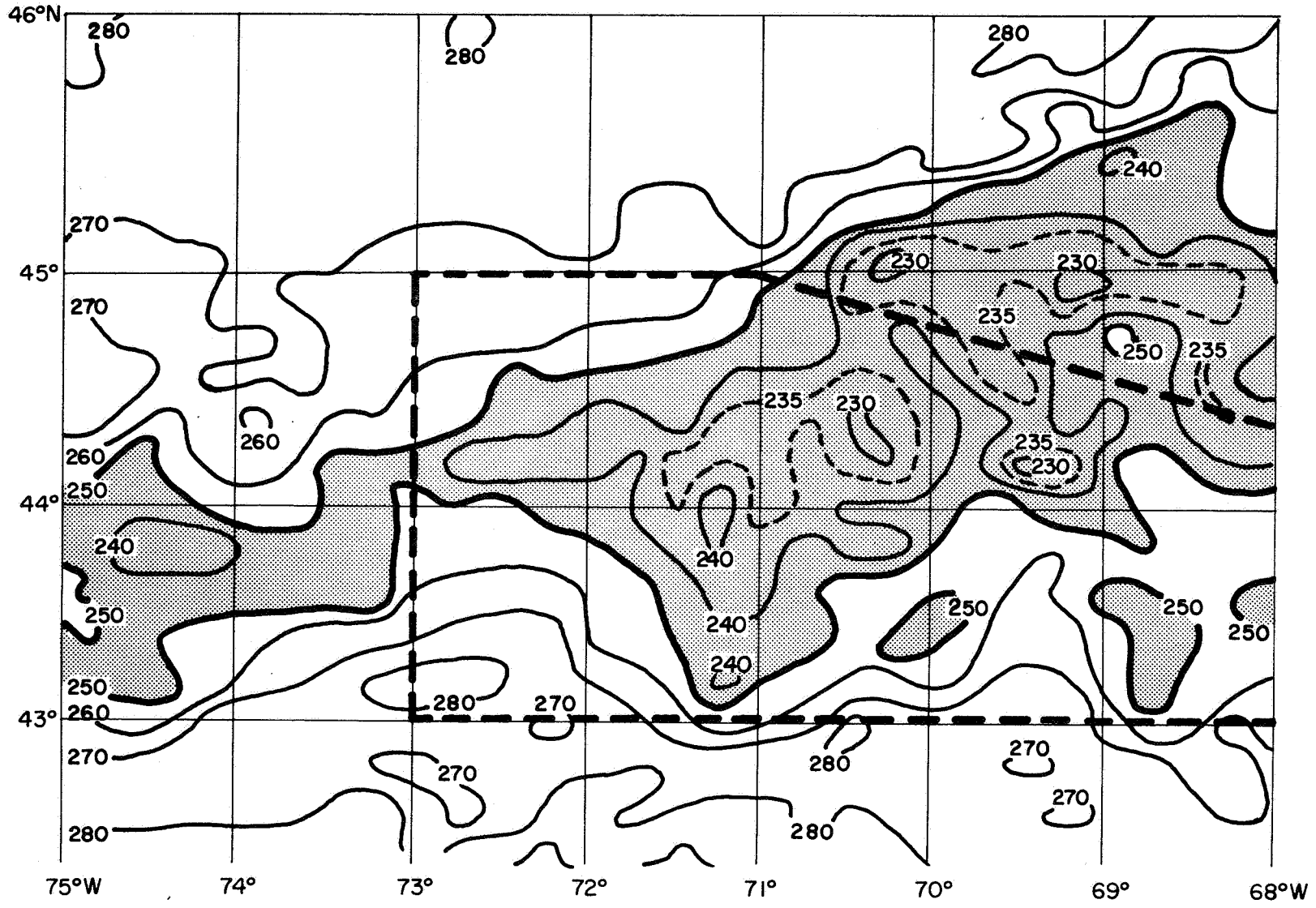

Figure 24 Analysis of Machine Mapped HRIR Data. Shaded Area Indicates Cloud Tops Colder Than 250°K. Area Enclosed by Large Dashed Line Represents Area of Figure 25.

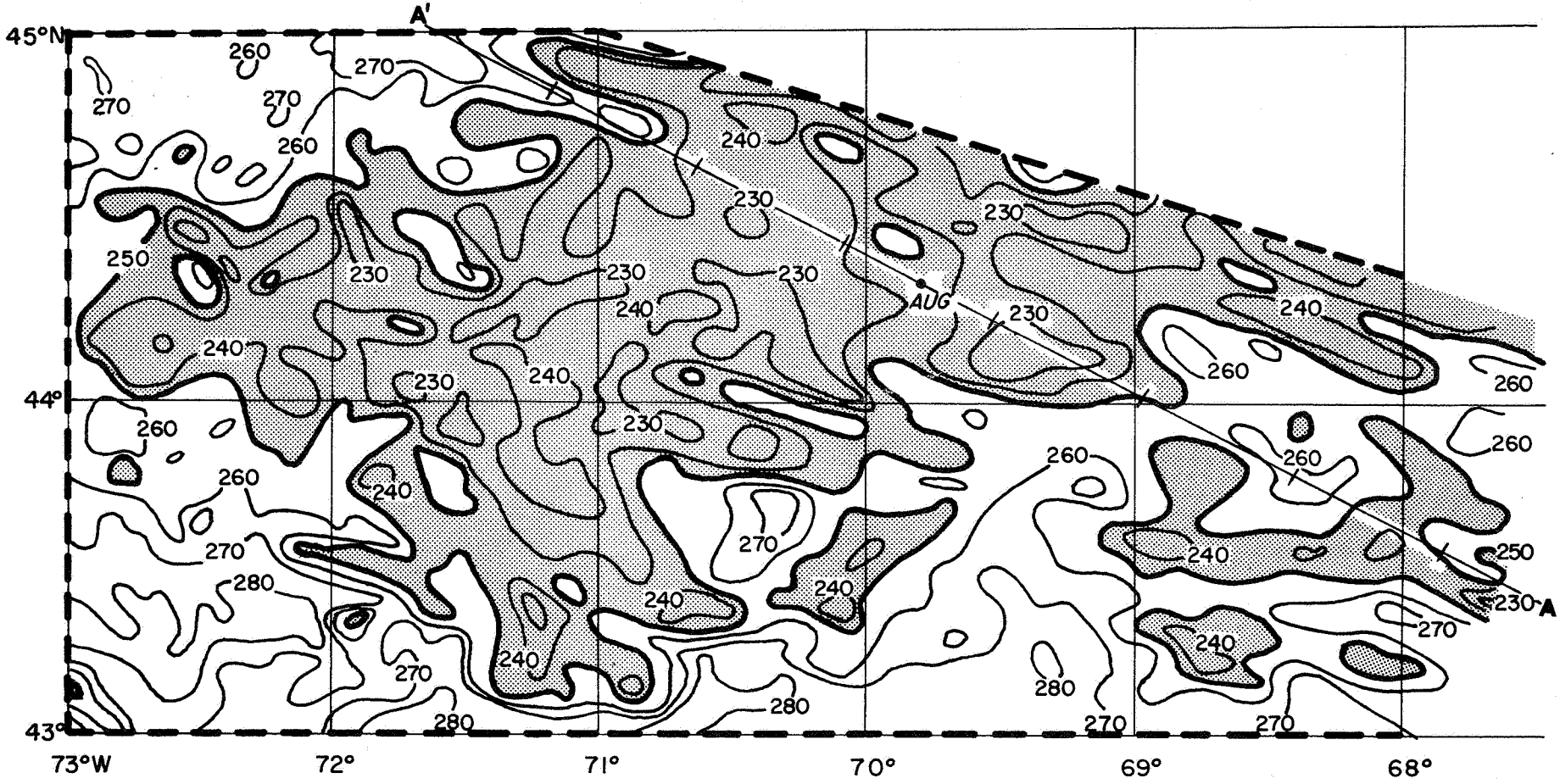

Figure 25 Analysis of Hand Plotted HRIR Data. Line AA' Represents Cross Section Line Through Augusta Used as Basis for Figure 27. (Short Cross Marks on this Line Represent Time Segments.)

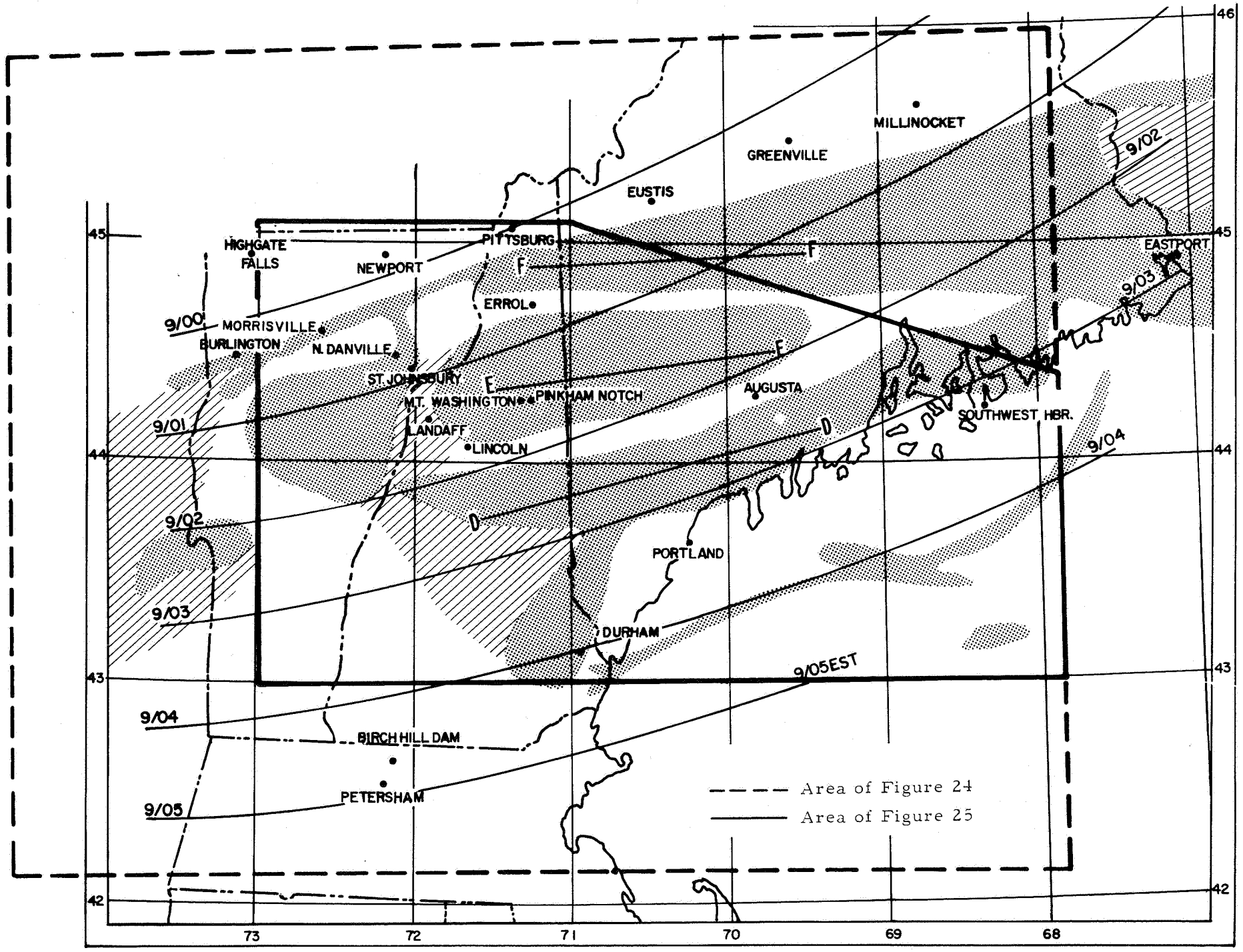

Figure 26 Enlarged Rectification of the Part of the Cloud Pattern in Figures 24 and 25. Isochrones of Frontal Positions Labeled in EST. Dotted Pattern Represents Bright White Area While Slashed Area Represents Grey Areas in Pictorial Data from Figure 23.

The entire New England area received relatively small amounts of precipitation during the passage of this frontal band.† The largest amounts were of the order of .5 in., in the area of northwestern Vermont and central New Hampshire; elsewhere amounts averaged near .2 of an inch, with even smaller amounts occurring in Massachusetts. The precipitation data used for the study were taken from the hourly precipitation data for New England, September 1964, as published by the U.S. Dept. of Commerce, Weather Bureau. In that summary, total amounts occurring within the hour are reported at the end of each hour, and only measurable amounts (greater than .01 in.) are reported. Therefore, all trace amounts are omitted and no analysis of precipitation at increments smaller than one hour were possible. This data form, coupled with the fact that most of the data were from non-Weather Bureau stations where records are kept by untrained observers, probably degraded the correlations with the IR data.

3.2.2 Correlation of Precipitation to Cloud Top Temperatures

Various authors have attempted to relate precipitation rates to cloud thickness, cloud top height, or radar echo depth. For example, Boucher (1959) related hourly precipitation rates to radar echo depth. His Figure 8 is reproduced here as Figure 27. In Boucher's study, he attempted to determine an approximate curve which related cloud radar echo depth to precipitation rates. It must be remembered that, for the type of radar used in Boucher's study, the top of the radar echo almost certainly does not represent the top of the cloud as seen by the HRIR sensor. Hence, the cloud top temperatures which would correspond to Figure 27, would tend to be somewhat warmer than those observed by the HRIR sensor. However, a reasonable relationship between precipitation rates and cloud depth (and, hence, cloud top height) is demonstrated.

An attempt was made to correlate the occurrence of precipitation with cloud top temperature as obtained from the detailed analysis shown in Figure 25. The technique used was to plot a cross section line, on the detailed analysis, through the station in question. The orientation of the cross section was first determined from the mean 12 hour frontal speed (00 GMT to 12 GMT, 9 September) which encompassed the HRIR observation time ($\simeq$ 0600 GMT). Since the structure was determined to be

---

† In fact, it was chosen for study not as an optimum case, but as one of the few Nimbus HRIR I cases over an area of readily available and reasonably dense data.

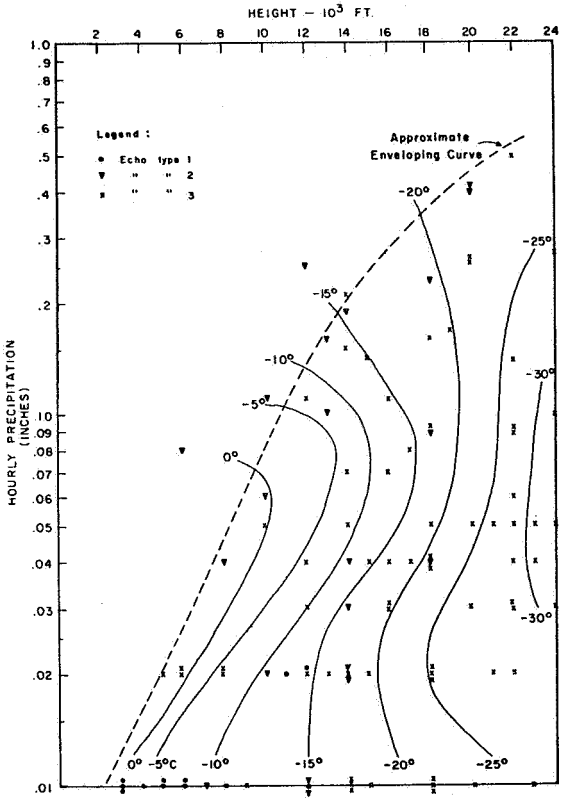

Figure 27 Hourly Precipitation as a Function of the Depth and Type of Vertical Echo. Isotherms Refer to Temperature at Top of Echo.

cellular in nature, an estimated component of the movement of the cells was then added to the frontal speed to get the resultant cross section line. This component was derived by using the 700 mb wind direction, and 80% of the 700 mb wind speed. The use of such an estimate for cell velocity has been shown, by personnel at NSSL, to be a reasonable first approximation. One such cross section line has been indicated on Figure 25 (line AA', through Augusta, Maine). Data taken along this line, at one hourly intervals, are shown plotted in Figure 28, for a time period from 3-1/2 hours before to 3-1/2 hours after the HRIR observation time. This example is typical of many prepared for this analysis. For some stations the correlation was not as good as that shown in this figure. However, for periods within $\pm$ 2 hours of the HRIR observation, correlations were generally good to excellent; i.e., when the HRIR temperature became colder than approximately 250°, precipitation occurred in measurable amounts. This indicates that, when cloud top heights are in the vicinity of 500 mb or higher (especially for the cellular cloudiness apparent in this frontal band) measurable amounts of precipitation are typically recorded.

Data taken from 14 stations in New England, which were either under or near the edge of the frontal cloud band at the HRIR observation time (see Fig. 26), were used to obtain a frequency diagram of (1) number of occurrences of measurable precipitation or of no measurable precipitation, vs (2) 5°K temperature categories. For this analysis, data were extracted from the plots prepared for each station (similar to Figure 28). Mean temperatures for each hour were computed and, were compared to the occurrence of precipitation. The results are shown in Figure 29.

This type of analysis of course implies a quasi-steady state condition of the frontal clouds over some period of time; in this case, the time period selected ranged from approximately six hours prior to the HRIR observation time to three hours after the observation time (a rather long time period). In addition, several other assumptions had to be made to perform this analysis. First, since only measurable precipitation was reported, no account could be taken of the occurrence of trace amounts. Hence, the probabilities can only reflect measurable precipitation (> 0.01 in.) Since, in most cases, recording type rain gauges were used, it was often difficult to determine after the fact when very small amounts (on the order of .01 in.) occurred. Therefore, some ambiguity is probably present in the data reported in this form. The frontal movement, as taken from conventional NMC weather maps, appeared to be non-uniform over the 24 hour period, 12 GMT, 8 September to 12 GMT, 9 September. The front moved relatively rapidly prior to 00 GMT, 9 September, slowed appreciably through the period to 06 GMT, 9 September, and then moved somewhat faster through the period to 12 GMT, 9 September. Since

Figure 28 Occurrence of Measurable Precipitation vs. HRIR Cloud Top Temperature for Augusta, Me., 8-9 September 1964.

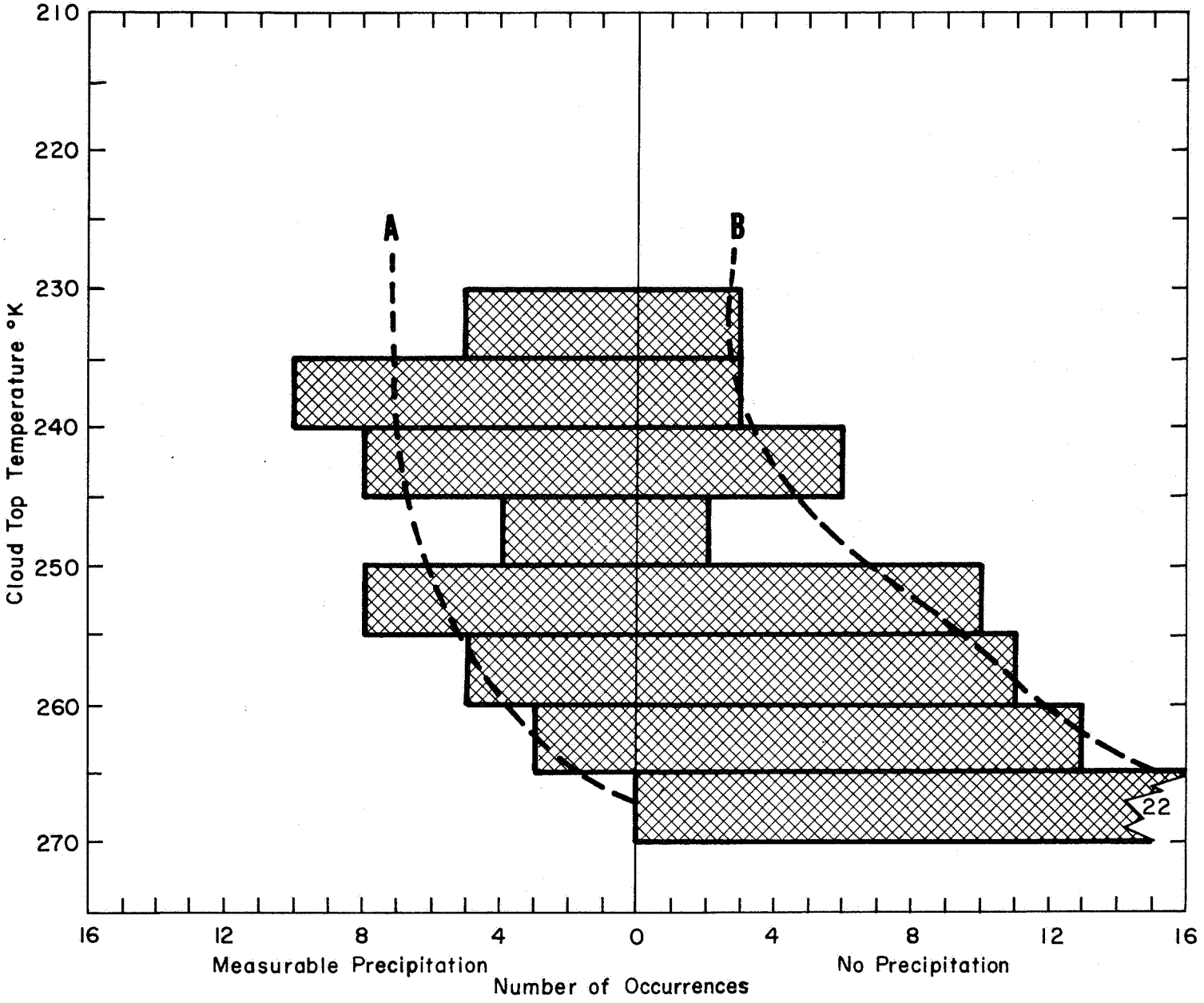

Figure 29 Frequency Distribution for Both Occurrence and Non-occurrence of Measurable Precipitation vs. HRIR Cloud Top Temperature

the HRIR observation occurred near 06 GMT, some difficulty in assigning a frontal speed was encountered. After some analysis, it was determined that a mean frontal speed, based on the 00 GMT, 9 September and 12 GMT, 9 September frontal placements, would suffice for this study. Thus, the resulting probabilities, derived from the data shown in Figure 29, cannot be expected to be extremely good.

The frequency distribution (of the occurrence of both precipitation and non-precipitation) have been approximated by smooth curves as shown in Figure 29. Line A represents the number of occurrences of precipitation, while line B represents the number of occurrences of no precipitation for the various temperature categories shown. Based on the actual data and on the curves (lines A and B), the probabilities of measurable precipitation vs temperature categories have been tabulated in Table 2. The probability distribution of the occurrence of measurable precipitation increases from approximately zero, when the cloud top temperature is greater than 266°K, to probabilities of approximately 75% when cloud temperatures lie between 230° and 235°K. Although these data are based on the passage of a single frontal band, many stations have been used in the compilation and the data are believed to represent a reasonable first approximation to the probability of precipitation vs HRIR cloud top temperatures at the mesoscale. However, before much significance can be placed on these probabilities, several other similar cases should be analyzed. Funds in the present study did not allow such analyses, but they are recommended for future study since the results seem to be encouraging.

Table 2

Probability of Precipitation Occurrence

Versus Cloud Top Temperatures

Temperature Increments °K	Probability % Sample	Smoothed
230 - 235	65	75
236 - 240	75	70
241 - 245	55	60
246 - 250	65	50
251 - 255	45	45
256 - 260	30	30
261 - 265	20	20
266 - 270	0	0

3.3 Further Study of an Apparently Anomalous Bright Band

Widger, et al, (1966) presented case examples of daylight HRIR data. In one such case, Data Orbit 206/207, 11 September 1964, they discovered a very narrow, bright band extending across southeastern England, apparently bodering the northern edge of a band of cirrus (presumed to be associated with the jet stream).

An enlarged portion of the pictorial data is shown in Figure 30. The grid on this figure has been modified slightly from the computer grid, using landmarks. The narrow bright band lies across southeastern England and over the North Sea.

The corresponding digitized HRIR data have been plotted at full resolution, and analyzed at a 4^{o}K isotherm interval, in an attempt to determine whether or not the narrow bright band was real, or only a product of contrast reactions of the human eye. A portion of this analysis (with an 8^{o}K isothermal interval for illustrative purposes) is shown in Figure 31. The narrow band of very warm temperatures is in evidence (between A and A'). The band was composed of warmer cells, rather than having the more or less continuous appearance of the pictorial form. In fact, in the area east of 2.5^{o}W, a second band (between B and B'), or a widening of the overall band, appears.

The shaded area in Figure 31 includes all blackbody temperatures (T_{bb}) greater than 298^{o}K. Surface (shelter) temperatures at 00Z (approximately 11 hours prior to the HRIR data) were 289^{o}K. Allowing for a 7^{o}K diurnal increase in temperature (the probability is 90% that a diurnal increase of 7^{o} will not be exceeded at London in September, see Merritt, E. S., 1961), the shaded area of (Fig. 31) is still warmer than the surface. Therefore, the radient energy reaching the HRIR sensor was almost certainly composed of some reflected energy, as well as ground or cloud emitted energy.

Figure 32 is a montage of Nimbus I AVCS data taken during the same pass as the HRIR data. Geographic outlines have been added to the computer grid originally inscribed on the pictures. Comparing this grid to that on Figure 31, the bright band of the HRIR data (Fig. 30) would appear to lie generally on a line between the two large arrows. Some aspects of this grid appear questionable when the cloud and clear features on Figures 30 and 32 are compared. The band may be oriented more to the northeast (i.e., from about the left arrow to about 52.5^{o}N, 0^{o} on the grid). Furthermore, we have not been able to verify to the precision required for this case, the geographical location of the digitized HRIR data.

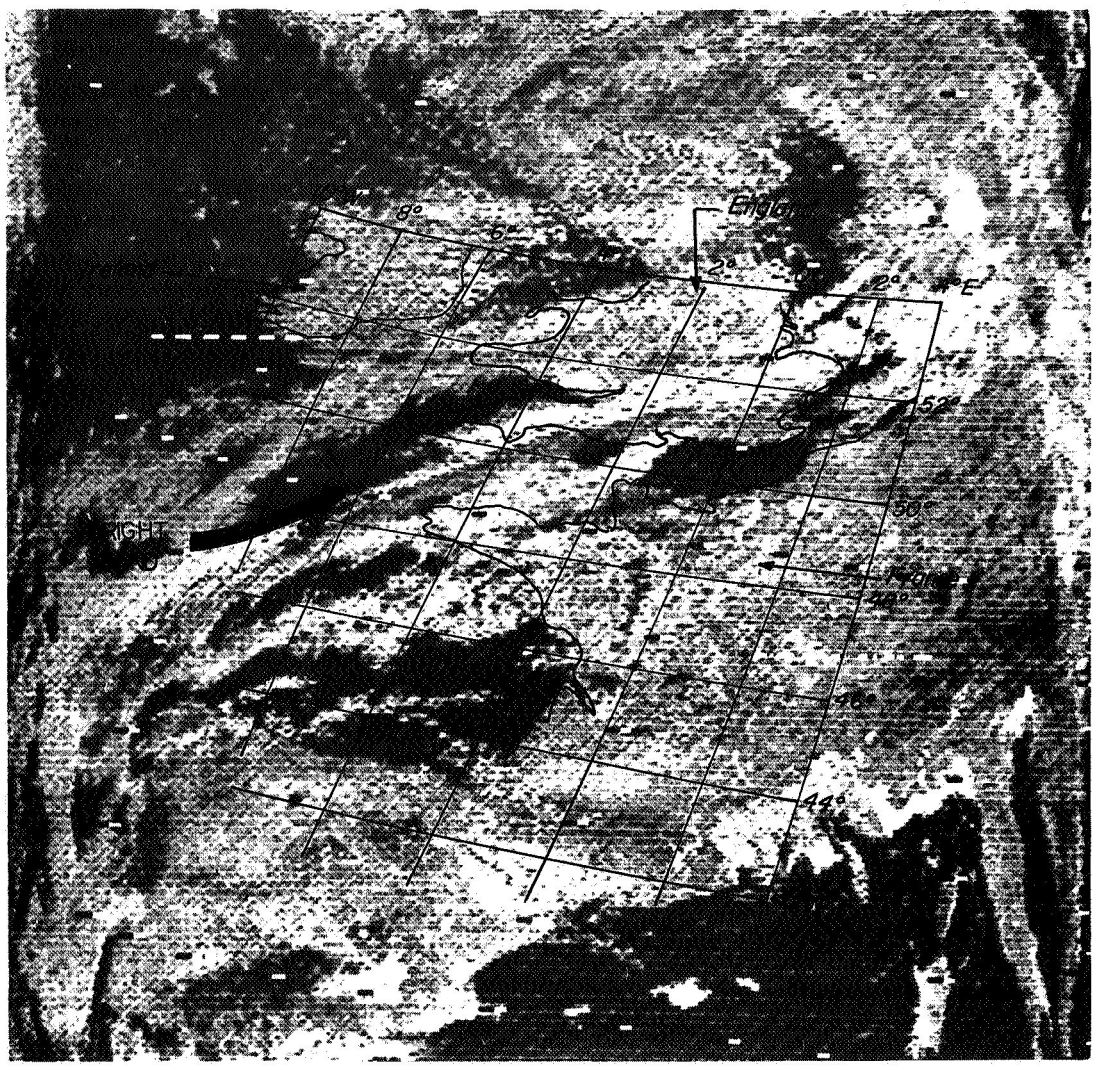

Figure 30 Enlarged Portion of HRIR Pictorial Data.

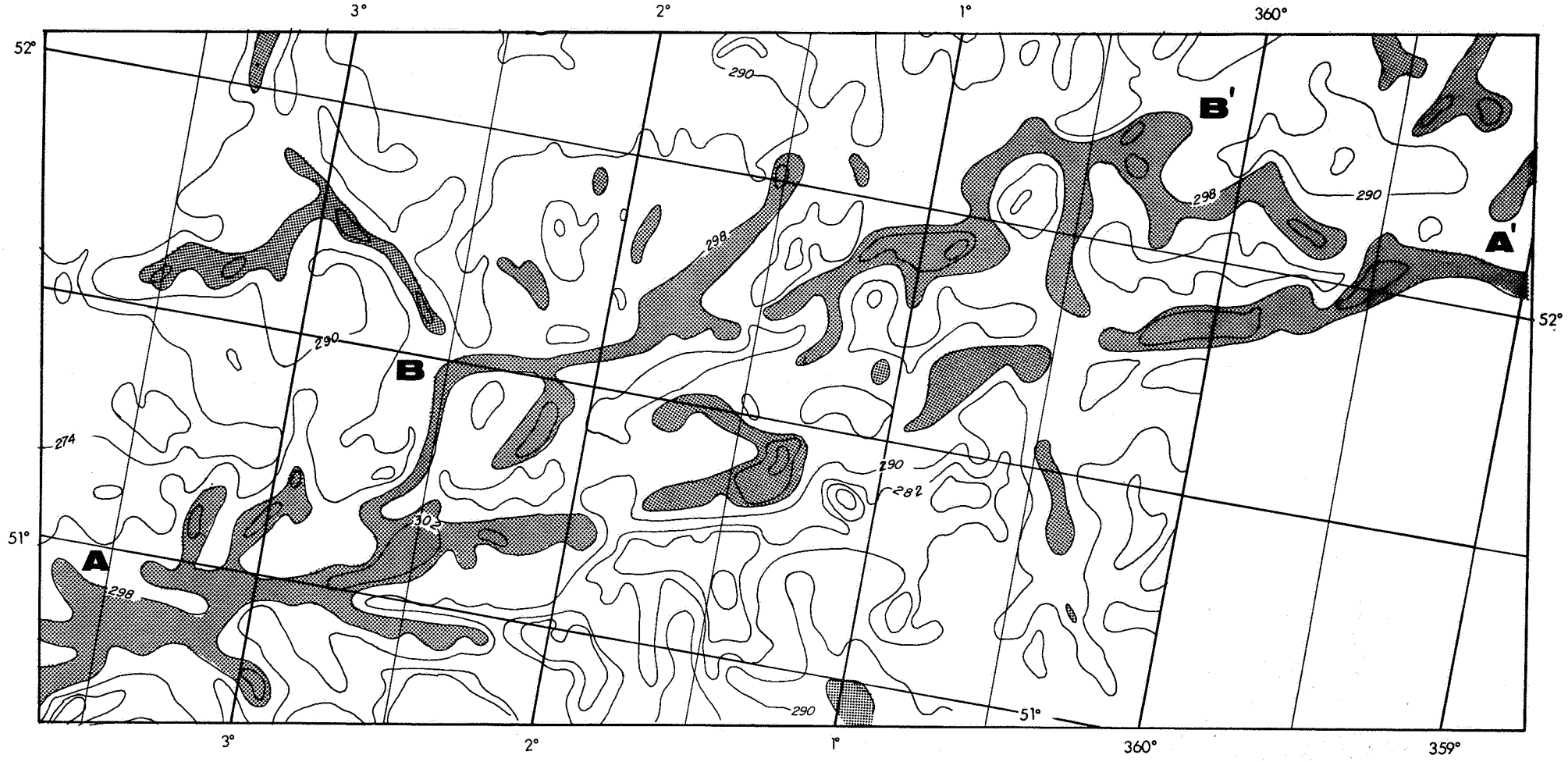

Figure 31 Portion of Analysis Derived from Digitized Daylight Data at Full Resolution (Shaded Area includes all $T_{BB} > 298°K$)

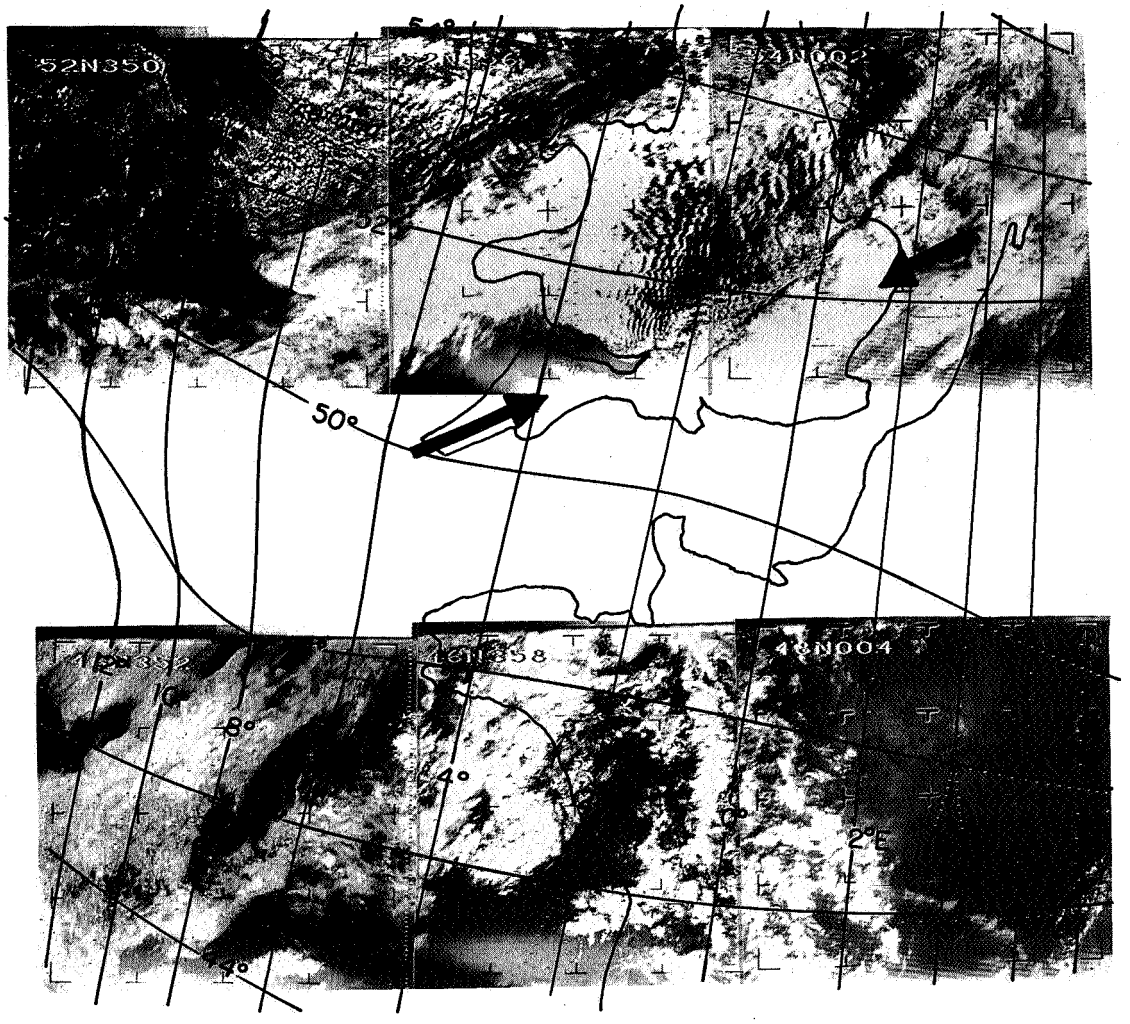

Figure 32 Nimbus AVCS Montage Taken on Same Pass as HRIR Data Shown in Figures 30 and 31.

The limited funds for this portion of the contract did not permit further analysis of this interesting and still unresolved case. These data indicate that the bright band observed by Widger et al, is in fact revealed on the digitized data, and was not an artifact. The questions raised by Widger in his earlier study still remain unanswered, and must be left to future research.

The starting point for further research would be an attempt to very precisely locate each of the three pieces of data (Figs. 30, 31, and 32), and especially to determine the precise location of the HRIR data relative to the AVCS data. This is because it would appear to be critical whether or not the bright band actually coincides, as suggested by Widger, with the clear, or possible cirrus shadow area, visible in the AVCS. If it does, then an anomaly requiring explanation would still seem to exist. If it does not, then the explanation is probably no more than joint high reflection and high emission from low level clouds.

4. CONCLUSIONS AND RECOMMENDATIONS

4.1 Diurnal Cloud Studies

Analyses of TIROS VII 8-12μ "window" observation of the Indonesian area (10N-10S, 95E-150E) have been prepared during June-September 1963, at two-hourly intervals during a composited "day." These analyses indicate a semi-diurnal cloud cycle, with pronounced amplitude over the land masses of the area. Cold areas (high cloud) appear over most land areas during the period 0200-0800 LMT and 1600-2000 LMT. The 16-20 LMT temperature minimum (high cloud maximum) is the primary feature. Warmer temperatures (lower clouds) appear during the periods 1200-1400 LMT and 2200-2400 LMT. The primary lower cloud maximum is at 2200-2400 LMT. Diurnal variations over tropical open oceans and small tropical islands have been shown to have a similar pattern.

Averages over the area for day (06-18L) and night (18-06L) show a pattern which is somewhat contrary to Rasool's (1964) finding of large, diurnal percentage of cloud cover variations. However, the observed variations are in line with TIROS VII data presented by Rasool (1965), in reply to a discussion by Winston (1965).

The observed semi-diurnal cloudiness variation suggests that atmospheric tidal effects may be important, especially around 2200 LMT.

4.1.1 Suggestion for Further Diurnal Studies

The techniques which have been employed here to derive a composited cloud "day" have many additional applications. These are unique to the inclined orbit TIROS radiometric observations. Some selected applications might be:

a. Evaluation of the diurnal cloud variations over the open ocean and atolls.

b. Evaluation of the diurnal variation in surface temperature (T_{bb}) in various arid regions to develop relationships between known rock conductivities and the daily satellite-observed surface temperature (T_{bb}) changes. This technique might be applicable to satellite determination of planetary surface rock structure.

c. Evaluation of the variation of specific land surface reflection with change in solar zenith angle.

4.2 Time Lapse Movie of Diurnal Cloud Cycle Over Indonesia

A 16 mm color, sound-on-film, motion picture has been prepared from the TIROS VII "window' radiation analyses over Indonesia and Malaysia. This motion picture provides a "four dimensional" look at cloud variations, from the viewpoint of a synchronous satellite centered over the Celebes. Explanations and visual examples of the use of the precession of the plane of the orbit to construct a composited day, are presented in the movie.

4.2.1 Suggestions for Further Applications of Time Lapse Movies of TIROS Radiometric Data

The time lapse movie technique presents many possible opportunities for application. These range from an application to the ocean/atoll diurnal variation study mentioned in Section 4.1.1 to the possible synthesis of a tropical or extra-tropical storm development sequence. The unique combination of radiation (particularly "window") observation and the time lapse technique provides an opportunity to observe in "four" dimension.

4.3 Hurricane Alma Analyses

The conclusions and suggestions for further study of this study are included in Appendix B.

4.4 HRIR Analyses

4.4.1 Vortex Case Study

Although the analysis of this case has been necessarily restricted and is not as detailed as might be desirable, the following conclusions can be drawn:

1. As expected, the vortex pattern can be easily recognized in the machine mapped IR data at the 1:2 million map scale.

2. Cold areas in the digitized data correlate well with larger bright areas in the pictorial HRIR presentation, narrow bands in the pictorial presentation are not resolvable at a 1:2 million machine mapped scale. This scale allows an analyses to be made to resolutions of about one-half to three-quarters degree of latitude. Each mapped data point is, however, a mean of from 30 scan spots for nadir angles near 60 degrees, to nearly 70 scan spots for areas along the subpoint track. The pictorial presentation provides greater resolving power (resolutions less than 5 n.mi. for Nimbus I) than this map scale.

3. The time series of AVCS, HRIR and TIROS IR data provides a good description of the cyclone cloud system and its movement. The advantages of the joint or integrated use of the several data sources are evident.

4. For the purposes of identification of large synoptic scale systems, as were demonstrated in a subsequent case study, (see Section 3.2), hand plotted data using nearly all data scan spots are more desirable (and perhaps necessary) for better identification of mesoscale systems within larger synoptic scale patterns.

4.4.2 Recommendations for Further Study

The resources for the current study did not permit an exhaustive study of this case. It is recommended that the following analyses should be made, in order to derive the maximum benefit from the studies already performed.

1. Hand plotting of the HRIR digitized values, at a map scale large enough to accommodate at least every other data point. Analysis of this data should reveal mesoscale systems within the larger synoptic scale pattern, which may be relatable to the mid- or lower tropospheric dynamics (see for example Rogers and Sherr 1966). Analyses of this data at isoline intervals closer than 5^{o} would be desirable.

2. An attempt should be made to determine (probably from the nearest radiosonde data) the height of the various isothermal surfaces. This would result in a three-dimensional picture of this vortex at a very fine scale. While this may not be fully feasible over the open ocean, as this vortex is, such analyses should be great values when performed for similar cases over land.

4.4.3 Rain Band Case

The following conclusions can be drawn from this case study.

1. The choice of scale of presentation of the HRIR data contributes to the interpretability of the data. The pictorial presentation appears to be a convenient scale for comparing HRIR data to AVCS data forms, but does not allow detailed analyses (especially at sub-synoptic scales) of the three dimensional cloud structures to be accurately represented. 1:2 million machine mapped data allow easy recognition of sub-synoptic scale cellular cloud structures, but do not allow mesoscale analyses to be performed. Hand plotted data at full resolution do allow mesoscale interpretation, but make larger scale pattern recognition more difficult.

2. The occurrence of measurable precipitation seems to be reasonably correlated with cloud top temperature. In particular, when cloud top temperatures are colder than 250°K (at least for this case), the probability of measurable precipitation is somewhat greater than 50%. When cloud top temperatures lie between 230 and 235°K, the probability of measurable precipitation is on the order of 75%.

4.4.4 Recommendation for Further Research

This case study has indicated the value of the HRIR data in various formats. In particular, if the mesoscale structure of frontal bands, etc., are of interest, the detail can be provided by the HRIR data at its full fidelity. For sub-synoptic scale use, the machine mapped data is adequate. Thus, the data format selected for the entire study should be dependent on the specific objectives.

It would be desirable to obtain statistically significant data regarding the probability of measurable precipitation vs cloud top temperatures, for future operational use. Further studies along the lines of that initiated for this case could provide such information. Many cases of frontal bands are readily available in the Nimbus II and TIROS IR data, and should be studied for this purpose. The study could also be expanded to cover synoptic scale features, such as extratropical cyclones.

REFERENCES

Bandeen, W.R., 1962: TIROS II Radiation Data Users Manual, Supplement, Aeronomy and Meteorology Division, NASA, GSFC, Greenbelt, Maryland.

Boucher, R.J., 1959: "Synoptic-Physical Implications of 1.25-cm Vertical-Beam Radar Echoes," Journal of Meteorology, 16(3), pp. 312-326.

Elliott, R.D. and E.L. Hovind, 1965: "Heat, Water, and Vorticity Balance in Frontal Zones," Journal of Applied Meteorology, 4(2), pp. 196-211.

Haurwitz, B and J. Austin, 1944: Climatology, McGraw Hill Book Co., Inc. New York, pp. 410.

La Seur, N. and M. Garstang, 1964: Tropical Convective and Synoptic Scale Weather Systems and Their Statistical Contribution to Tropical Meteorology, Final Report, Grant Nos. DA-SIG-36-039-62-G23 and DA ARO 49-92-63-G23, Florida State University.

Merritt, E.S., 1961: Distribution of Station Temperatures, Pan American World Airways, Technical Memo No. 2.

Palmer, C.E., C. Wise, L. Stimpson, G. Duncan, 1955: The Practical Aspect of Tropical Meteorology, Air Weather Service Manual 105-48, Vol. I.

Ramage, C.S., 1962: Diurnal Variation of Summer Rainfall Over Malaya, Sci. Rep. No. 3, Contract No. AF 19(604)-6156, University of Hawaii.

Rasool, S.I., 1964: "Cloud Heights and Nighttime Cloud Cover from TIROS Radiation Data," Journal of Atmos. Sci., 21(2), pp. 152-156.

Rasool, S.I., 1965: Reply to "Comments on Cloud Heights and Nighttime Cloud Cover from TIROS Radiation Data," Jour. Atmos. Sci., 22(3), pp. 339-340.

Rogers, C.W C., and P.E. Sherr, 1966: Toward the Dynamic Interpretation of Satellite-Observed Extratropical Vortical Cloud Patterns, Final Report, Contract No. Cwb-10812, ARACON Geophysics Division, Allied Research Associates, Inc. (Available from the National Environmental Satellite Center, ESSA, Suitland, Maryland.)

Saha, K.R., 1966: A Contribution to the Study of Convection Patterns in the Equatorial Trough Zone Using TIROS IV Radiation Data, Technical Report No. 74, Dept. of Atmospheric Science, Fort Collins, Colorado.

Sherr, P.E., and C.W.C. Rogers, 1965: The Identification and Interpretation of Cloud Vortices Using TIROS Infrared Observations, Final Report, Contract No. Cwb-10812, ARACON Geophysics Company.

Sherr, P.E., 1966: "Some Problems in Using TIROS Radiation Data as Filed on Final Meteorological Radiation Tapes," Proc. 4th Symposium on Remote Sensing of Environment, University of Michigan, Inst. of Science and Technology.

Shiffrin, K.S., 1961: "Spectral Properties of Clouds," Geofis. Pura. Appl. 48, pp. 129-137.

Staff Members, Goddard Space Flight Center, 1962: TIROS III Radiation User's Catalog, NASA, Greenbelt, Maryland.

Staff Members, Aeronomy and Meteorology Division, 1965: TIROS VII Radiation Data Catalog and User's Manual, Vol. 1, NASA Goddard Space Flight Center, Greenbelt, Maryland.

Widger, W.K., Jr., J.C. Barnes, E.S. Merritt, and R.B. Smith, 1966: Meteorological Interpretation of Nimbus High Resolution Infrared Data, NASA CR 352, National Aeronautics and Space Administration.

Winston, J.S., 1965: "Comments on "Cloud Heights and Nighttime Cloud Cover from TIROS Radiation Data," Jour. Atmos. Sc., 22(3), pp. 333-338.

APPENDIX A

COMPOSITED TIROS VII 8-12μ "WINDOW" ANALYSES

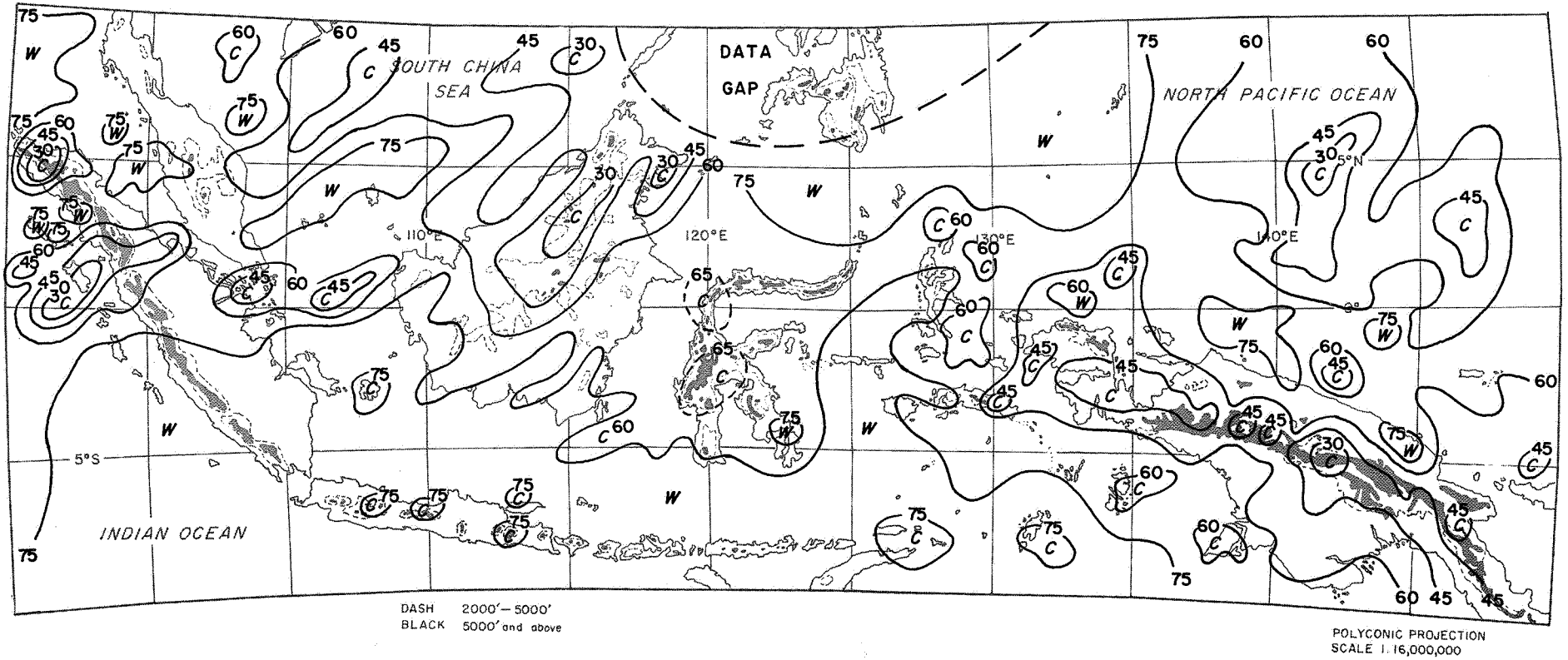

Figure A-1 COMPOSITED TIROS VII 8–12 μ "WINDOW" ANALYSIS – 0000 LOCAL

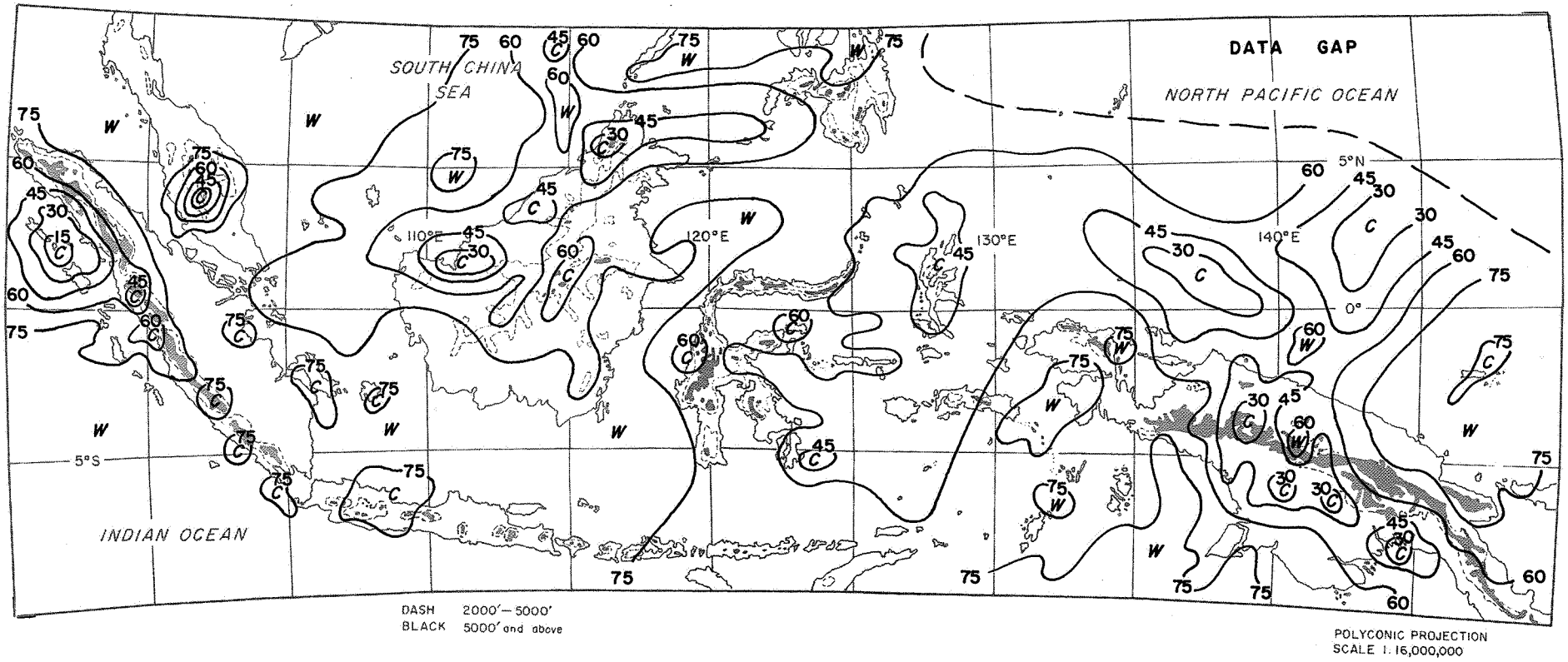

Figure A-2 COMPOSITED TIROS VII 8-12 μ "WINDOW" ANALYSIS — 0200 LOCAL

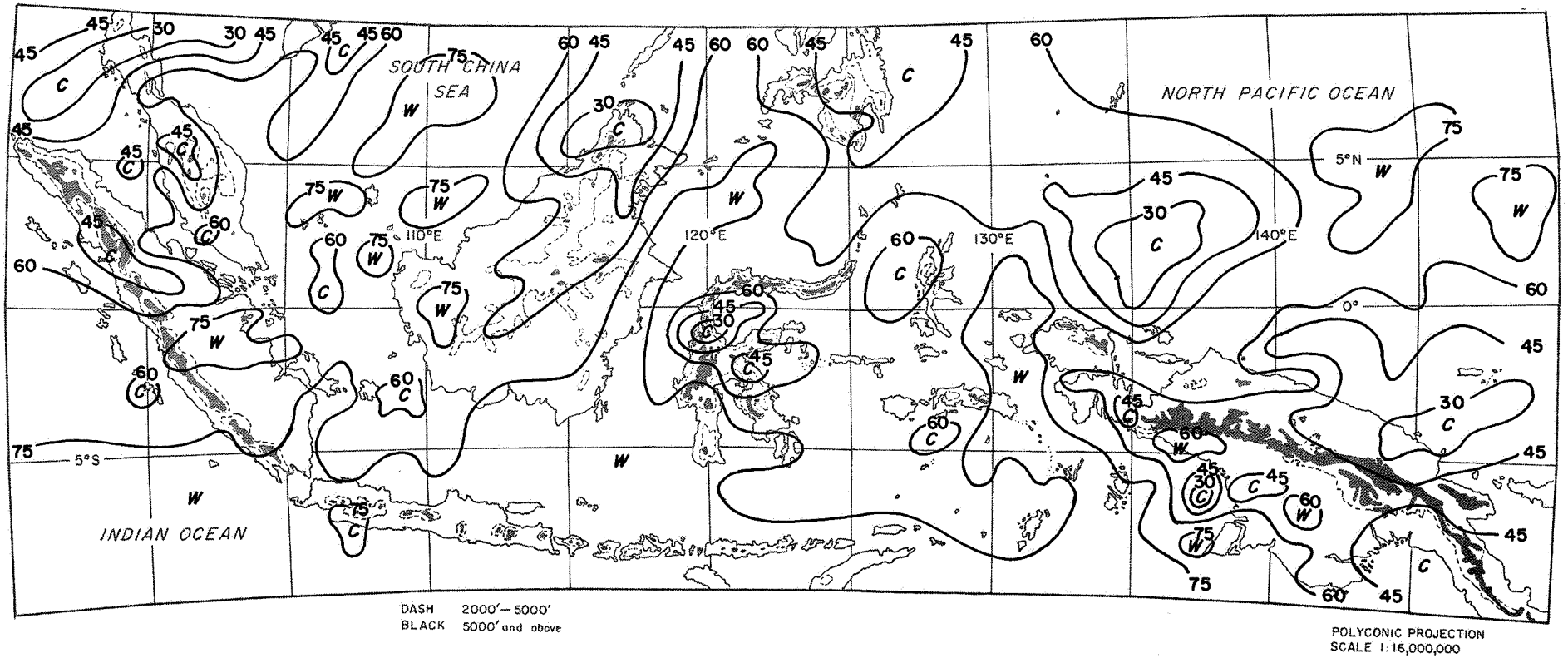

Figure A-3 COMPOSITED TIROS VII 8-12 μ "WINDOW" ANALYSIS – 0400 LOCAL

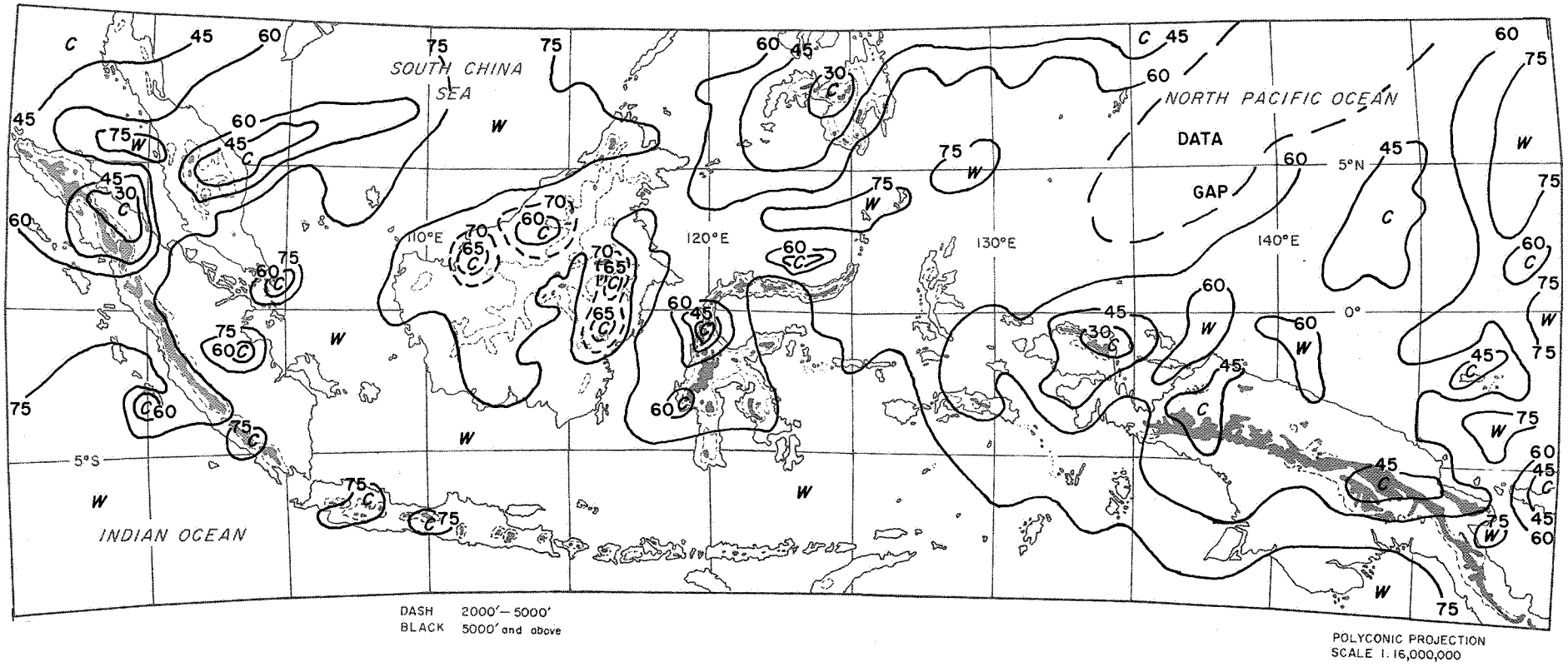

Figure A-4 COMPOSITED TIROS VII 8–12μ "WINDOW" ANALYSIS – 0600 LOCAL

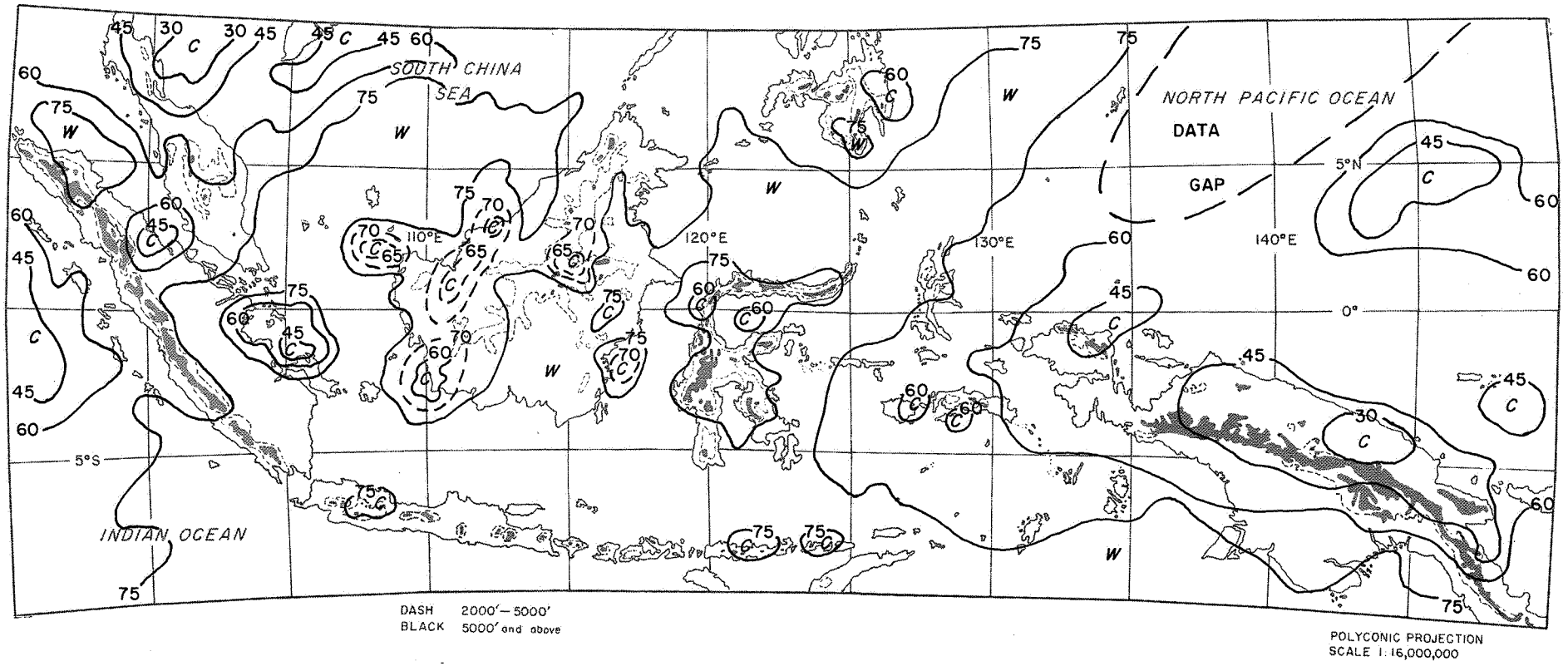

Figure A-5 COMPOSITED TIROS VII 8–12μ "WINDOW" ANALYSIS – 0800 LOCAL

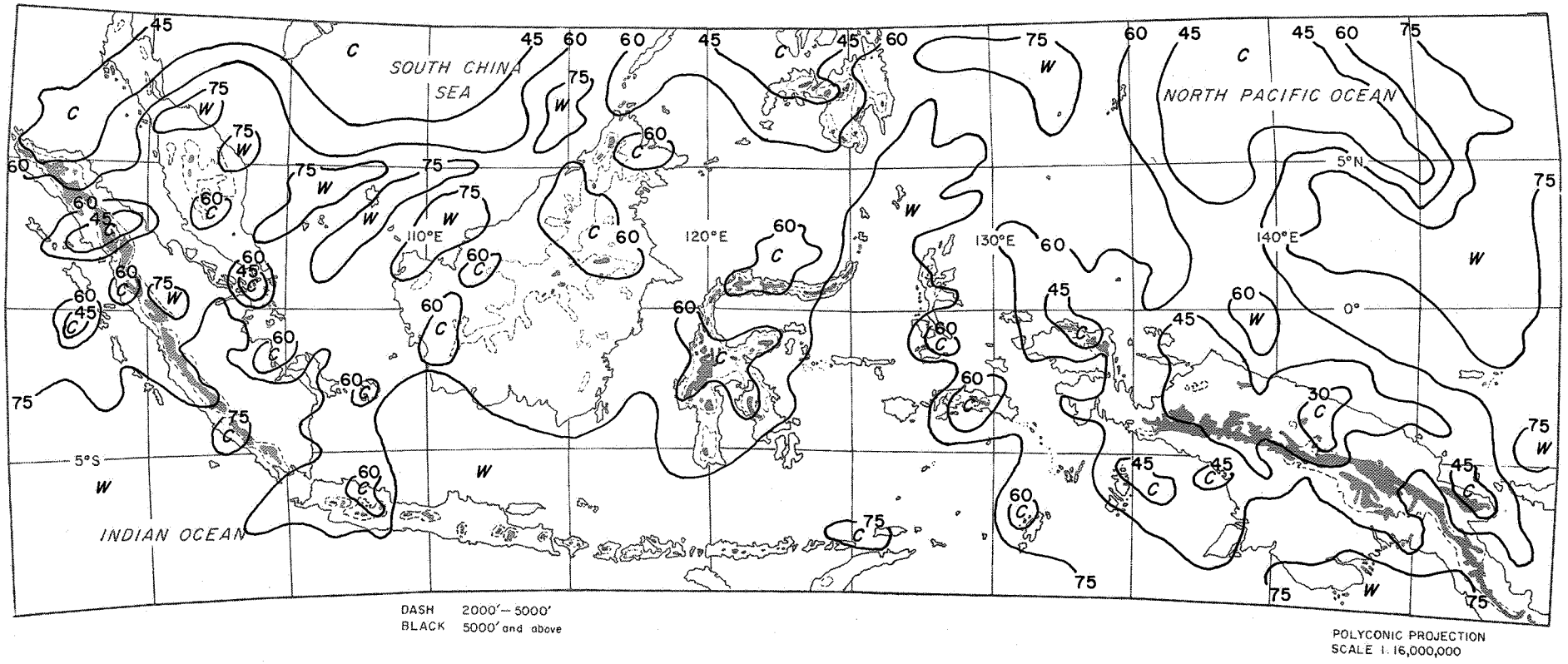

Figure A-6 COMPOSITED TIROS VII 8–12μ "WINDOW" ANALYSIS – 1000 LOCAL

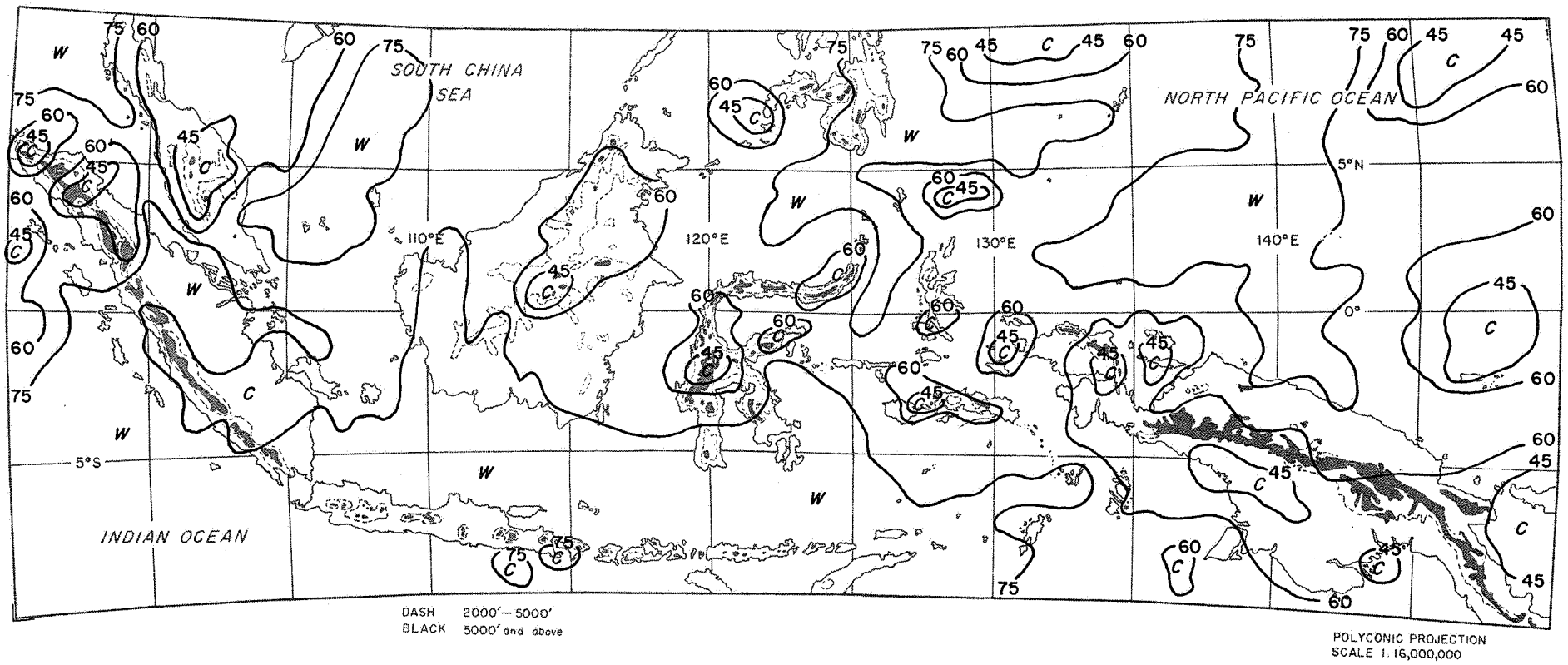

Figure A-7 COMPOSITED TIROS VII 8-12 μ "WINDOW" ANALYSIS - 1200 LOCAL

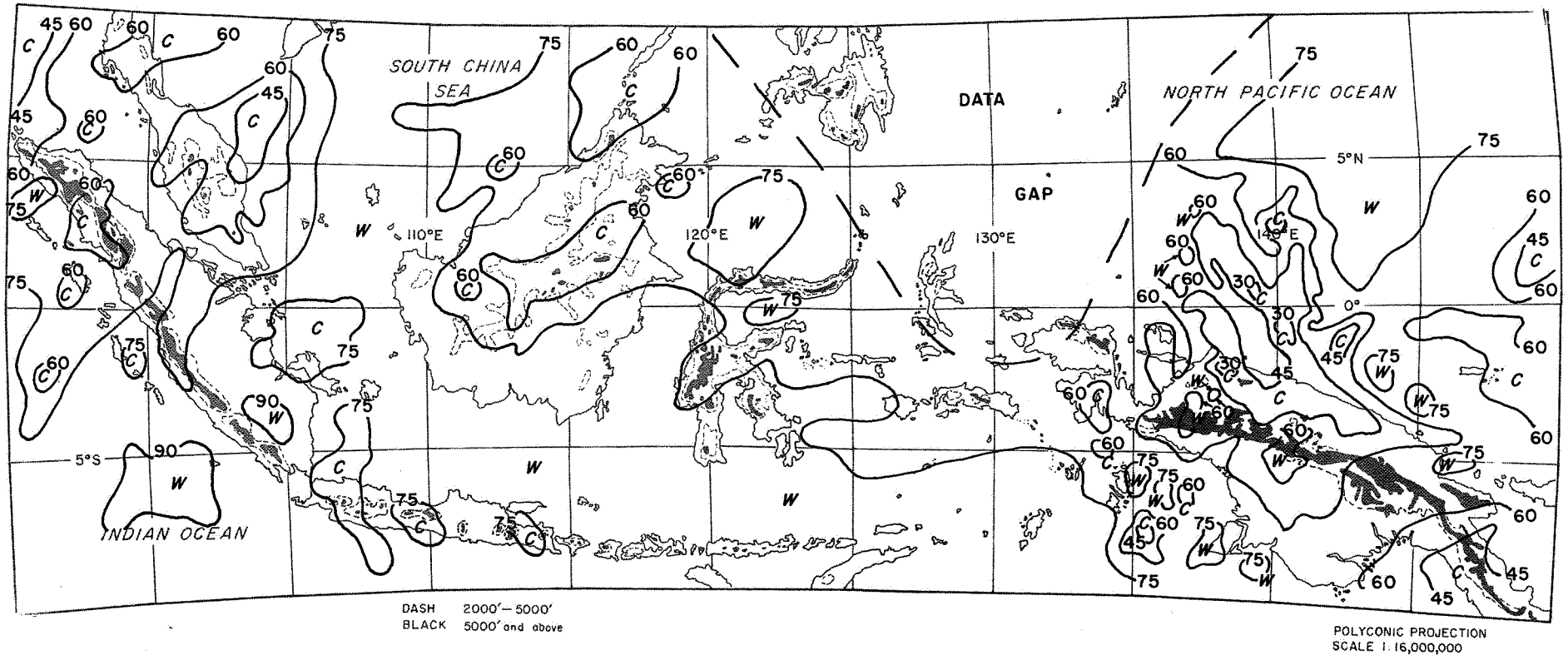

Figure A-8 COMPOSITED TIROS VII 8–12μ "WINDOW" ANALYSIS – 1400 LOCAL

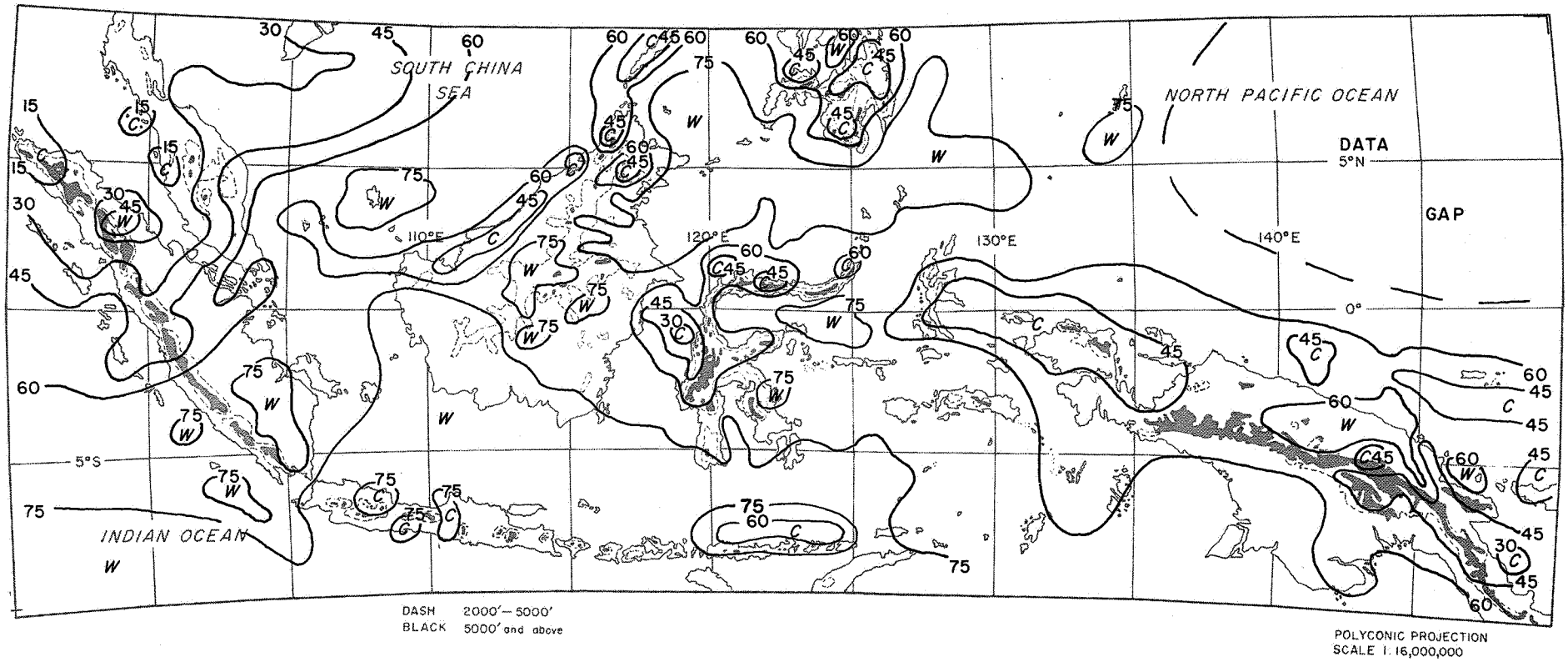

Figure A-9 COMPOSITED TIROS VII 8–12μ "WINDOW" ANALYSIS – 1600 LOCAL

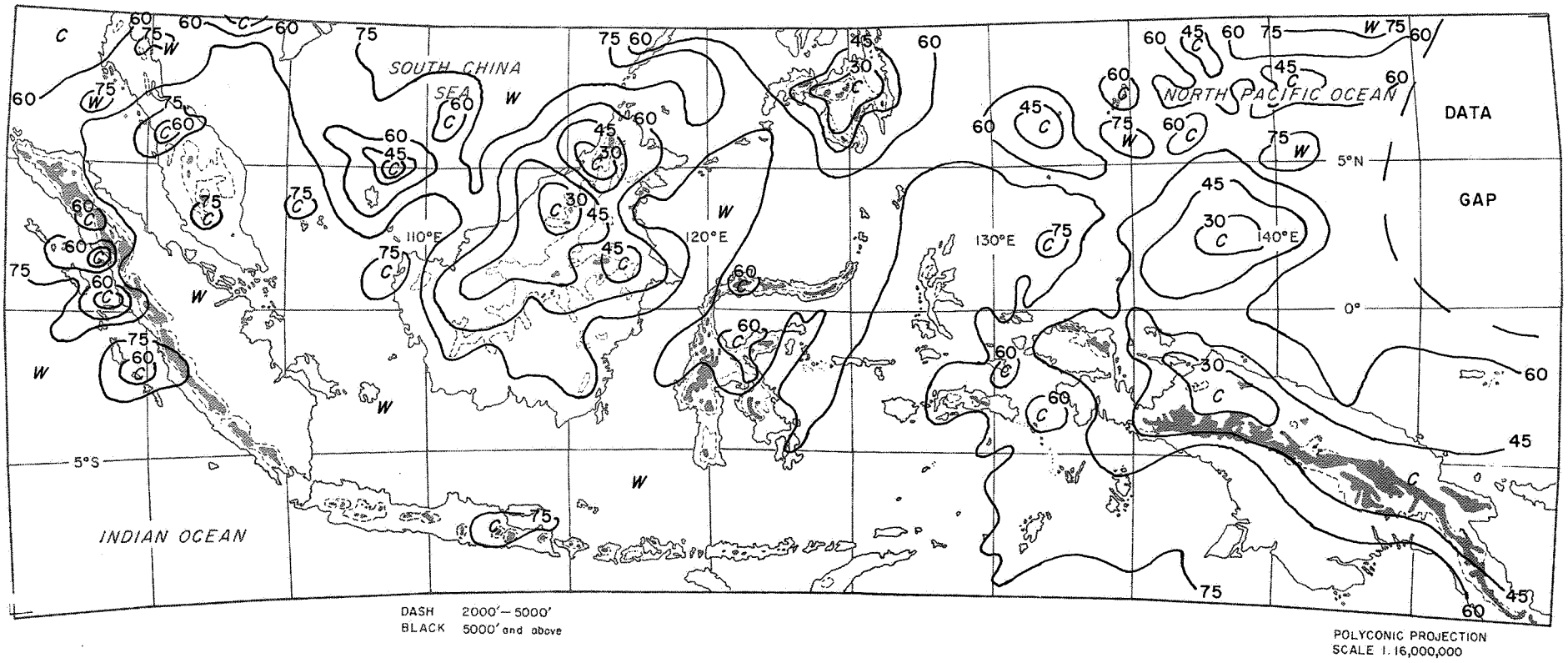

Figure A-10 COMPOSITED TIROS VII 8-12μ "WINDOW" ANALYSIS - 1800 LOCAL

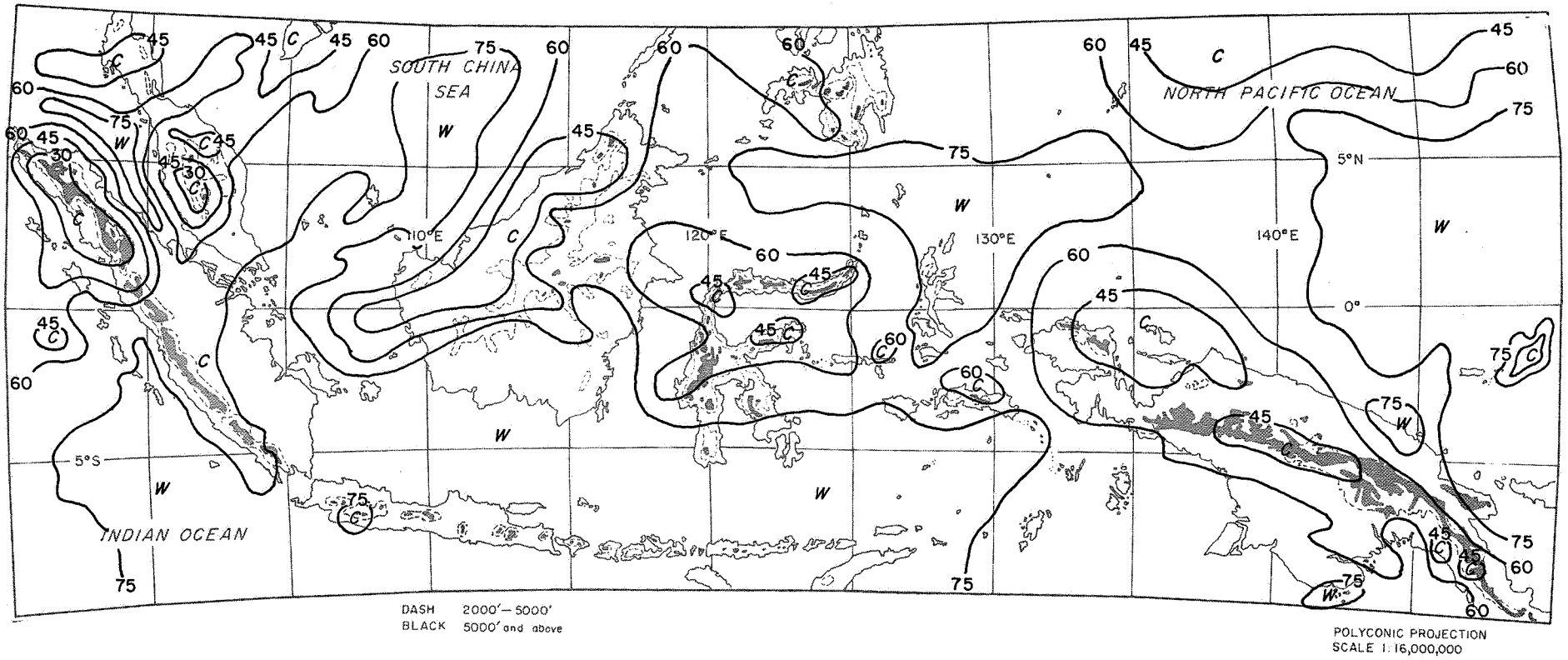

Figure A-11 COMPOSITED TIROS VII 8-12μ "WINDOW" ANALYSIS-2000 LOCAL

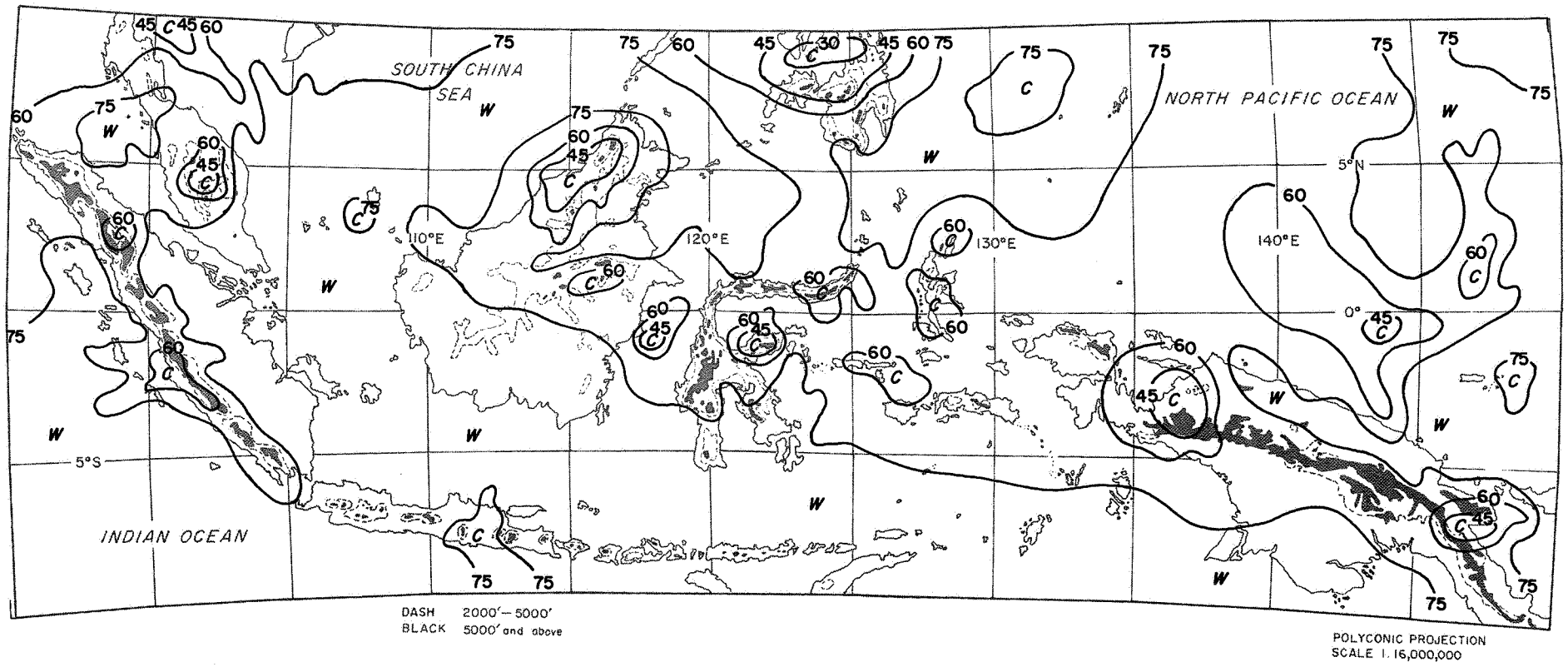

A.-12 COMPOSITED TIROS VII 8–12 μ "WINDOW" ANALYSIS – 2200 LOCAL

APPENDIX B

HURRICANE ALMA ANALYSES

B. 1 Introduction

The launch of Nimbus II in May 1966, and the fortuitous occurrence of Hurricane Alma early in June 1966, provide a unique opportunity to investigate, in detail, certain aspects of meteorological satellite-observed hurricanes.

Cirriform canopies of mature tropical cyclones have been studied by several investigators using observations from meteorological satellites. Among the more recent are those by Fritz et al (1966), and Wexler, Merritt and Chang (1966); both of which emphasized the visible spectrum canopy. Some pertinent results of these studies are:

1. The size and organization of the visible canopy in related to storm intensity (Fritz et al 1966).

2. The canopy character, i. e., the distribution of sharp and diffuse edges and, in part, size, is determined by the field of motion in the upper troposphere (Wexler, Merritt, and Chang, 1966).

3. The change in size of the canopy during intensification appears to be closely linked to the percentage area covered by cumulus towers ("hot towers"), which influence the outflow layer (Wexler, Merritt and Chang 1966).

Hurricane Alma, observed more frequently by meteorological satellites than any previous hurricane, provides a basis for study of some of these features. It also offers, through the Nimbus MRIR data, a chance to observe the canopy in visible, infrared "window," and absorption portions of the spectrum simultaneously. The following sections report on a detailed analysis of these aspects of Hurricane Alma.

B. 2 Data and Analysis

B. 2. 1 Data

B. 2. 1. 1 Conventional

Conventional surface and radiosonde data were collected, for the period 6-10 June 1966, for the area within 900 miles of the center of Hurricane Alma. Aircraft observations by NHRP aircraft were requested but were not available.

B.2.1.2 Satellite

Meteorological satellite observations are available for each day of Hurricane Alma from 4 June to 10 June 1966. Data are also available for the period following landfall on 10 June; however, they will not be considered during this study. Table B-1 provides a listing of each of the satellite observations collected for study. Some use will be made of each observation; however, the major portions of this study will be directed toward the Nimbus AVCS and MRIR observations for 9 June 1966.

Table B-1

Satellite Observations of Hurricane Alma

		Pass	
4 June 1966	ESSA-1	1743	TV
5 June 1966	ESSA-1	1757	TV
6 June 1966	Nimbus II	291	HRIR
7 June 1966	Nimbus II	305	HRIR
7 June 1966	ESSA	1786	TV
8 June 1966	Nimbus II	324	MRIR
8 June 1966	Nimbus II	324	AVCS
9 June 1966	Nimbus II	332	HRIR
9 June 1966	Nimbus II	338	APT, AVCS, MRIR
10 June 1966	Nimbus II	344	HRIR

B.2.2 Analysis Procedures

Observations from conventional and satellite sources indicate that Alma reached hurricane intensity late on 6 June 1966. Satellite observations suggest that little change in intensity occurred until 10 June, when the storm entered the Florida panhandle and weakened.* We have assumed, therefore, for analysis purposes, that Alma was a steady state storm from 6-10 June 1966. This assumption permits compositing, in storm coordinates, all the conventional surface and radiosonde observations for the 6-10 June period. Analyses, at standard constant pressure levels, of the streamline, isotach, temperature, moisture and tropopause height fields have been prepared for each of the composited data arrays. In addition, rectifications of Nimbus II "window" (10-11μ) and "H_2O" (6.4-6.9μ) observations

*Some subsequent re-intensification occurred later, when the storm moved off the Atlantic coast.

have been prepared at the same scale as the streamline isotach, etc. analyses to facilitate comparison.

B.3 Observations

B.3.1 General

Hurricane Alma was a small storm, which moved as shown in Figure B-1. Canopy size and organization, determined from the satellite visible spectrum observations using techniques developed by Fritz et al (1966), suggest maximum surface winds in the 60-80 kt range. Wagner (1966) indicates, however, that Alma, in spite of her small size, was a prolific rain producer: " . . . up to 30 inches of rain in Honduras . . ." and 8 inches in 24 hours in Wilmington, North Carolina (a new record) after the storm had moved inland over southeastern United States. We may, therefore, assume Alma was a well-organized tropical cyclone, which a priori, had an ample amount of intense convection.

B.3.2 Satellite

B.3.2.1 AVCS Mosaic

A Nimbus II AVCS mosaic taken at 1200 local time, 9 June 1966, is shown as Figure B-2. Alma is just about to enter the Florida panhandle. The thin cirriform streamers extending to the north and northeast of the storm center are indicative of the outflow wind patterns frequently observed in meteorological satellite photographs of tropical cyclones. Sharp edges, attributed to subsidence by some investigators, e.g., Fett (1964), lie along the south through west sides.

B.3.2.2 MRIR

The MRIR experiment on Nimbus II provides observations in the five spectral bands as indicated in Figure B-3. One archival form of the data is all five channels imaged in photofacsimile format on a single 8 by 10 inch sheet (Figure B-3). The observations of Alma are at 30N 80W, an area which is upside-down in Figure B-3. Figure B-4 presents a slightly enlarged section covering the portion over Hurricane Alma, with north now in the normal orientation. Note

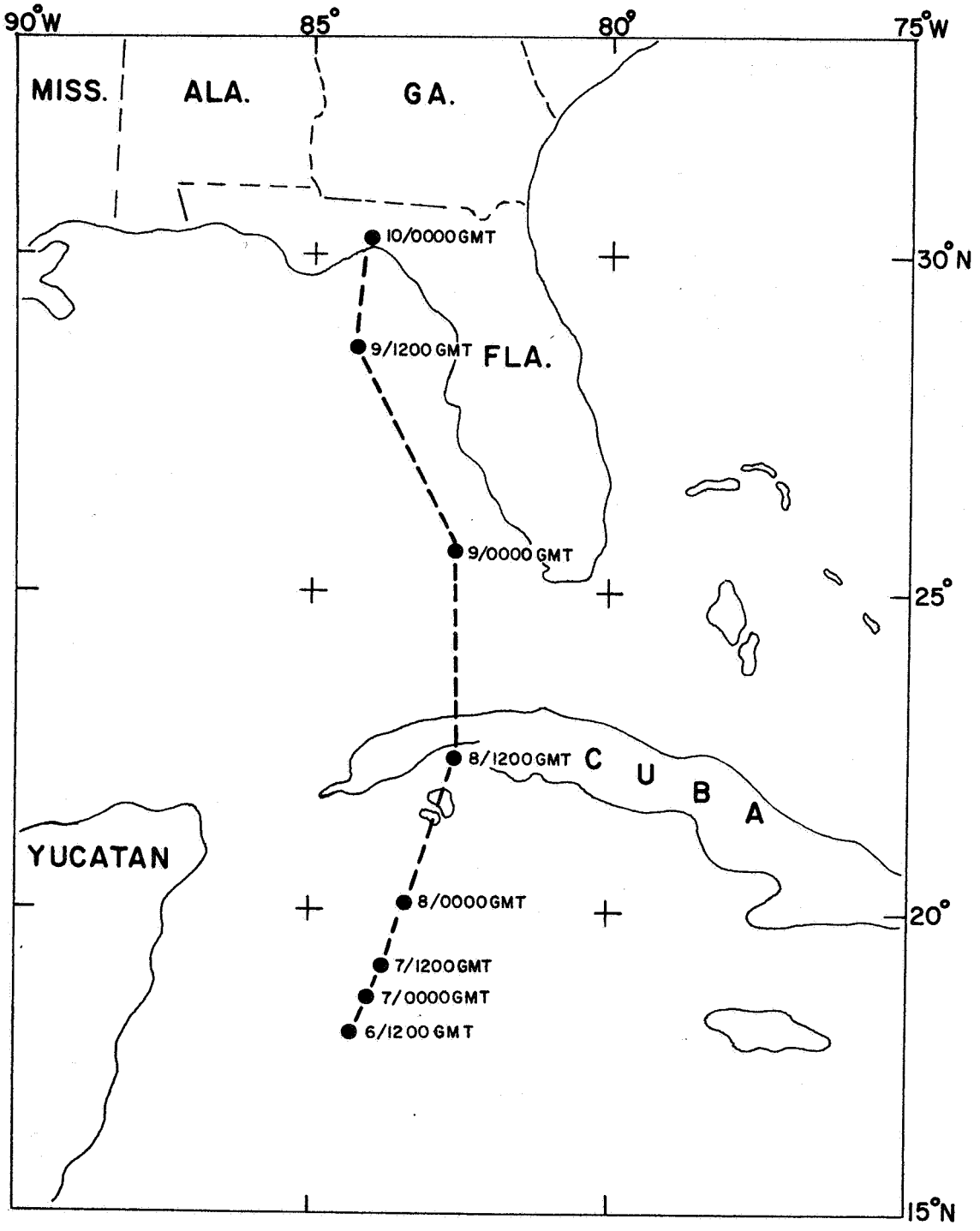

Figure B-1 Hurricane Alma Positions 6-10 June 1966

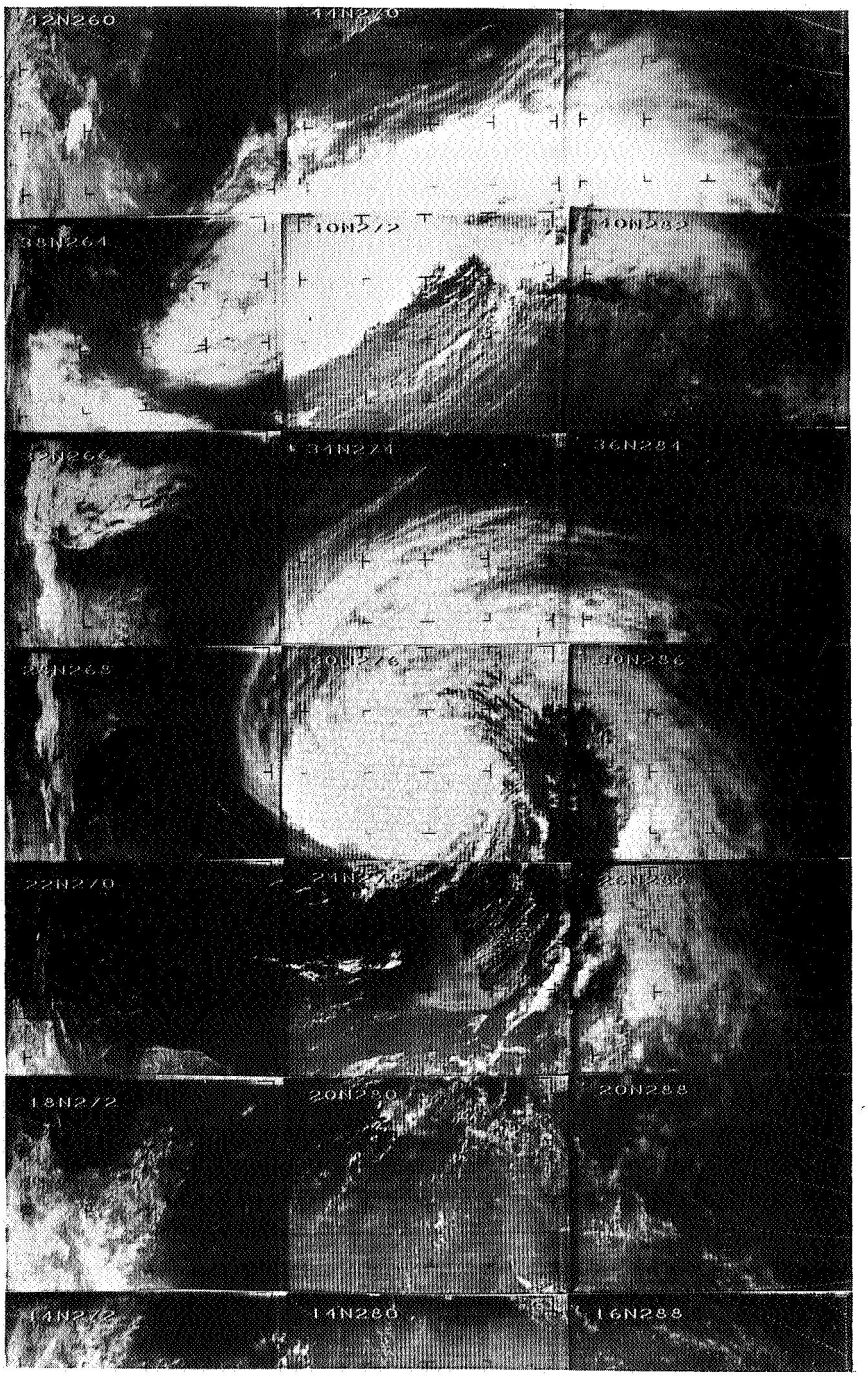

Figure B-2 Nimbus II AVCS Photograph, Hurricane Alma
~ 1200 LMT, 9 June 1966

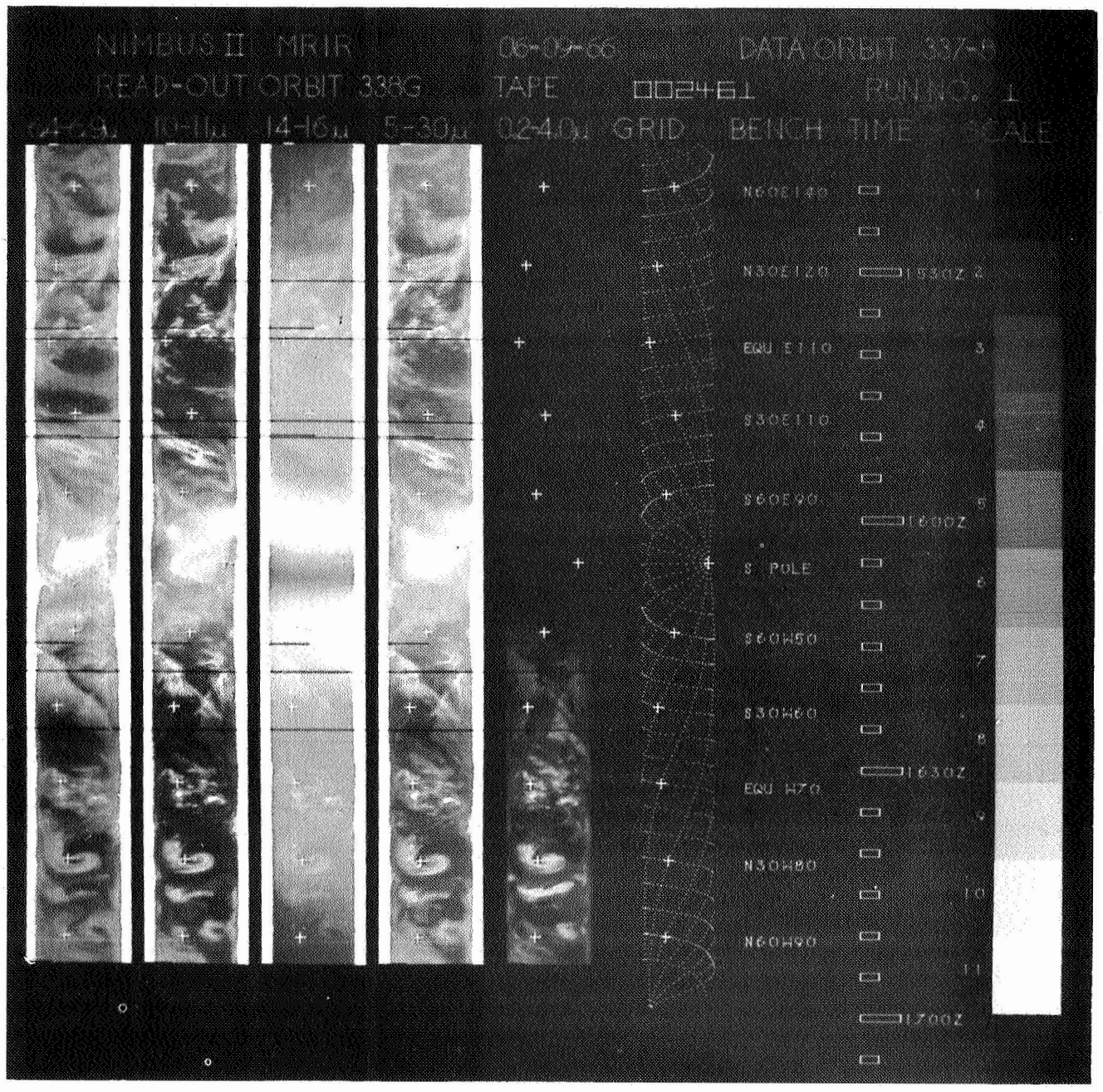

Figure B-3 Nimbus II MRIR Archival Sheet
Data Orbit 337, 9 June 1966

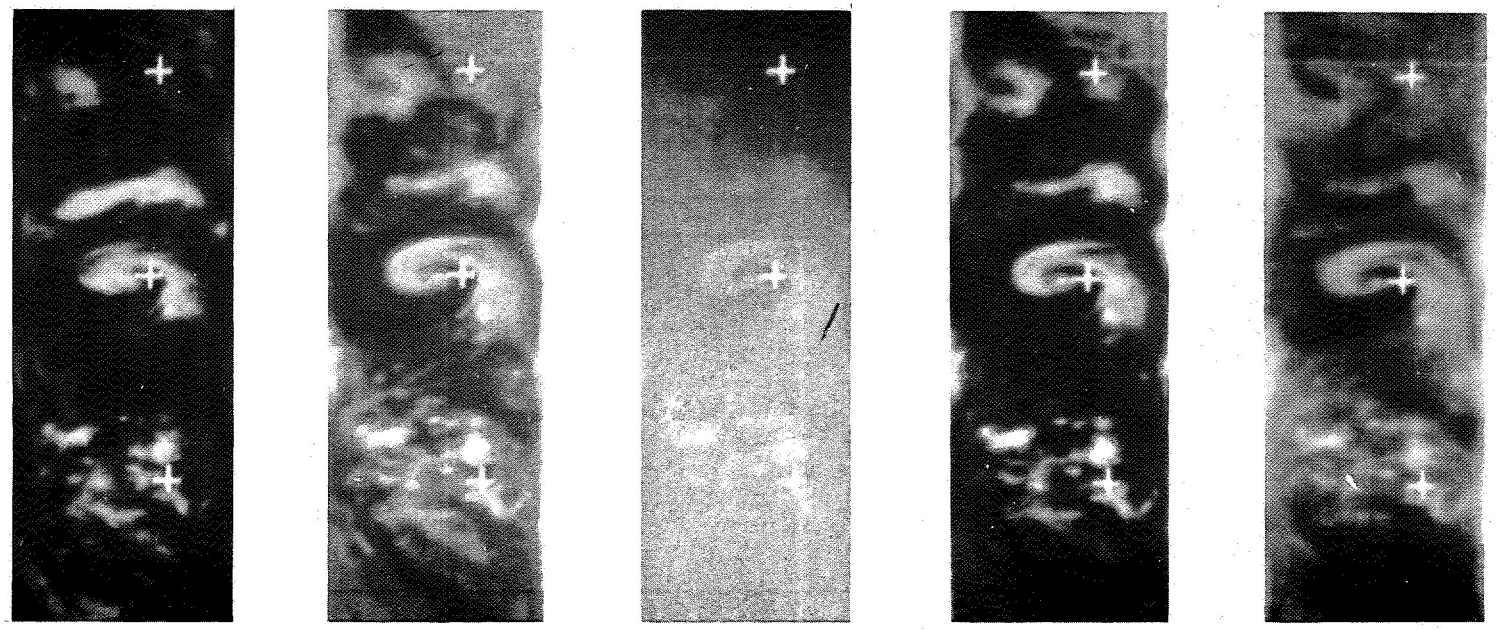

0.2-4.0μ 5-30μ 14-16μ 10-11μ 6.4-6.9μ

Figure B-4 MRIR Enlarged Section Over Hurricane Alma
Orbit 337, ~1200 LMT, 9 June 1966

that the high clouds associated with Alma's canopy are readily visible in all bands, including the 14-16μ CO_2 band which is only slightly influenced by clouds below about 10 km. The the top of Alma's canopy is at a level about 10 km.

In order to permit direct comparison of the MRIR observations, both in the "window" (10-11μ) and in "H_2O" (6.4-6.9μ), with the streamline, both isotach and moisture analyses and with each other, rectifications (Figs. B-5 and B-6) were prepared. These rectifications show the various tones of gray converted to their appropriate digital temperatures (see Nordberg et al, 1966). An error of estimate of the order of the temperature range of at least one gray scale step is common in these converstions; thus only relative use should be made of the values presented. The most significant feature observed,in a comparison of the two rectified images, is the difference in overall size of the canopy as seen in H_20 (6.4-6.9μ) and in the "window" (10-11μ). This difference occurs mainly in the regions on the west through northeast sides of the canopy. The apparent reason for this disparity will be discussed during the comparison of these rectifications with the conventional streamline analyses.

B.3.2.3 Summary of Satellite Observations

Nimbus II AVCS and MRIR observations of the cirriform canopy of Hurricane Alma indicate a fairly typical outflow pattern on 9 June 1966. Detailed rectifications of the canopy observations in the "window" (10-11μ) and in the H_20 (6.4-6.9μ) spectral bands show that the H_2O "canopy" is larger in specific sectors than the "window" canopy.

Definition of the "canopy" is difficult. However, we are describing, as canopy, those bright cloud areas lying to the west, north and east of the center of circulation. The major band to the east of the storm center running on a northeast southwest line is associated with a low level asymptote of convergence and is not considered as part of the canopy.

B.3.3 Streamline and Isotach Analyses

Figures B-7 through B-11 present streamline/isotach analyses at the following standard constant pressure surfaces: SFC, 600 mb, 400 mb, 300 mb and 200 mb. These analyses indicate that the strongest winds in Alma were on the east side, a typical situation for northward moving hurricanes. Vertical wind shear was

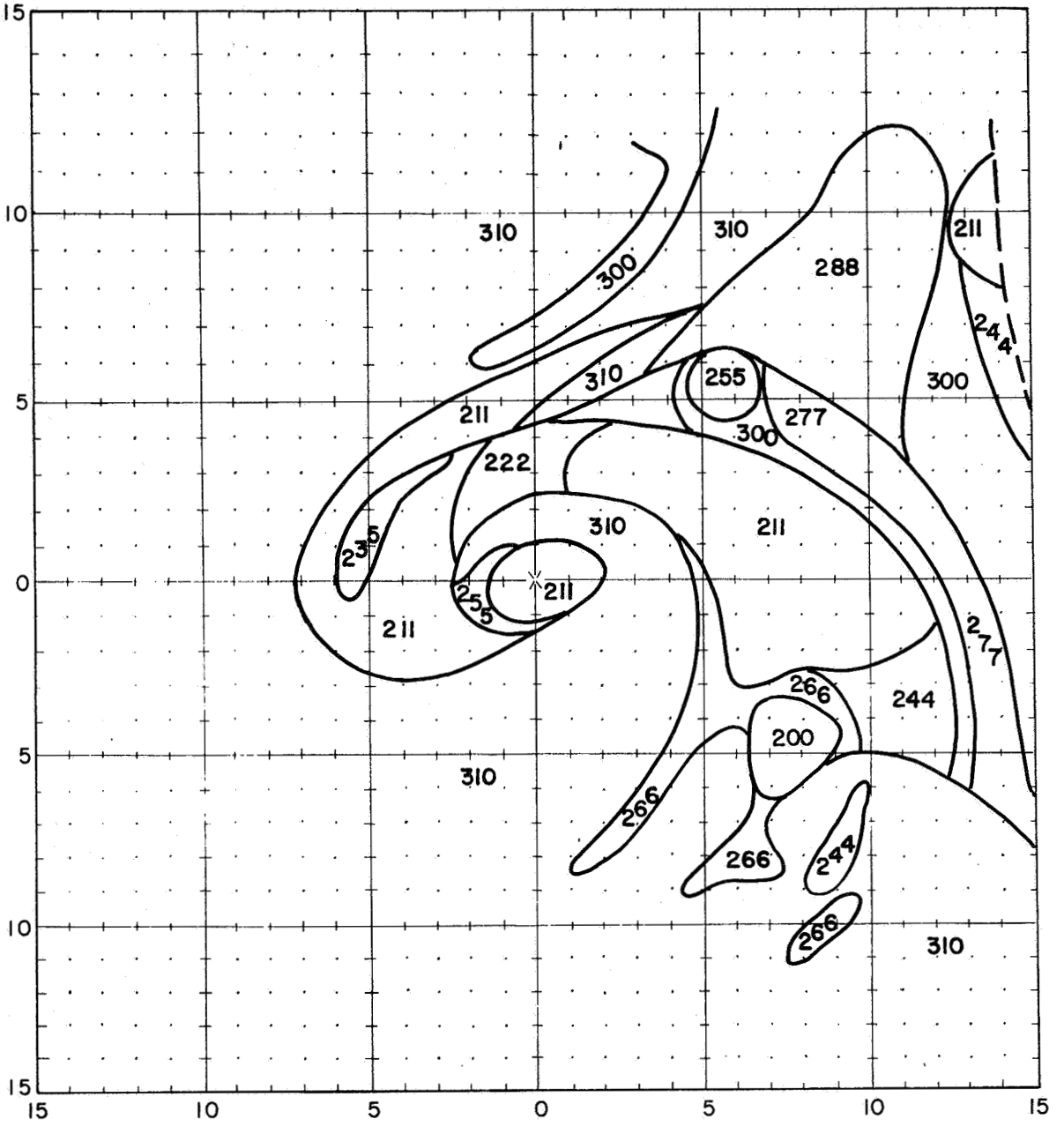

Figure B-5 10-11μ Observations Hurricane Alma ~ 1200 LMT 9 June 1966. (Note; Rectifications at same scale as composite streamlines. The grid interval is 5 degrees with one degree subdivisions.)

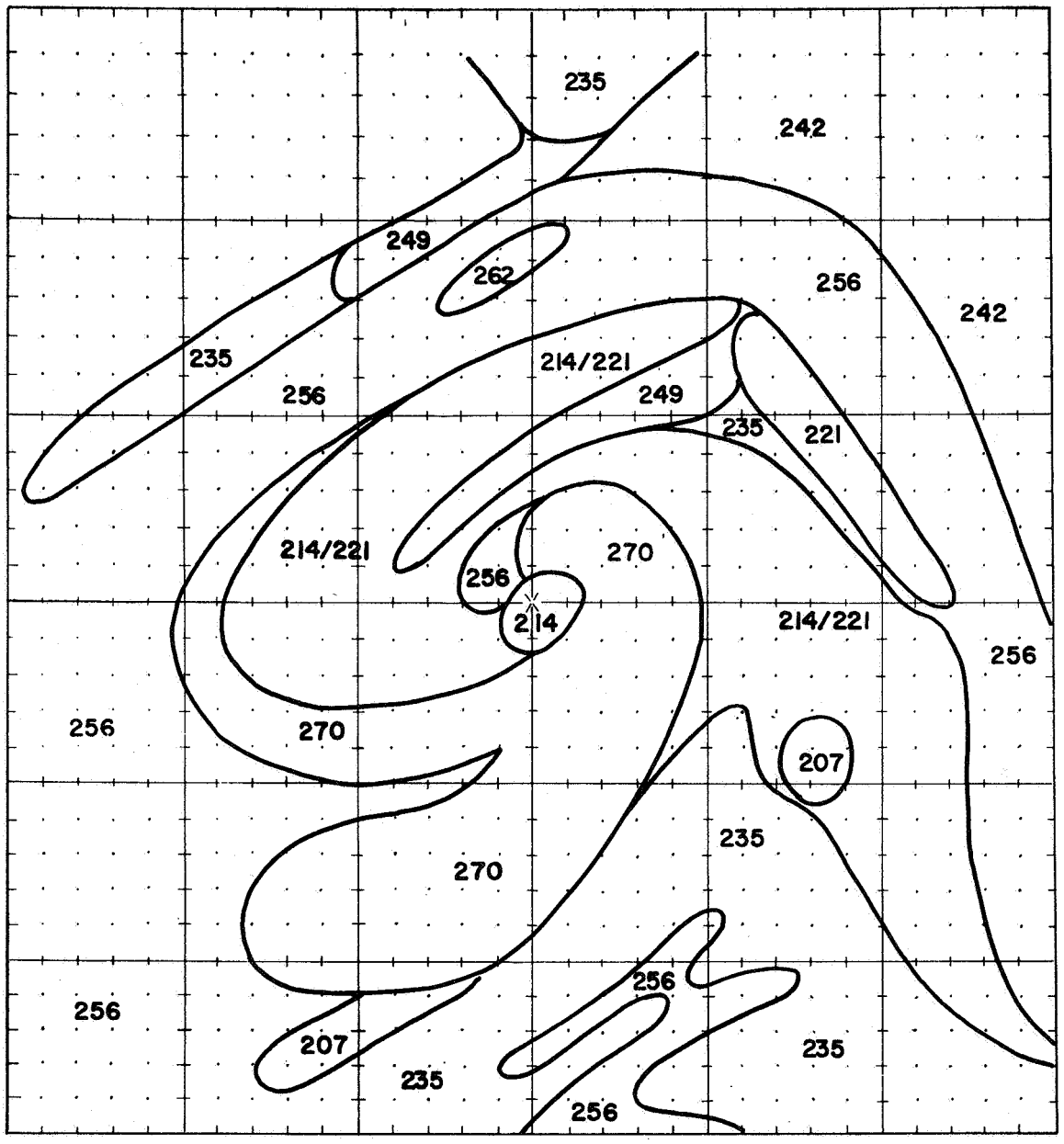

Figure B-6 6.4-6.9μ Observations Hurricane Alma ~ 1200 LMT 9 June 1966. (See Note on Figure B-5).

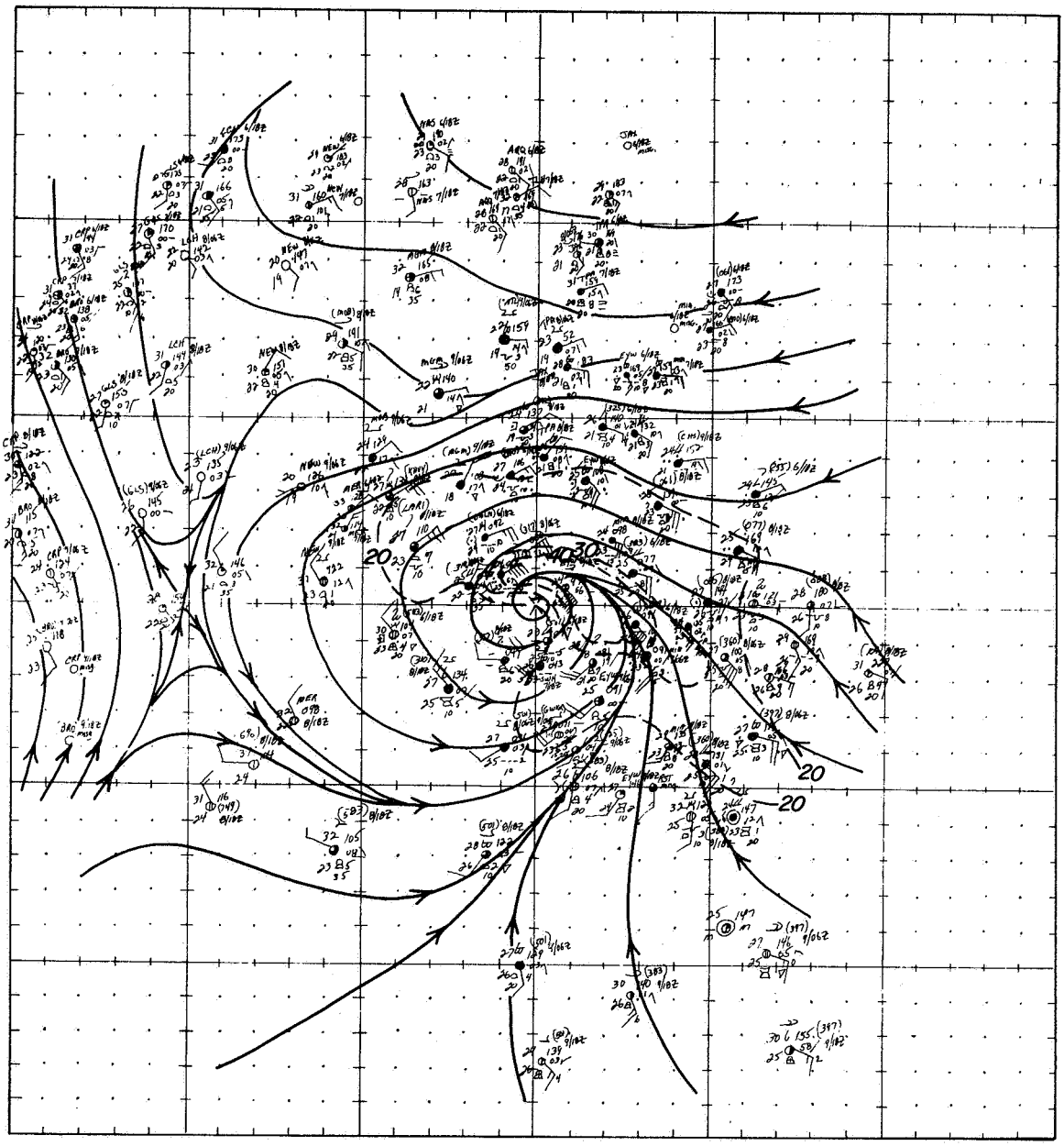

Figure B-7 Surface Streamline/Isotachs, (Composited in Relation to Alma Locations 6-10 June 1966).

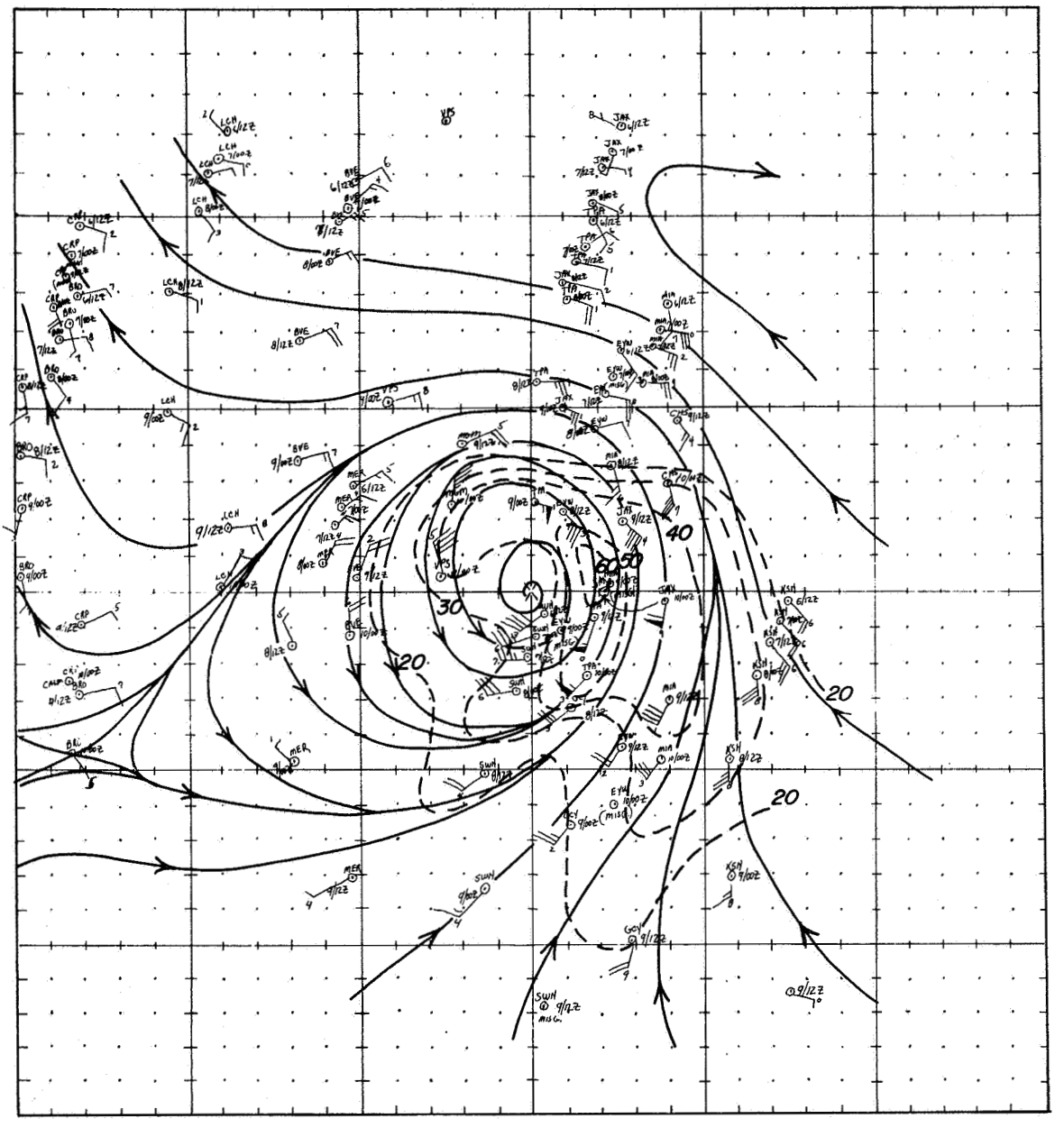

Figure B-8 700 mb Streamline/Isotachs, (Composited in Relation to Alma Locations 6-10 June 1966).

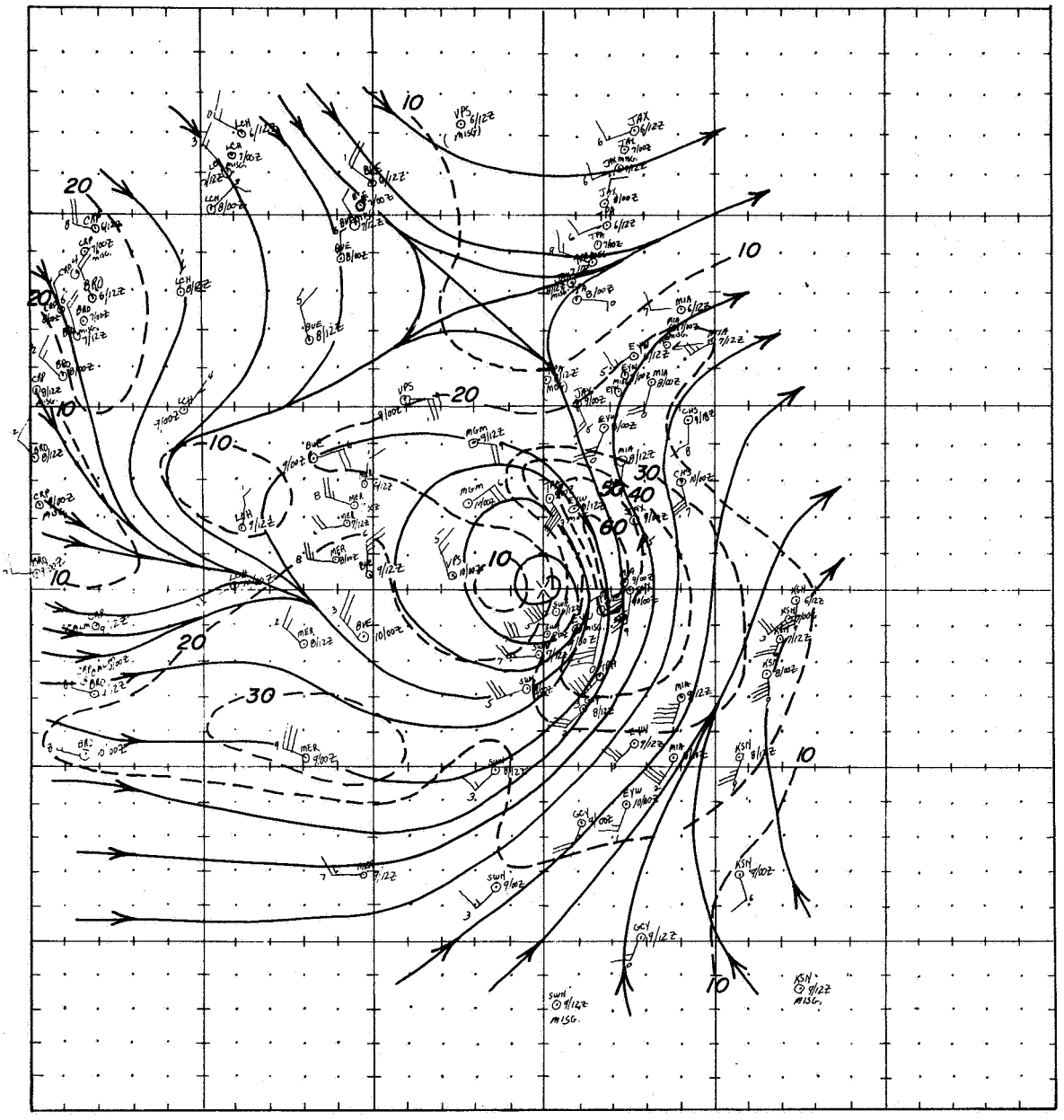

Figure B-9 400 mb Streamline/Isotachs, (Composited in Relation to Alma Locations 6-10 June 1966).

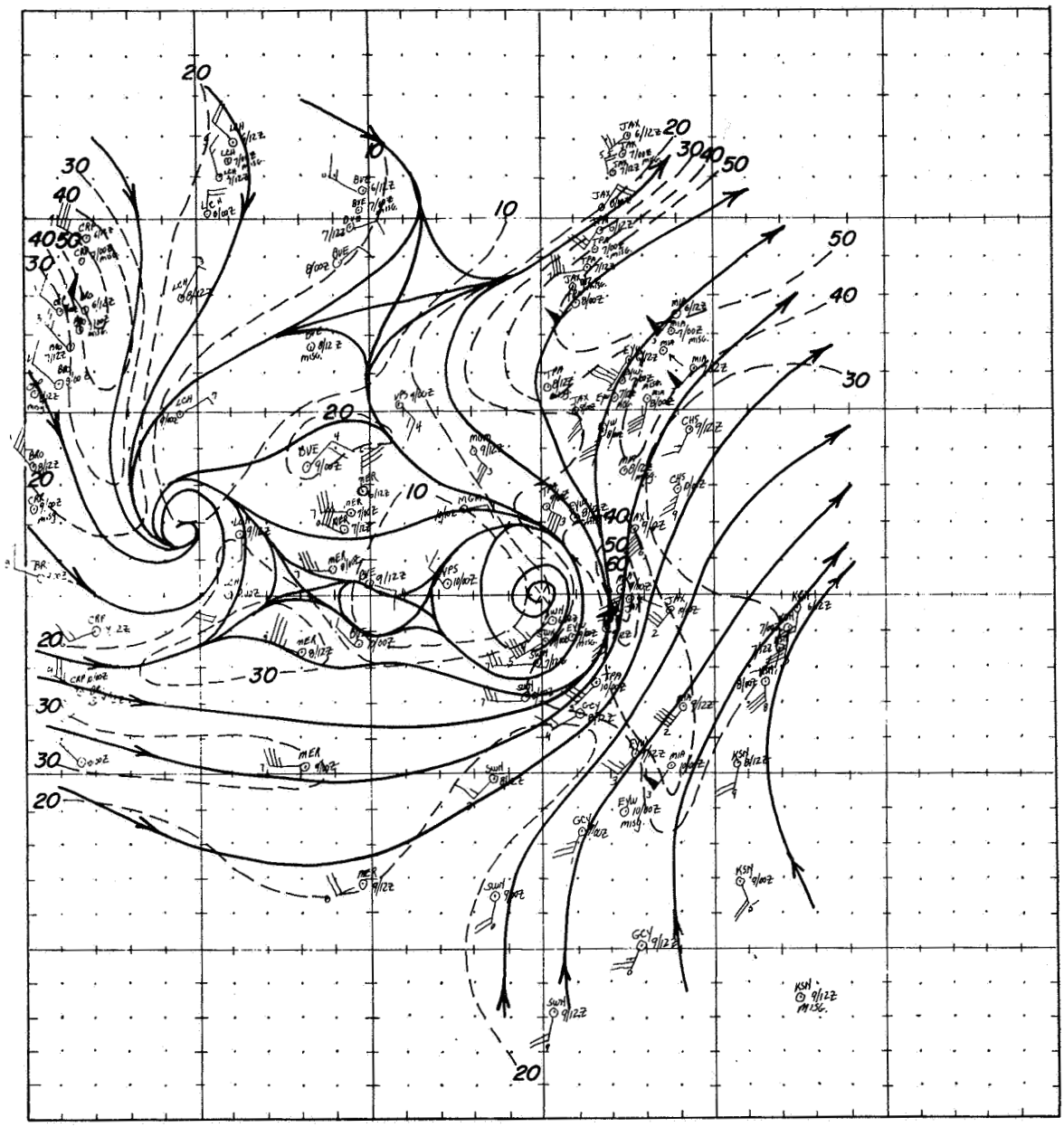

Figure B-10 300 mb Streamline/Isotachs, (Composited in Relation to Alma Locations 6-10 June 1966).

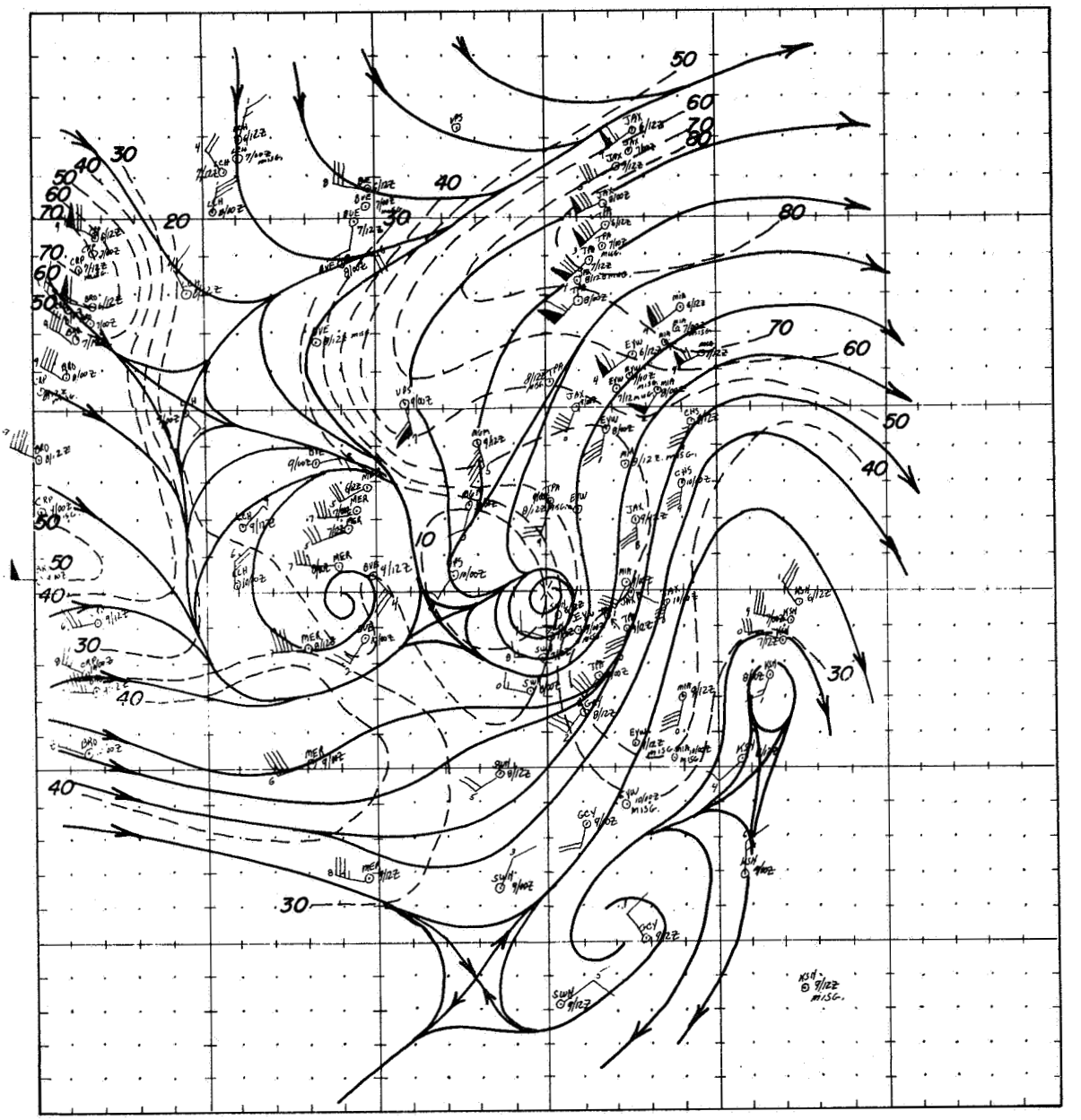

Figure B-11 200 mb Streamline/Isotachs, (Composited in Relation to Alma Locations 6-10 June 1966).

least on the east and south sides, and greatest on the north through northeast sides. The area south of the storm center in Figure B-2 (the AVCS mosaic), shows several small bands parallel to the wind flow. Malkus (1963) found a similiar relationship between small bands, wind flow, and vertical shear in cloud lines over the Pacific.

Inflow into the storm existed primarily in the southwest through south and southeast sectors, e.g., see the surface streamlines in Figure B-7. Outflow occurred primarily in the northwest through east sectors of the storm. (See, for example, Figures B-9, B-10, and B-11 at 400 mb, 300 mb and 200 mb respectively.) Radial outflow is occurring in those regions where the H_2O "canopy" is larger than the "window" canopy.

Less intense cyclonic circulation in the upper troposphere (300 mb and 200 mb; Figures B-10 and B-11) are found on the west side of the storm. These appear similar to those discussed in Widger, et al (1966), in an HRIR analysis of developing Typhoon Wilda 1964. The role of these small scale circulations is not clear. However, they appear to be colder than the immediate environment and could therefore produce acceleration by forming, with the warm core hurricane system, a vertical solenoidal cell.

B.3.4 Comparisons

The observations in the 10-11μ "window" and in the 6.4-6.9μ H_2O band, shown in Figures B-5 and B-6, pose some important questions. In particular, what is the cause of the size differences between the "window" and H_2O canopies. Wexler, Merritt, and Chang (1966) have shown that the canopy character, size, sharp or diffuse edges, etc., can be directly related to the field of motion at cirrus levels. Comparison of the "cirrus layer" field of motion, approximated by the 200 mb chart (Fig. B-11), with the rectified "window" and "H_2O" canopies, indicates that the areas where the H_2O "canopy is larger than the 'window" canopy are areas of significant outward radial components.

B.3.4.1 Parcel Motions

In order to examine parcel motions outward from and inward toward the storm, we have prepared cross-sections along appropriate trajectories, as shown in Figure B-12. Cross-section No. 1 (Fig. B-13) provides a sample of an outflow

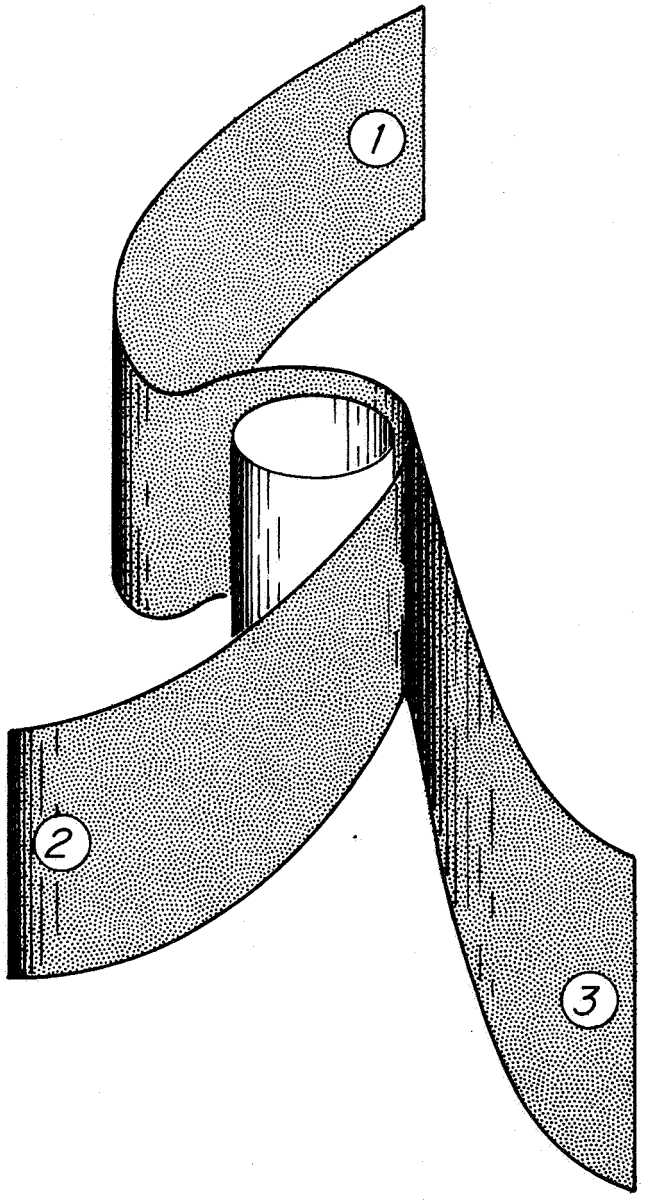

Figure B-12 Location for Cross-sections in Figures B-13, B-14, and B-15.

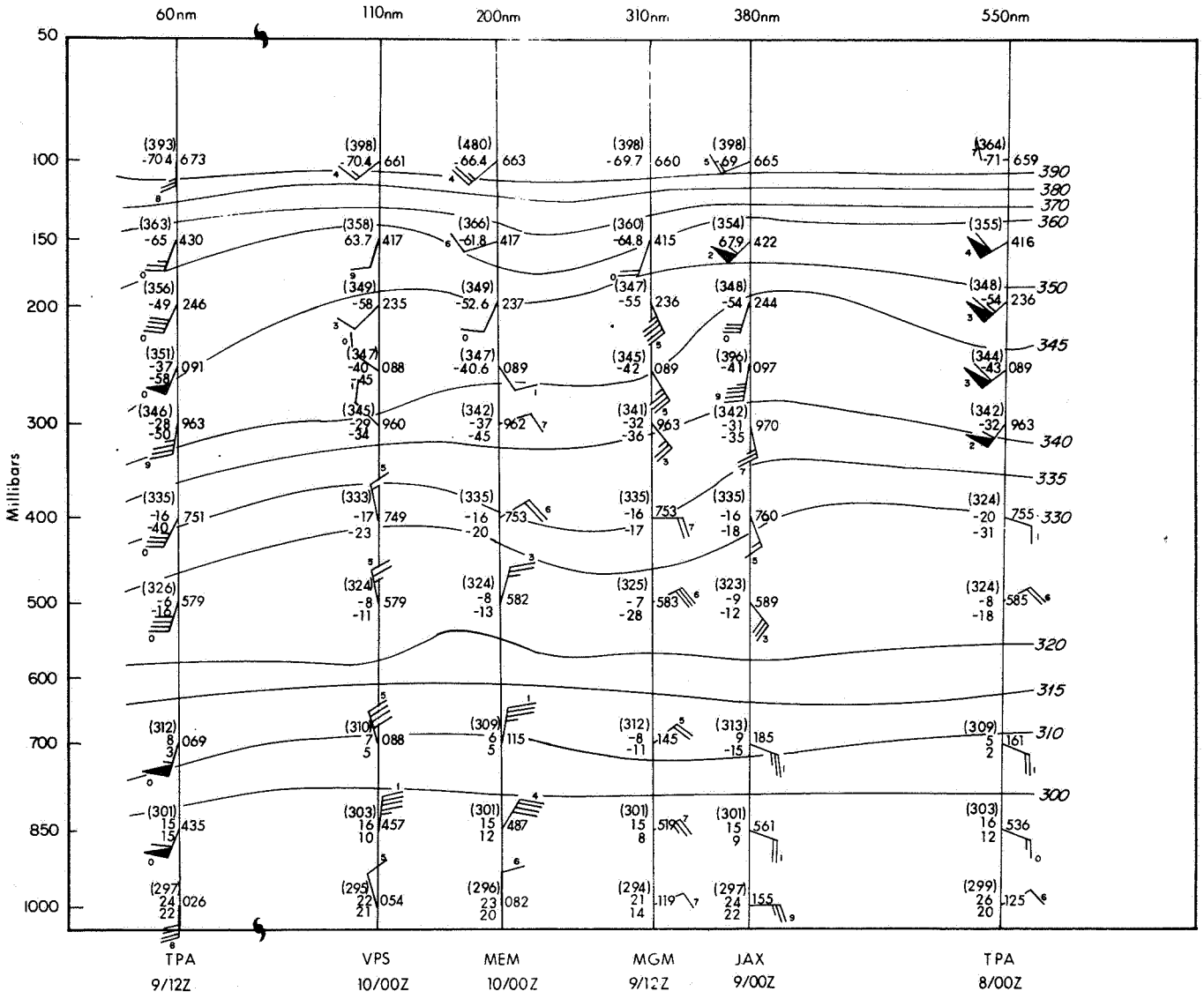

Figure B-13 Cross-Section No. 1 Along Cloudy Zone Outflow Trajectory, Hurricane Alma, (Data Derived from 6-10 June 1966 Composites).

trajectory, while sections No. 2 and 3 (Figs. B-14 and B-15) sample the clear zone and cloudy zone inflow trajectories from the west and south.

Cross-section No. 1 (Fig. B-13)

As shown in Figure B-12, cross-section No. 1 (Fig. B-13) was prepared along an outflow trajectory at 200 mb. An air parcel is assumed to move from the east side of the storm center around the north side, then anticyclonically north and northeastward. On an isentropic surface of about 360 K, a parcel moves slightly upward for the first 110 n.mi. of travel (condensation may occur if the ascent exceeds about 2 km). Descent occurs during the following 150 n.mi. If we start with a cloud parcel on the 360 K surface, and it descends the indicated 45 mb, a majority of the cloud would be evaporated. We would, therefore, have a concentration of water vapor and cloud particles (ice). The amount of cloud particles remaining will, of course, depend on the initial volume content of cloud particles. The area of assumed evaporation coincides to some degree with the area of the "window" canopy (Fig.B-5), where the temperatures warm from 222 K to 255 K. This area, however, is about 60 miles from the area where the "window" canopy essentially ends, but the "H_2O" canopy continues and then extends for its greatest distance along an outflow trajectory. Differences in the mean times of the composited data and of the Nimbus observation may be partially responsible for the lack of exact correspondence between the area of downward motion and the boundary of the "window" (and presumably the visible) canopy.

Cross-section No. 2 (Fig. B-14)

The inflow from the west occurs in essentially clear air. Figure B-14 shows a cross-section of the composited data along a trajectory at about 400 mb. Note the general absence of directional shear in all the soundings (excepting BRO below 500 mb), and the uniformity of lapse rates. A very slow descent seems to occur, throughout the entire trajectory, in parcels moving along 320-340^{o}K potential temperature surfaces. A slight ascent is to be noted at about 350-500 n.mi. from the storm center at levels between about 300 and 150 mb. This region appears cloudless in the MRIR data (Fig. B-5). However, the surface composite, Figure B-7, indicates that some cirrus was scattered throughout this region during the compositing period. The 9 June AVCS mosaic indicates only low level cumulus in this area. This observation is, however, some twenty-four hours after the mean of the compositing period.

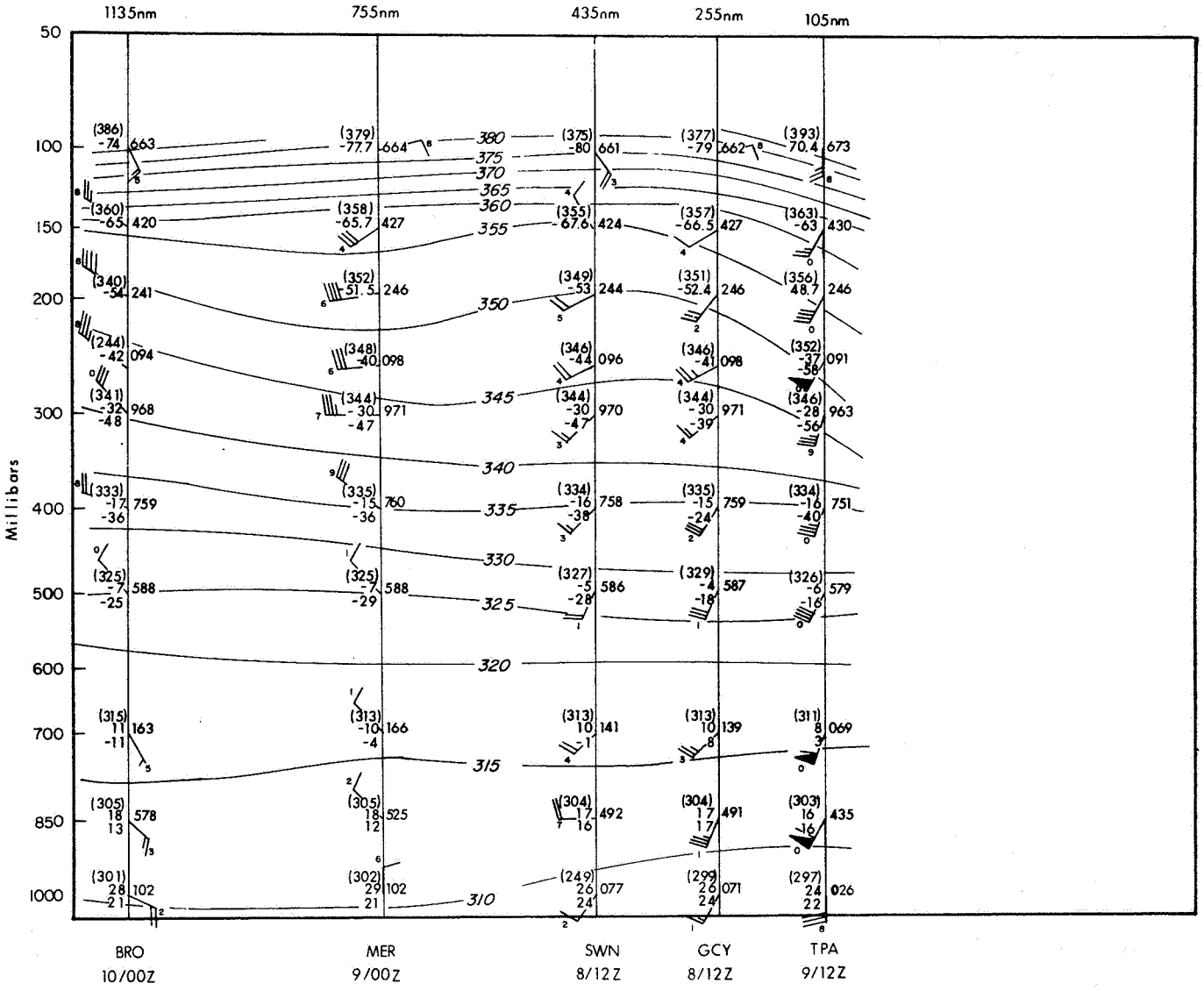

Figure B-14 Cross-Section No. 2 Along Clear Zone Inflow Trajectory, Hurricane Alma, (Data Derived from 6-10 June 1966 Composites).

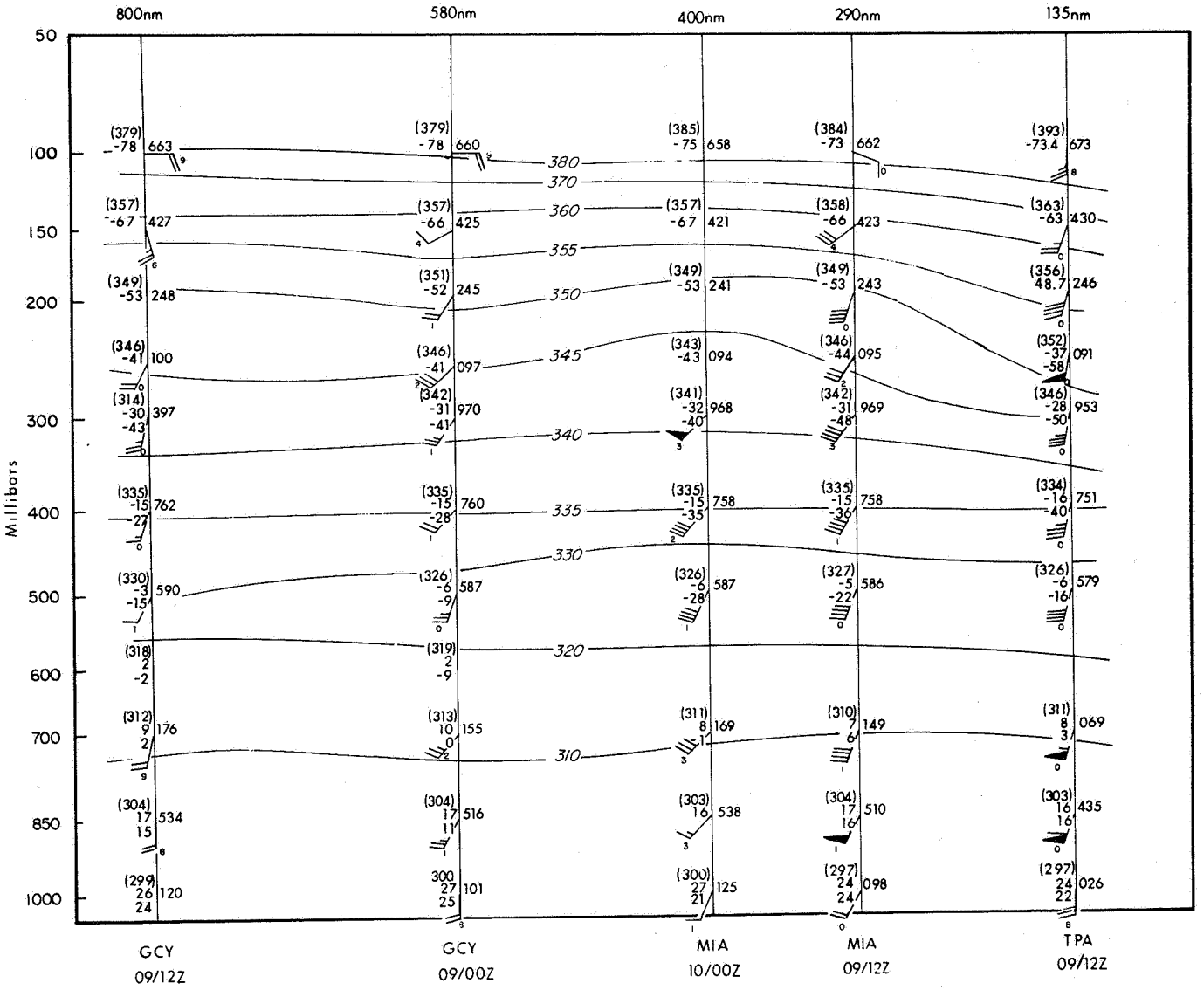

Figure B-15 Cross-Section No. 3 Along Cloudy Zone Low Level Convergence Inflow Trajectory, Hurricane Alma, (Data Derived from 6-10 June 1966 Composites).

Cross-section No. 3 (Fig. B-15)

This composited cross-section, Figure B-15, provides a look at the atmosphere along a surface -850 mb trajectory which approximates an asymptote of convergence in the storm. Comparison with the MRIR rectifications, Figures B-5 and B-6 indicate that this trajectory is just on the edge of the large cold band east of the storm center. This area (as was that of the previous cross-section, No. 2) is notably free of vertical directional shear (excepting the areas above 150 mb). Some slight ascent is observed for parcels moving in the layer encompassed by the $330^{o}K$-$350^{o}K$ potential temperature surfaces. Comparison with the surface analysis (Figure B-7), shows this ascent to be associated with the beginnings of overcast skies and precipitation.

B.3.4.2 Summary of Parcel Motion Analyses

Comparisons between conventional data analyses, and MRIR observation in the 10-11μ "window" and in the 6.4-6.9μ H_2O spectral band, indicate the following:

1. The difference in horizontal extent of the "window" and "H_2O" canopies occurs in a region of significant outward radial component in the 300 mb - 150 mb layer.

2. Parcel descent, along an isentropic surface, is noted in the region where the most significant differences in size between the "H_2O" and "window" canopies occurs.

3. Minimum vertical directional shear is found where essentially clear skies appear in the MRIR observation; while maximum vertical shear occurs in the regions where overcast skies occur.

4. The sharpest edges of the visual AVCS canopy occurs in regions of minimum outward radial components, in correspondence with the findings of Wexler, Merritt, and Chang (1966).

B.4 Time Change in Canopy Size

B.4.1 Results of a Previous Study

As mentioned previously, the studies by Wexler, Merritt, and Chang (1966) showed that the time change in canopy size was closely related to estimates of the percent of the storm area covered by cumuliform towers influencing the outflow region. An estimate by Malkus et al (1961) of four percent of the total area within

a radius of 200 n.mi., was used in that study to determine the mean vertical velocities associated with observed canopy changes (derived from the field of motion at 200 mb). The following simple model was used: (1) the rate of production of cirrus volume equals ωA_c, where A_c is the area of cumulus towers and ω is a mean updraft at the base of the cirrus. (2) Assuming a steady state, an incompressible fluid, and a cirrus layer of constant depth, the rate of cirrus production by the cumulus towers equals the rate of increase of cirrus volume, or

$$A_c \omega = H \frac{dA}{dt}$$

where H is the estimated cirrus layer thickness and A is the horizontal area of cirrus.

Values of the rate of increase in area, dA/dt, were estimated (by Wexler, Merritt, and Chang) from time changes in the canopy edge computed from outflow patterns. These values were 5×10^4 km^2 hr^{-1}, and 4×10^4 km^2 hr^{-1}, for two representative cases. Mean updrafts, assuming the Malkus estimate, i.e., four percent, were 1.2 - 1.6 m sec^{-1}, which are assumed reasonable as a mean updrafts for the entire cumulus tower area.

B.4.2 Procedure for Estimating Cirrus Area and its Change with Time in Hurricane Alma

The extensive satellite observations of hurricane Alma provided by ESSA and Nimbus, have now provided an opportunity (1) to determine the rate of change of canopy size for an actual storm history, and (2) to relate this, through the simple Wexler et al model, to an estimate of the area distribution of significant cumuliform towers.

Estimates of canopy area are complicated by the frequent inability to determine just which areas are cirriform, and which are not. For the purpose of this study, we have attempted to circumvent this problem by defining an ellipse delineating the area of cloudiness which may be directly related to the outflow from the center of the storm. Figure B-16 shows, schematically, the procedure used in fitting the ellipse.

The area of the ellipse is used as the area of the significant outflow cirrus. Since we are concerned only with the change in area, dA/dt, this procedure may be sufficient.

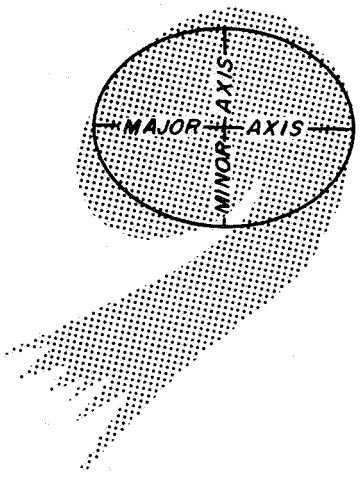

Figure B-16 Schematic of Procedure for Describing Area of Alma Canopy

Observations of Alma by ESSA 1, and by the Nimbus II APT, were presented as the Picture of the Month in the Monthly Weather Review, and are included here as Figure B-17. Measurements of the areas determined from these observations were supplemented by HRIR observations and AVCS observations. The computed ellipse areas are presented in Figure B-18. Note the decrease in dA/dt as the period of maximum intensity is approached, with dA/dt becoming approximately zero at the time of maximum intensity.

The average rate of canopy area increase dA/dt, during the period 5 June to 7 June, is 4×10^4 km^2 hr^{-1} and is approximately equal to the values obtained by Wexler, et al for the canopy change due to advection of cirrus within the outflow layer.

B.4.3 Cumuliform Tower Considerations

The simple model used by Wexler et al, i.e.,

$$A_c \omega = H \frac{dA}{dt},$$

and a cumulus "hot tower" area coverage of four percent leads to mean vertical velocities of 1.2 to 1.6 m sec^{-1}.

PICTURE OF THE MONTH

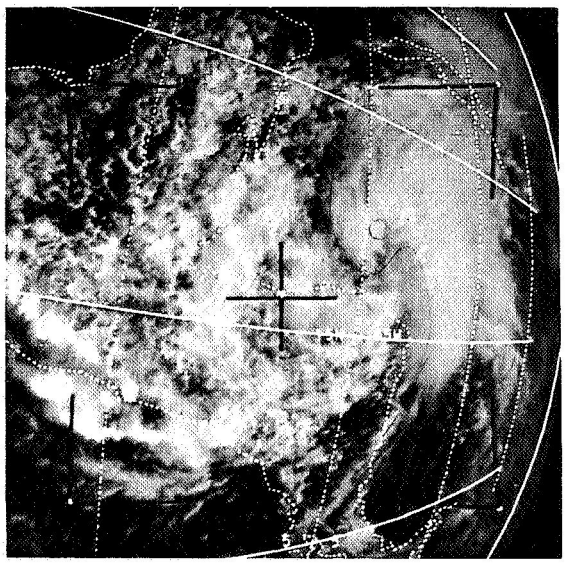

(a) ESSA–1, Pass 1743, Camera 1, Frame 7, June 4, 1966, 1943 GMT.

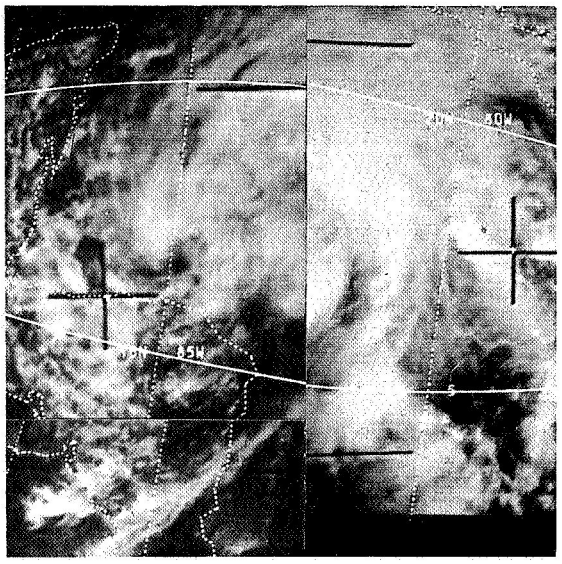

(b) ESSA–1, Pass 1757, composite of three photos, June 5, 1966, approximately 1908 GMT.

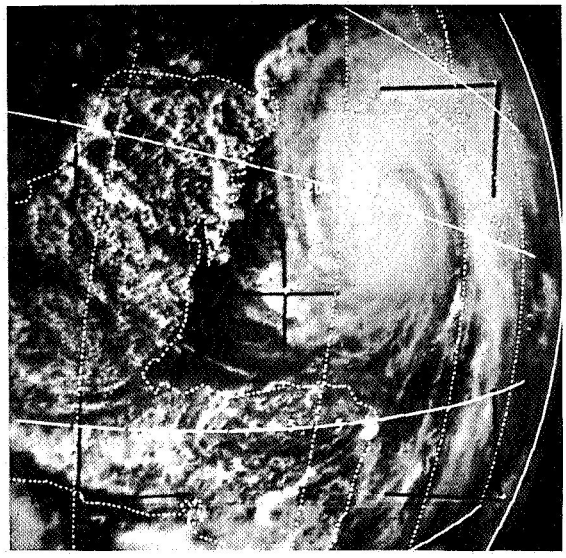

(c) ESSA–1, Pass 1786, Camera 1, Frame 6, June 7, 1966, 1938 GMT.

(d) Nimbus II, Pass 338, APT, June 9, 1966, 1641 GMT.

Figure B-17 Monthly Weather Review Picture of the Month Hurricane Alma, June 1966.

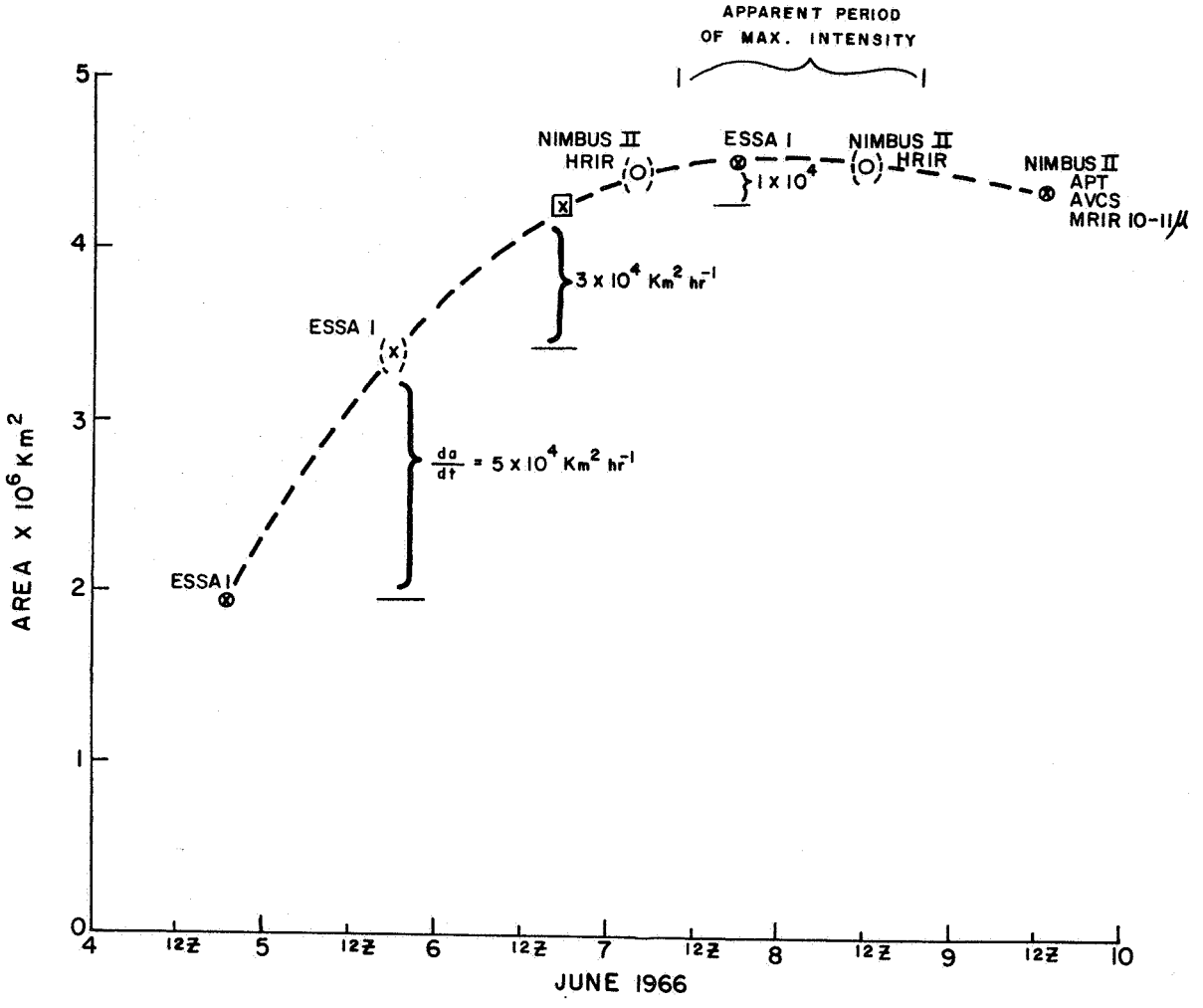

Figure B-18 Hurricane Alma Canopy Area Change with Time, 4-10 June 1966.

Hurricane Alma, however, was not at maximum intensity during the 5-7 June period. We must, therefore, assume cumulus towers covered at least four percent of the storm area out to 200 miles radius prior to the hurricane stage, if the mean vertical velocities are not to exceed 2 m sec^{-1}. This observation is somewhat counter to Malkus, et al (1961), who estimated, from radar and photographs of Daisy (1958) a cumuliform tower area of one percent on the day of upgrading to tropical storm and of four percent on the day of maximum intensity. However, observations and a model prepared by Yanai (1964) suggest that the cumulus convection should in fact precede maximum storm intensity to transport the heat necessary to produce a warm core structure. Yanai (1964) states that a radial gradient of temperature in the upper troposphere, formed through upward transport of sensible and latent heat,may induce further development of the storm.

In summary, Hurricane Alma appears to have had at least four percent of its area, within a radius of 200 miles, covered with significant cumulus towers during the 2-3 day period prior to reaching hurricane intensity. During the time of maximum storm intensity, a balance had been achieved between cirrus production and dissipation.

B.5 Conclusions, and Recommendations for Further Research, Derived from the Study of Hurricane Alma

B.5.1 Conclusions

This observational study of certain facets of Hurricane Alma, 1966, using conventional data as well as satellite observations from Nimbus II and ESSA 1, has re-emphasized the value of meteorological satellite observations in the study of tropical cyclones. Specific findings are as follows:

a) The Hurricane Alma canopy, viewed in satellite observations in the visible spectrum, indicates sharp edges in areas where minimum radial outward components occur, and diffuse edges in areas of maximum radial outward components. This essentially confirms the study of Wexler, Merritt and Chang (1966), regarding the evolution of sharp edges in the visible spectrum canopy.

b) The existence of thin bands, parallel to the wind, to the south of Alma on 9 June 1966, provides support to observations of Malkus since the bands parallel the wind in an area where there is a minimum of directional shear in the vertical.

c) The difference in size between the visible or "window" canopy, and the "H_2O" emission "canopy," observed by the Nimbus II MRIR, suggests that subsidence and attendent evaporation is, in fact, taking place around the edge of the canopy. The differences in canopy size are greatest in the areas of maximum outward radial components. This finding introduces some new questions into the problem of canopy evolution. Fett (1964) suggests that subsidence is responsible for sharp edges, while Wexler et al (1966) shows in a model approach that sharp edges can occur through advection alone. Thus we find support for both concepts, although the requirement for subsidence to produce sharp edges still seems in question.

d) The rate of increase in "canopy" area with time suggests that the "hot towers," thought to be primarily responsible for cirrus production, must exist in the pre-tropical storm stages. This observation is somewhat counter to those of Malkus et al (1961). However, the observation is compatible with the hurricane models proposed by Yanai (1964), and others, which require initial formation of the warm core in the middle and upper troposphere. These models postulate that the heating takes place through upward transport of sensible and latent heat in "hot towers."

e) The observation of a decrease in the rate of change of canopy size just prior to maximum storm intensity suggests that a balanced, steady state between cirrus production and evaporation is achieved when the storm has reached maximum intensity. Creation of new hot towers appears required for further development.

B.5.2 Recommendations for Further Research

B.5.2.1 "Window" versus "H_2O" Canopy

The observations of the Nimbus II MRIR, which reveal a difference in size between the (1) visual (TV) and "window" infrared canopy, and (2) the "H_2O" emission "canopy," pose two interesting problems desirable of further study. These are:

a) Is the "H_2O" canopy size difference the result of evaporation around the edge of the (TV) and "window" infrared canopy, leaving only a high concentration of water vapor, or is it caused by a combination of (1) evaporation (leaving a moderate water vapor concentrate) and (2) amounts of ice crystals which are below the (TV) resolution? Further studies of this type, with concurrent aircraft studies of moisture and ice particle concentrations, are required.

b) Is the apparent evaporation caused by subsidence occurring in a major branch of the hurricane vertical circulation? If so, does the subsidence in this branch reach a maximum at the hurricane stage of the storm? Further studies of storms at varying degrees of intensity may resolve this question.

B.5.2.2 Canopy Increase with Time

The rate of increase in canopy size with time, in Alma, was somewhat counter to the observations of Malkus et al (1961), but is in line with the development model of Yanai (1964). If, in fact, the "hot towers" associated with the canopy increase are present prior to tropical storm intensity and this can be demonstrated in more than a single storm, we may have considerable support for Yanai's model. This model speculates warming in the upper troposphere, through the transport of sensible and released latent heat, prior to storm intensification. The advent of the synchronous meteorological satellite may permit an extensive study of this possibility. Additionally, detailed analyses of HRIR observations may provide a measure of the percentage area of "hot towers" in the early stages of storm development.

REFERENCES

Fett, R.W., 1964: "Aspects of Hurricane Structure: New Model Considerations Suggested by TIROS and Project Mercury Observations," Mon. Wea. Rev., 92, pp. 43-60.

Fritz, S., L.F. Hubert, and A. Timchalk, 1966: "Some Inferences from Satellite Pictures of Tropical Disturbances," Mon. Wea. Rev., 94, pp. 231-236.

Malkus, J.S., C. Ronne, and M. Chaffee, 1961: "Cloud Patterns in Hurricane Daisy, 1958," Tellus, 13, pp. 8-30.

Malkus, J.S., 1963: "Cloud Patterns Over Tropical Oceans," Science, 141 (3583), pp. 767-668.

Merritt, E.S., and C.J. Bowley, 1966: Analyses of Diurnal Variations in TIROS VII "Window" Radiation Over Indonesia and Malaysia, Second Quarterly Report, Contract No. NAS 5-10151, Allied Research Associates, Inc.

Nordberg, W., A.W. McCulloch, L.L. Foshee, and W.R. Bandeen, 1966: Preliminary Results from Nimbus II, Goddard Space Flight Center, Document No. X-620-66-349.

Picture of the Month, August 1966: Mon. Wea. Rev., 94(8), p. 534.

Wagner, A.J., 1966: "The Weather and Circulation of June 1966 — A Month with Variable Weather and Several Extremes," Mon. Wea. Rev., 94(9), pp. 587-594.

Wexler, R., E.S. Merritt and D. Chang, 1966: Cirrus Canopies in Tropical Storms, Final Report, Contract No. Cwb-11305, Allied Research Associates, Inc.

Widger, W.K., J.C. Barnes, E.S. Merritt and R.B. Smith, 1966: Meteorological Interpretation of Nimbus High Resolution Infrared (HRIR) Data, NASA Contract Report, NASA CR-352.

Yanai, M., 1964: "Formation of Tropical Cyclones," Reviews in Geophysics, 2(2), pp. 367-414.